LEVEL II (12) B.S.

CR 80.026

CIVIL ENGINEERING LABORATORY
Naval Construction Battalion Center
Port Hueneme, CA

Sponsored by
NAVAL FACILITIES ENGINEERING COMMAND

DESIGN CRITERIA FOR DEFLECTION CAPACITY OF
CONVENTIONALLY REINFORCED CONCRETE SLABS,
PHASE I - STATE-OF-THE-ART REPORT

October 1980

An Investigation Conducted by

CONSTRUCTION TECHNOLOGY LABORATORIES
Structural Analytical Section
5420 Old Orchard Road
Skokie, Illinois 60077

N68305-79-C-0009

AD A091738

DDC FILE COPY

80 11 04 012

SECURITY CLASSIFICATION OF THIS PAGE (When Data Entered)

REPORT DOCUMENTATION PAGE	READ INSTRUCTIONS BEFORE COMPLETING FORM

1. REPORT NUMBER	2. GOVT ACCESSION NO.	3. RECIPIENT'S CATALOG NUMBER
CR-80.026	AD-A091 738	

4. TITLE (and Subtitle)	5. TYPE OF REPORT & PERIOD COVERED
DESIGN CRITERIA FOR DEFLECTION CAPACITY OF CONVENTIONALLY REINFORCED CONCRETE SLABS, PHASE I. STATE-OF-THE-ART REPORT.	Final Jan 1979 - Aug 1979
	6. PERFORMING ORG. REPORT NUMBER

7. AUTHOR(s)	8. CONTRACT OR GRANT NUMBER(s)
Mohammad/Iqbal Arnaldo T./Derecho	N68305-79-C-0009

9. PERFORMING ORGANIZATION NAME AND ADDRESS	10. PROGRAM ELEMENT, PROJECT, TASK AREA & WORK UNIT NUMBERS
CONSTRUCTION TECHNOLOGY LABORATORIES A Division of the Portland Cement Association 5420 Old Orchard Rd., Skokie, Illinois 60077	YF60.534.091 01.412B

11. CONTROLLING OFFICE NAME AND ADDRESS	12. REPORT DATE
Civil Engineering Laboratory Port Hueneme, Ca. 93043	Oct 80
	13. NUMBER OF PAGES
	148

14. MONITORING AGENCY NAME & ADDRESS(if different from Controlling Office)	15. SECURITY CLASS. (of this report)
	Unclassified
TER 534	15a. DECLASSIFICATION/DOWNGRADING SCHEDULE

16. DISTRIBUTION STATEMENT (of this Report)

Approved for public release; distribution unlimited.

17. DISTRIBUTION STATEMENT (of the abstract entered in Block 20, if different from Report)

18. SUPPLEMENTARY NOTES

19. KEY WORDS (Continue on reverse side if necessary and identify by block number)

Blast Resistant Design	Ultimate Deflection
Reinforced Concrete	Tensile Membrane Action
Reinforced Concrete Slabs	

20. ABSTRACT (Continue on reverse side if necessary and identify by block number)

In this Phase I report, data obtained from a literature search of static and dynamic tests on uniformly loaded reinforced concrete one-way and two-way slabs are tabulated. Analytical methods for predicting incipient collapse deflection are summarized and compared to the test results. A method for predicting incipient collapse deflection, when tensile membrane resistance can be developed, is recommended for further study in Phase II of a three phase study. The recommended relationship gives incipient collapse deflection as a function of the short span of the slab and the rupture strain of the reinforcing steel.

DD FORM 1473   EDITION OF 1 NOV 65 IS OBSOLETE
1 JAN 73

TABLE OF CONTENTS

TABLE OF CONTENTS (Continued)

-iii-

1. INTRODUCTION

1.1 Objective and Scope

The primary objective of this investigation is to develop design criteria for conventionally reinforced concrete slabs under static uniform load based on the incipient collapse condition. Major emphasis is placed on the deflection capacity associated with incipient collapse. This involves a reexamination of the relevant design criteria contained in NAVFAC P-397, "Structures to Resist the Effects of Accidental Explosions" (1), in the light of experimental and analytical data that have become available since the publication of the manual in 1969.

The investigation has been subdivided into three phases. Under Phase I, a definition of incipient collapse for conventionally reinforced concrete slabs is proposed. Then, based on an evaluation of available analytical and experimental data, recommendations on an appropriate analytical method of estimating this incipient collapse deflection of reinforced concrete slabs under static uniform load is presented.

Phase II of the investigation will mainly involve a parametric study of a number of variables to identify the most significant among these in terms of their effect on incipient collapse. Design criteria that will account for the major design parameters will then be developed and presented in useful format.

Minimum design and construction requirements necessary to develop the tensile membrane behavior at incipient collapse will also be developed.

The work under Phase III will consist mainly in summarizing the work under Phases I and II in the form of a supplement to NAVFAC P-397.

The scope of this investigation is limited to one-way and two-way slabs under uniformly distributed static load near incipient collapse.

Work accomplished during the first phase of the investigation is presented in this report. Of the two major objectives of this report, the first consists of a literature review of experimental and analytical work on reinforced concrete one-way slabs, two-way slabs, and flat slabs with drop panels. Slabs with and without lateral and rotational edge restraints are considered. Particular emphasis is placed on studies considering tensile membrane action. This is followed by a review of current design criteria for estimating the incipient collapse deflection of the reinforced concrete slabs. Based on the review, a method for determining the incipient collapse deflection of conventially reinforced slabs under static uniform loads is recommended.

1.2 Background

NAVFAC P-397 (1) is a government standard for designing structures subject to accidental explosions. Although this standard is simple to apply, it does not take into account the influence of slab geometry, section properties, boundary conditions, material properties, and load distribution on incipient collapse deflection of reinforced concrete slabs. There is a need to re-examine the approach used in the the manual by providing realistic design critera for the incipient collapse deflection of conventionally reinforced concrete slabs. If NAVFAC P-397 is overconservative,then a significant reduction in the cost of protective structures for certain specific uses can be achieved.

The use of yield-line theory (2) for calculating the collapse load of reinforced concrete slabs is prescribed by NAVFAC P-397. Yield-line theory, which considers only flexural action in slabs, gives collapse load values that are theoretically upper bounds, i.e., "on the unsafe side." However, experimental investigations show that the actual maximum load, and in many cases, the collapse load, are usually higher than those calculated using yield-line theory. This enhancement in strength is attributed to membrane action. Several analytical and experimental researches have been reported in the literature. However, design criteria for reinforced concrete slabs near incipient collapse have not been presented.

1.3 Definition of Incipient Collapse

Incipient collapse for conventionally reinforced concrete slabs is defined here as that state of a slab characterized by a drop in the load capacity following mobilization of tensile membrane action. The collapse condition is associated with tensile rupture of the flexural reinforcement. It is assumed that the slab is properly designed to preclude premature bond or shear failure. It is further assumed that concrete is effectively confined within the reinforcing mesh so that no major gaps occur in the slab as a result of concrete fragments falling off.

-2-

2. METHODS OF SLAB ANALYSIS FOR DESIGN PURPOSES

2.1 Elastic vs. Plastic Theory

A slab system may be designed using either elastic or plastic theory. These two theories serve different purposes. According to elastic theory, when a slab is loaded with small loads within the elastic region, stresses are proportional to strains. Plastic theory, on the other hand, considers the behavior of a slab when loaded well into the inelastic range.

An advantage of elastic theory is that it provides information under the action of permissible loads. It may thus be used to calculate deflection and stress distribution under such loads. A slab analysis using elastic theory necessarily involves a study of flexural and torsional moments at several points in a slab. For irregularly shaped slabs, it is often laborious and sometimes impossible to apply effectively.

With the widespread use of electronic computers, the finite element method has become the most important tool for analyzing complex structures. Use of simplified elastic models, however, can only give an approximate description of structural behavior. Results are limited to load levels within the elastic range.

When structural safety is of prime importance, information beyond the elastic limit is essential. Consequently, there has been an increasing interest in understanding the behavior of reinforced concrete in the inelastic range. Inelastic methods of reinforced concrete design have been accepted in several codes.

Plastic theory provides a relatively simple means for calculating the capacity of slabs and for determining design moments that result in a suitable safety factor against failure. It does not give a unique solution, but an infinite number of solutions. For example, it is possible to decrease the amount of reinforcement at one section if a corresponding increase is introduced at another section. These solutions are not equivalent for design purposes, because they lead to differences in deflection, crack width, and construction costs. When plastic theory is accepted in a building code, some restrictions on its applications are required to prevent the selection of unsuitable solutions.

2.2 Slab Design Using Plastic Theory

At present, there are four methods for designing slabs using plastic theory. These are:

1. Yield-Line Theory

2. Lower-Bound Approach
   Strip Theory

3. Upper Bound Method including the effect of membrane action.

2.2.1 <u>Yield-Line Theory</u>. Present knowledge of the yield-line design of reinforced concrete slabs is based on Johansen's work (2), first published in 1943. The theory has proved broadly successful in predicting initial hinging load in reinforced concrete slabs with negligible membrane forces.

Yield-line theory is based on the premise that a certain characteristic pattern of cracks (yield-lines) is formed that leads to failure at ultimate load. Along these yield-lines the plastic moment capacity of the slab cross section is assumed to have been reached thereby transforming the slab into a mechanism. Yield-line theory is based on the pure moment capacity of a slab section in the direction of the reinforcement, and as such uses a principal moment yield criterion. The deformation of the slab takes place due to rotation of slab segments along yield-lines. The portion of the slab between yield-lines is assumed to remain rigid. In addition, all elastic deformations are neglected, as shown in Fig. 1.

In the early 1960's, yield-line theory came to be recognized as being only a part of the more general limit analysis of plates. Solutions obtained from it were known to give an upper bound to the ultimate load. Collapse loads calculated using yield-line theory were then considered essentially as unsafe solutions since the true collapse load was thought to be less than or equal to that calculated from the theory.

2.2.2 <u>Lower-Bound Approach</u>. For a proper estimate of the collapse load, an upper bound solution itself is insufficient and a corresponding lower bound solution should be available. Lower bound solutions are those that satisfy equilibrium and boundary conditions and provide a strictly admissible moment field without violating yield conditions anywhere in the slab. This is essentially a safe solution since the collapse load may be greater than or equal to the calculated value. In addition, lower bound solutions provide valuable information on the required distribution of positive and negative reinforcement (3). A unique solution is obtained when yield-line theory and the lower bound solution provide identical collapse loads. Unfortunately, very few lower bound solutions have been found to agree closely enough with the corresponding upper bound solutions. Those that are available are restricted to relatively simple cases (3,6).

<u>The Strip Method</u>. The strip method, developed by Hillerborg (7), is based on the lower bound approach. Usually a slab is designed to have reinforcement in orthogonal X and Y directions. Hillerborg considered it appropriate to deliberately eliminate the twisting moment, M_{xy}, from the plate equilibrium equation. Thus the total load carried by the slab
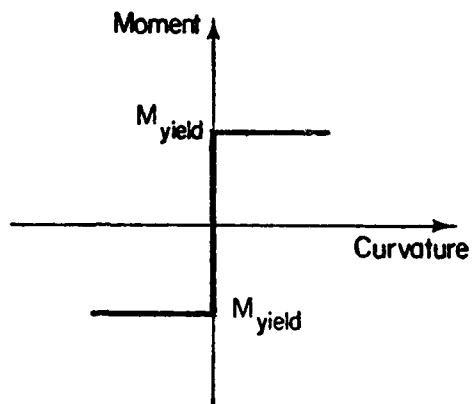
Fig. 1   Moment-Curvature Relationship for Reinforced
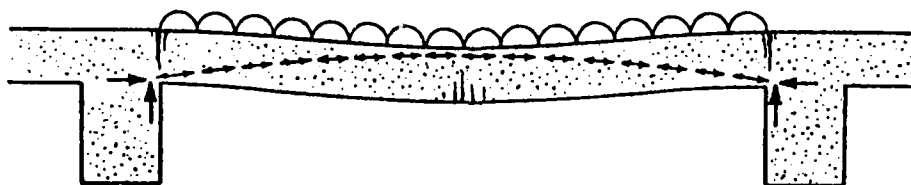Concrete Slab Assumed in Yield-Line Theory

Fig. 2   Arching Action in Restrained Reinforced
Concrete Slabs (from Ref. 13)

is split into two parts. Part of the load is assumed carried by strips in the X-direction and the remainder by strips in the Y-direction. The strip method provides a simple and powerful technique for the design of two-way slabs. It is particularly useful for design of flat plate structures (8,9). The approach is allowed in the Swedish Code (10), but is practically unknown in North America.

Wood and Armer (9) examined Hillerborg's strip method critically and found it a powerful alternative to yield-line theory. Armer (11) tested seven half-scale model slabs designed by the strip method and found the method to be safe and satisfactory.

   2.2.3 <u>Membrane Action in Reinforced Concrete Slabs</u>. As mentioned earlier, both yield-line theory and lower bound solutions are based on the pure moment capacity of the slab cross-section and do not take into account in-plane forces. The presence of in-plane forces results in an increase in the ultimate load to a magnitude beyond that predicted by the yield-line theory.

Efforts to understand and utilize the considerable reserves of strength in reinforced concrete slabs, have steadily intensified since 1955 when Ockleston (12) tested to destruction a slab in a dental hospital building in Johannesburg. It was noted that the interior panel of the underreinforced floor system, which acted as a restrained slab, carried more than double the load predicted by the yield-line theory. In a later paper, Ockleston (13) showed that the unexpected results could not be ascribed to strain hardening of the reinforcement or to the effect of the tensile strength of the concrete. Nor could catenary action due to tensile membrane stresses account for the observed behavior. It was concluded that the large increase in slab capacity was due to the development of in-plane compressive forces, termed "arching" or "dome action".

For underreinforced slabs, a substantial shift occurs in the neutral axis position in the post-cracking range. This creates a tendency for the slab edge to move outwards as slab deflection increases. If the outer edges are restrained against movement, compressive forces are induced in the slab, as shown in Fig. 2. Arching action occurs because the compressive force at the center of slab acts above the slab mid-depth, while along the edges it acts below the slab mid-depth. Due to arching action, the load-carrying capacity of a restrained slab is increased substantially above that predicted by yield-line theory. The beneficial effect of compressive forces on slab yield is the second factor leading to the enhancement of slab capacity (14).

2.3 Load-Deflection Relationship

The load-deflection relationship of uniformly loaded reinforced concrete slabs is significantly influenced by the boundary conditions along the slab edges, as shown in Fig. 3. The dashed
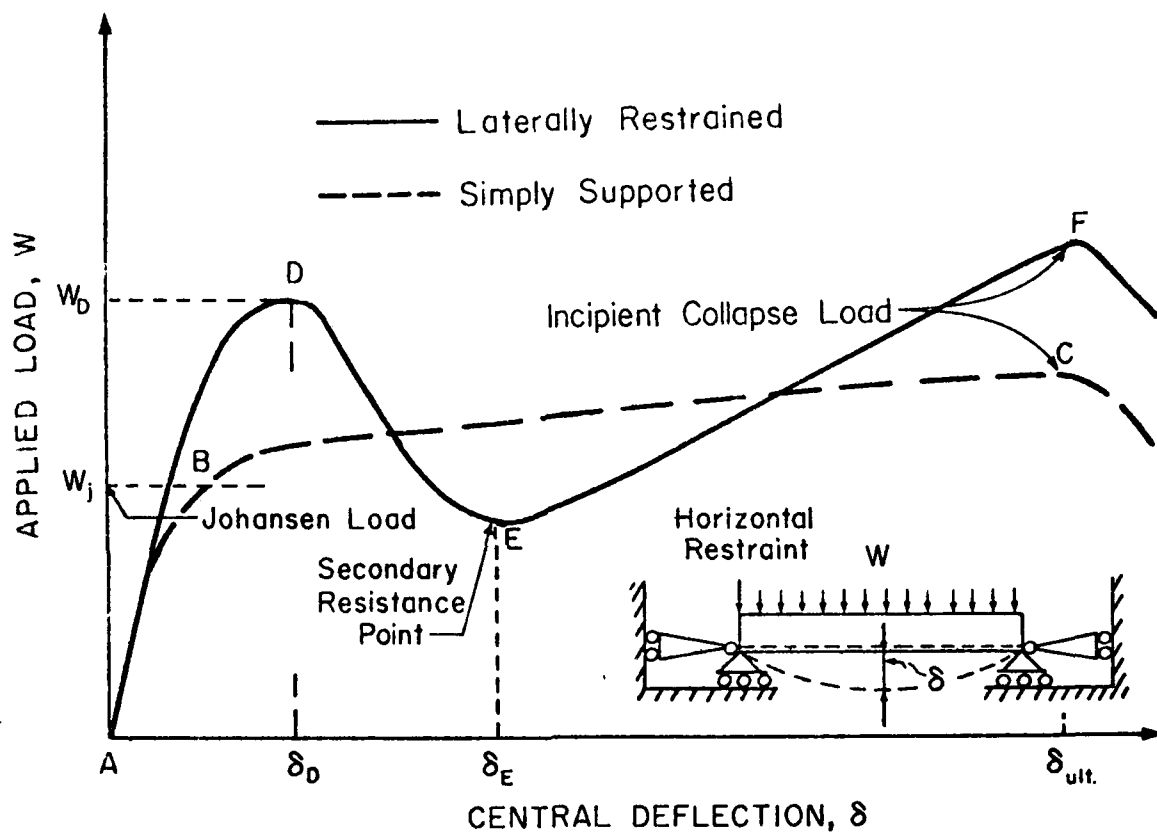
Fig. 3 Load-Deflection Relationship for Two-Way
Reinforced Concrete Slabs

curve in the figure shows that a simply-supported slab deflects elastically and then elasto-plastically as the load is increased from A to B. Near load stage B, a yield-line pattern develops and the slab deflects at a faster rate. Beyond this stage, the slab acts as a tensile membrane until reinforcement ruptures at load stage C.

When the slab edges are restrained against lateral movement, slab capacity is enhanced due to arching (compressive membrane) action, as shown by point D on the solid curve in Fig. 3. Beyond D, the load carried by the slab decreases rapidly because of a reduction in the compressive membrane force. As point E is approached, membrane action in the central region of the slab changes from compressive to tensile. Beyond E, the slab carries load by the reinforcement acting as a plastic tensile membrane with cracking penetrating the slab thickness. The slab continues to carry greater load with increasing deflection until the reinforcement ruptures at F.

In both simply-supported and restrained slabs, rupture of reinforcement precipitates collapse. Alternately, failure of bond between reinforcement and concrete may trigger premature collapse.

3. COMPRESSIVE MEMBRANE ACTION IN TWO-WAY RESTRAINED SLABS

3.1 Review of Previous Investigations

During the last three decades since Ockleston (12) published his test results, extensive research into limit behavior and strength of reinforced concrete slabs has been completed. A number of slabs have been tested. A brief review of these efforts is given below.

3.2 Ockleston's Work

Ockleston (12) conducted two tests on full-scale two-way slabs on the second floor of an existing three-story dental hospital building in Johannesburg. The slabs in both tests were 15'-10½" x 13'-6" in plan and 4-1/2" thick. They were bounded by transverse main beams spaced 16 ft apart, and by secondary beams spaced equally on either side of the longitudinal center-line of the floor, as shown in Fig. 4. Table 1 lists the dimensional and geometric properties of the slabs investigated.

Both slabs were tested under uniform load. In the first test, load was applied to only one of the interior slabs. In the second test, two adjacent slabs were loaded simultaneously. In both tests the slabs behaved in a similar manner.

Results showed that at working load level the slabs behaved elastically. Deflection and steel stresses at these low loads were much less than predicted by the usual design methods. At the maximum resistance level, W_D (corresponding to point D in Fig. 3) the slabs developed yield-line patterns in reasonable agreement with those predicted by Johansen's yield-line theory. However, the loads at which a decrease in loading capacity occurred (W_D) were higher than those calculated using yield-line theory. As shown in Table 1, the ratios of observed to calculated loads were 2.55 and 2.73. Maximum crack width at load W_D was about 0.1 inch, with cracks extending right through the slab thickness. The deflection δ_D was about 2-1/2 inches. This corresponds to an edge rotation of 1.54 degrees.

Ockleston also tested small-scale single-panel slab models and showed that the observed load increased by arching action due to development of compressive membrane forces. Arching action is caused by a substantial shift in the neutral axis accompanying cracking of concrete and yielding of the tensile reinforcement. This creates a tendency for the slab edge to move outwards as slab deflection increases. If the outer edges of the slab are restrained against any movement, compressive forces are induced in the slab, as shown in Fig. 2. As a result, the load-carrying capacity of the slab is substantially increased and a load greater than that predicted by yield-line theory is reached. Another factor contributing to the enhancement of the
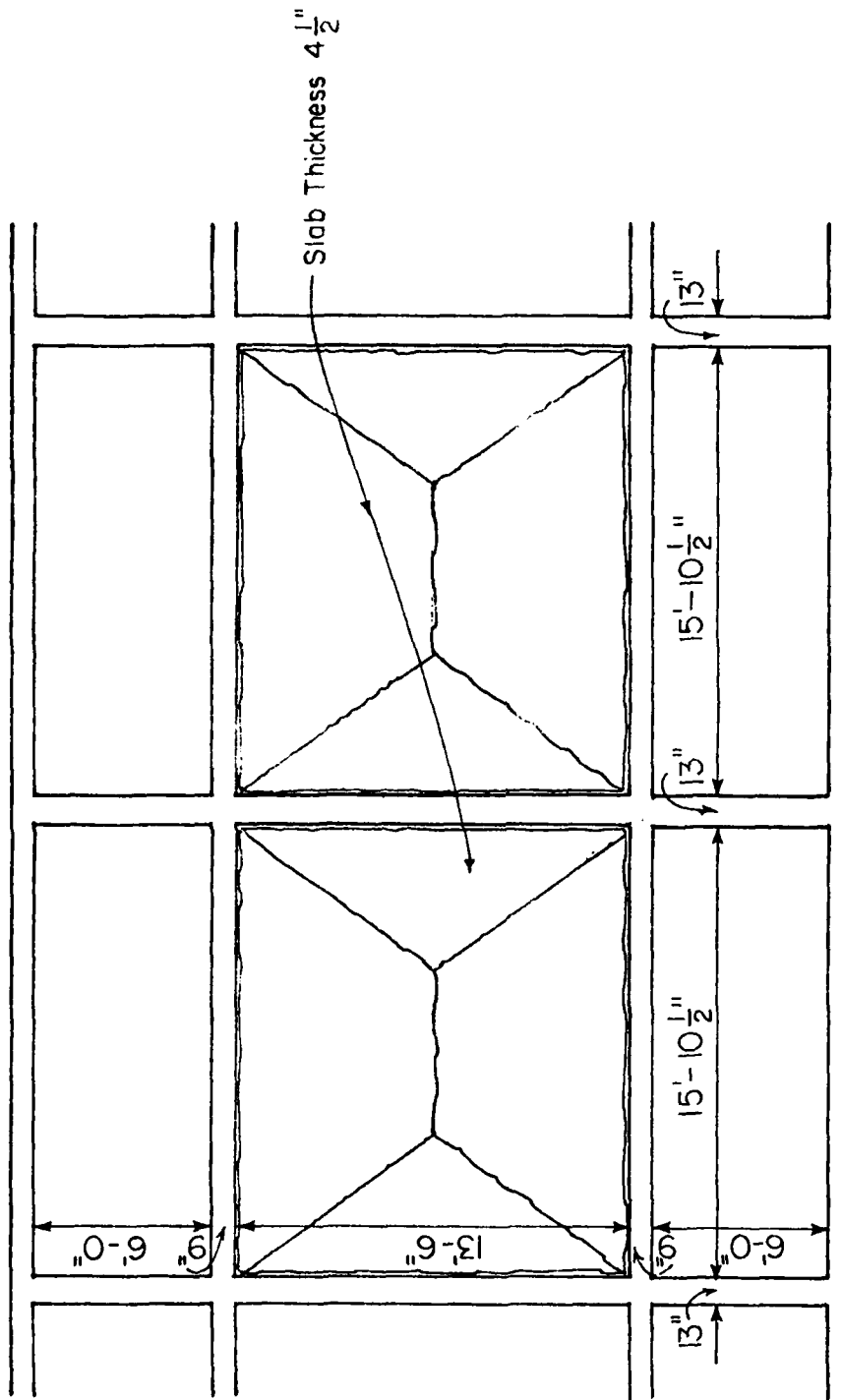
Fig. 4 Plan and Yield Pattern of Ockleston's Test Slabs (from Ref. 12)

loads is the beneficial effect of compressive forces on the moment resistance of the slab cross section.

The effect of arching action is most noticeable in underreinforced slabs in which cracking causes large movement of the neutral axis. Arching can occur only if the deflections are small and the horizontal spreading at the support is restrained. If the deflection becomes sufficiently large, arching action will disappear and may, with further increase in deflection, be replaced by tensile membrane action.

Ockleston's unique test of the continuous floor panels in an existing building is difficult to interpret. First, variable reinforcement in the slabs makes the analysis difficult. Second, the supporting beams deflected considerably under load. Third, partial restraint against spreading along outer edges did not permit development of full membrane action. Also, the incipient collapse deflection level of the slab was not reached during the test.

At about the same time in 1956, Powell (15) tested nine small-scale rectangular isotropic slabs with fully restrained edges. The reinforcement in each slab was varied, as shown in Table 1. Results showed that the peak resistance of a slab, W_D (corresponding to point D in Fig. 3) is significantly influenced by the slab steel ratio. For a slab with a steel ratio of 0.25%, the measured peak resistance, W_D, was 8.2 times higher than that given by yield-line theory.

Powell's test results further confirmed the major role that membrane forces play in enhancing the capacity of a slab. Further, it was shown that the effect of membrane forces on slab strength is greater in the range of lower steel ratios. However, no attempt was made to analyze the results of the experiment.

3.3 Wood's Work

3.3.1 Experimental investigation. Wood (9) tested several single-panel slabs under 16-point loading. Among these, five tests are of special interest when examining the nature of membrane action in slabs. As Table 1 shows, slab Specimens FS12 and FS13 were fully clamped along all four edges. Specimens G5 and G6 were supported on four encased steel beams, and Specimen L2 had two opposite edges free and the other two simply supported. Specimen L2 acted essentially as a one-way slab.

The first slab, Specimen FS12, showed no sign of cracking at the Johansen load, W_j. Deflections were very small, and due to compressive membrane action, the slab carried a load of nearly three times W_j with just a tiny diagonal crack appearing on the tension side. Except for this crack, the slab at this stage showed no sign of distress, as indicated in Fig. 5.

Fig. 5 Clamped and Horizontally-Restrained Square Slab, FS12, with Only Bottom Reinforcement (0.25 per cent). State of the Slab at Nearly Three Times the Johansen Load W_j. - Wood (from Ref. 4)

At a load over five times W_j, cracks near the center were observed. At this load, the deflection was only 10% of the slab thickness. As the load increased to 10.9 times W_j, the center deflection increased to about half the slab depth, with *no signs of punching shear around the edges.* This was followed first by a rapid increase of deflections and then sudden collapse, as shown in Fig. 6. The associated yield-line pattern, shown in Fig. 7, indicates distinct cracking along the diagonals and around the periphery of the slab. This yield-line pattern verifies Johansen's hypothesis that the energy in a slab near the limit of flexural capacity is concentrated in the bands of cracking along the diagonals and periphery of the slab.

On reloading, a central tensile membrane developed, accompanied by increasing diagonal crushing and cracks extending through the slab thickness. Unlike compressive membrane action, tensile membrane action is stable. Both moment and stretch redistributions occurred, but because of the favorable change in geometry, the deflections remained controllable. The test was terminated when the deflection was about 6 in., corresponding to a load of 3.6 times W_j. The load versus deflection relationship is shown in Fig. 6.

The second slab, Specimen FS13, had both top and bottom steel but with a reduced concrete strength. Behavior of this specimen was similar to that of FS12, but the incipient collapse load of FS13 was 4.38 times W_j.

After evaluating the above tests and others, Wood concluded that, for a clamped slab, the important feature is not the negative support reinforcement but rather the restraint against lateral expansion. In a clamped slab, a peripheral compression develops and induces "self-prestress" in the slab, thereby reducing cracking and deflection. As a result, yield moment and the corresponding peak load increases. Wood argued that arching action is not a good enough description for compressive membrane action. Rather, it is the favorable increase in moment resistance due to compressive forces in the slab that enhances the slab capacity.

   3.3.2 <u>Analytical Investigation</u>. Wood (4) presented methods to determine the strength of circular, clamped slabs, using a yield criterion including both bending and membrane stresses. He also noted that yield criteria for circular slabs are also applicable to clamped square slabs. This led to his proposing the following simplified equations for determining the collapse load of a clamped, square slab:

$$W_D = W_j \left(1 + 0.6 \frac{\delta_D}{h}\right) \qquad \text{Eq. (1)}$$

The above equation applies to reinforced slabs where the amount of steel is light, i.e. with a steel percentage $p = 0.0020$.

-13-
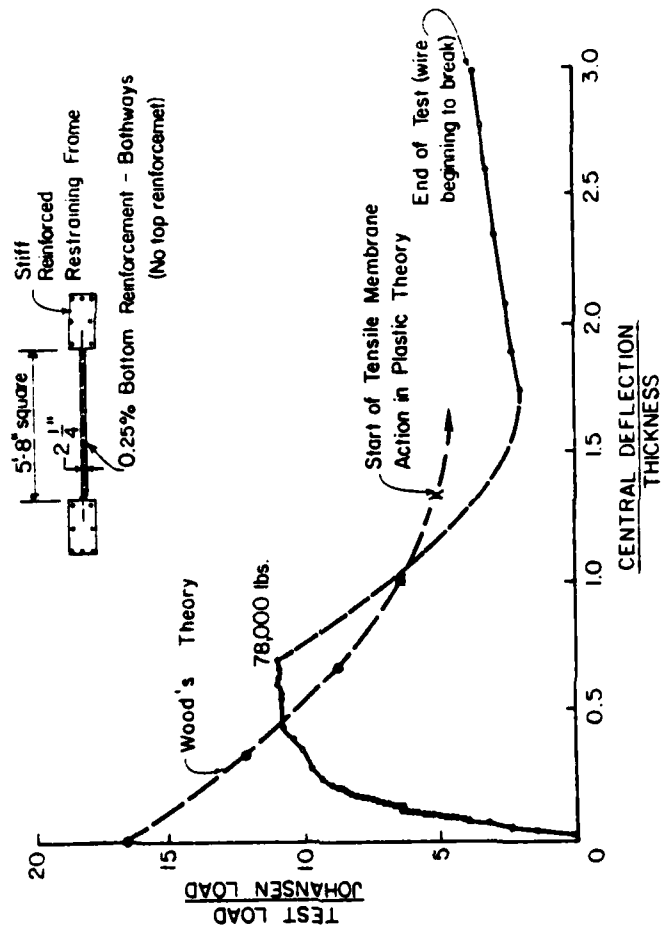
Fig. 6 Collapse of Square Reinforced Concrete Slab, FS12, with
Restraint Against Horizontal Expansion - Wood
(from Ref. 4)
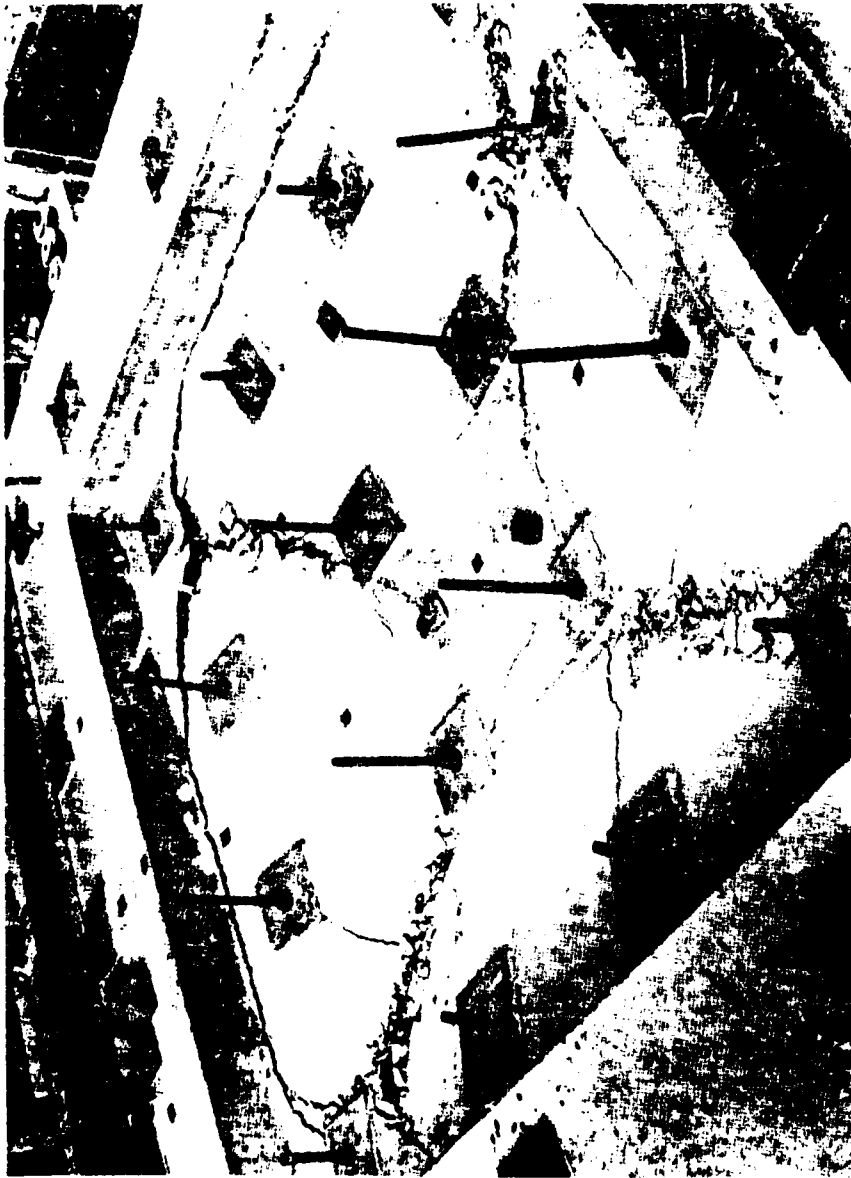
Fig. 7 The Same Slab as in Fig. 5 After Sudden Loss of Flexural and Compressive Membrane Capacity at 78,000 lb. (= 10.9 W$_j$, approx.) Note the absence of top reinforcement; also unusually heavy crushing on diagonals indicating strong cirucumferential compression. This photograph shows the development of a central tensile membrane zone on reloading. (from Ref. 4)

For heavily reinforced slabs with p = 0.0080, the equation becomes:

$$W_D = W_j \left(1 + 0.3 \frac{\delta_D}{h}\right) .$$

Eq. (2)

In these equations,

W_D = peak strength of the slab (corresponding to point D in Fig. 3)

W_j = Johansen's yield-line load

δ_D = deflection corresponding the point D in Fig. 3

h = slab thickness

Wood's design rule incorporates the observation that slab load enhancement increases as the percentage of slab reinforcement is reduced. Equations 1 and 2 require that a reasonable value be used for δ_D/h. When δ_D/h is limited to 0.5, then only a 15% increase is allowed when p = 0.0080.

The extreme conservatism in Eqs. 1 and 2 was justified by Wood as follows:

1. Compressive membrane action reduces deflection and cracking in a slab. This reduces incipient collapse warning. Because of the change in behavior near collapse from a "slow" to a sudden condition, the load factor should be raised.

2. Creep buckling is possible.

3. The subject is still in its infancy and much more research is needed.

4. A recommended load factor of 4 or 5 is intended not so much to guard against instability as to allow for the fact that the plastic theories are not on firm ground when concrete crushing is expected.

   3.3.3 Load-Deflection Relationship. Wood (4) was the first to analyze reinforced concrete slabs for compressive membrane action. He used large-deflection plate theory and assumed the material to be rigid-plastic. Due to the assumption that material behaves in a rigid-plastic manner, a rather surprising load-deflection relationship was obtained. As shown in Fig. 6, the maximum calculated load for clamped Slab FS12 occurs at zero deflection. In reality an appreciable deflection occurred before sufficient compressive forces were induced to increase the slab capacity beyond the Johansen load.

If compressive membrane action is to be utilized in the design of slab-beam floors, lateral restraint at the edges of each panel must be provided by the surrounding beams and panels. Lateral stiffness available has to be examined very closely because the development of membrane action is dependent on the restriction of very small horizontal translations. Furthermore, large horizontal forces are involved. Wood (16) showed that support stiffness, air gaps and prestressing significantly affect slab behavior. As shown in Fig. 8, slab failure can occur with little increase of load above that of a simple slab when a restraint of relatively low stiffness is provided. A very stiff surround might cause an enormous increase in load above Johansen's load and a corresponding decrease in slab deflection. An air gap showed an initial Johansen-type failure followed by recovery and delayed snap-through failure. Prestressing might increase the slab strength, but too much prestressing could destroy the arching action.

3.4 Sawczuk's Work

Sawczuk (17,18) applied the theory of plasticity to the analysis of compressive membrane action in reinforced concrete slabs. The slabs were restrained against lateral movement, but unclamped against rotation at the edges. Assuming that the energy of a slab near failure is concentrated in yield lines, and that the energy in the yield lines is a combination of bending and membrane stresses, Sawczuk put in mathematical form the energy equation for a slab, as follows:

$$\int_A pwdA = \sum_{i=1}^{n} (ML_i \dot{\theta}_i + NL_i \dot{\lambda}_i) \qquad \text{Eq. (3)}$$

where

p = intensity of uniformly distributed loads

w = rate of deflection

N = membrane stress

M = bending moment

$\dot{\theta}$ = rate of rotation at yield-line

L_i = yield-line length

n = number of yield lines

$\dot{\lambda}$ = rate of horizontal extension at yield lines

dA = element of slab area, A.

Equation 3 states that total energy due to plastic motion is equal to the sum of bending and membrane energy dissipated in
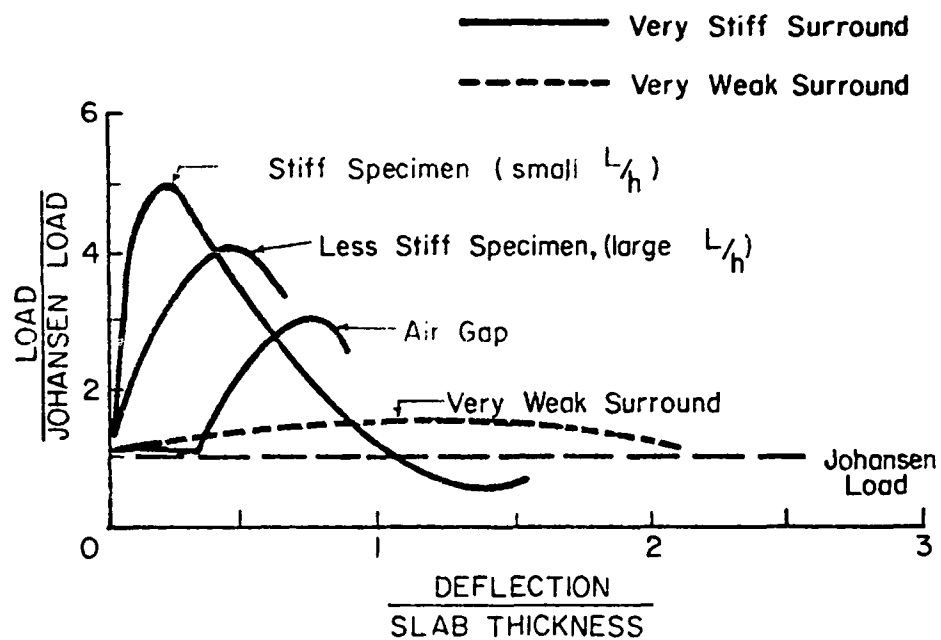
Fig. 8 Effect of Stiffness on Specimen and
Surround - Wood (from Ref. 16)

the yield lines. Using this energy approach, Sawczuk gave a load-deflection relationship:

$$W = \frac{W_J}{\mu(1 - \mu)} \left\{ 1 - 2\delta_D(1 - \mu)\left[\frac{(\eta - 2)(3 - 2) - \eta}{3 - \eta}\right] + \right.$$

$$\left. \delta_D^2\left[\frac{\eta + (3 - 2\eta)^2}{3 - \eta}\right]\right\}$$ Eq. (4)

where W_J = Johansen's yield-line load

   $\mu = A_s f_y / f_c' d$

   δ_D = deflection corresponding to peak load

   $\eta = \frac{1}{\alpha^2}\left(\sqrt{3\alpha^2 + 1} \; -1\right)$

   $\alpha = a/b$, ratio of slab sides.

Due to the tedious calculations involved, this method received little acceptance in slab design. However, the analysis is highly significant due to the innovative approach used in determining the collapse load of slabs including membrane effects. Hung and Nawy (19) extended this method to slabs with different boundary conditions. This is discussed later in the text.

3.5 Park's Work

One of the most notable contributions to the understanding of membrane action in reinforced concrete slabs is due to Park (20-23). Park conducted extensive tests on reinforced concrete slabs and attempted to analyze two-way rectangular slabs for compressive membrane action.

   3.5.1 Experimental investigation. The geometric and material properties of four single panel reinforced concrete rectangular slabs tested by Park under uniformly distributed load are given in Table 1. The test frame used is shown in Fig. 9a. The slabs, which were to be fully fixed against rotation and translation, were clamped to the frame as shown in Fig. 9b. Hold-down studs prevented rotation and horizontal screws bearing against steel plates at the slab edges prevented horizontal spread.

Uniformly distributed loading was applied upwards using a rubber bag placed underneath the slab and filled with water at the required pressure. The pressure was measured using a Bourdon pressure gauge. Load-deflection curves for all four specimens are shown in Figs. 10a and 10b. Examples of slab yield-line patterns after testing are shown in Figs. 11 and 12.

The test results confirmed the observation of earlier investigators that for restrained slabs the peak strength under mono-

-19-

(a)

40"

60"

(b)

Steel Bearing Plate

1"Dia. Steel Studs
@ 6" centres

12"x4" Channel

Slab

Rubber

Water

1" Dia. Horizontal
Screws @ 6" centres

Fig. 9 Steel Test Frame and Edge Support Details
- Park (from Ref. 20)

Fig. 10 Load-versus-Central Deflection Curves for Slabs
with All Edges Restrained - Park (from Ref. 22)
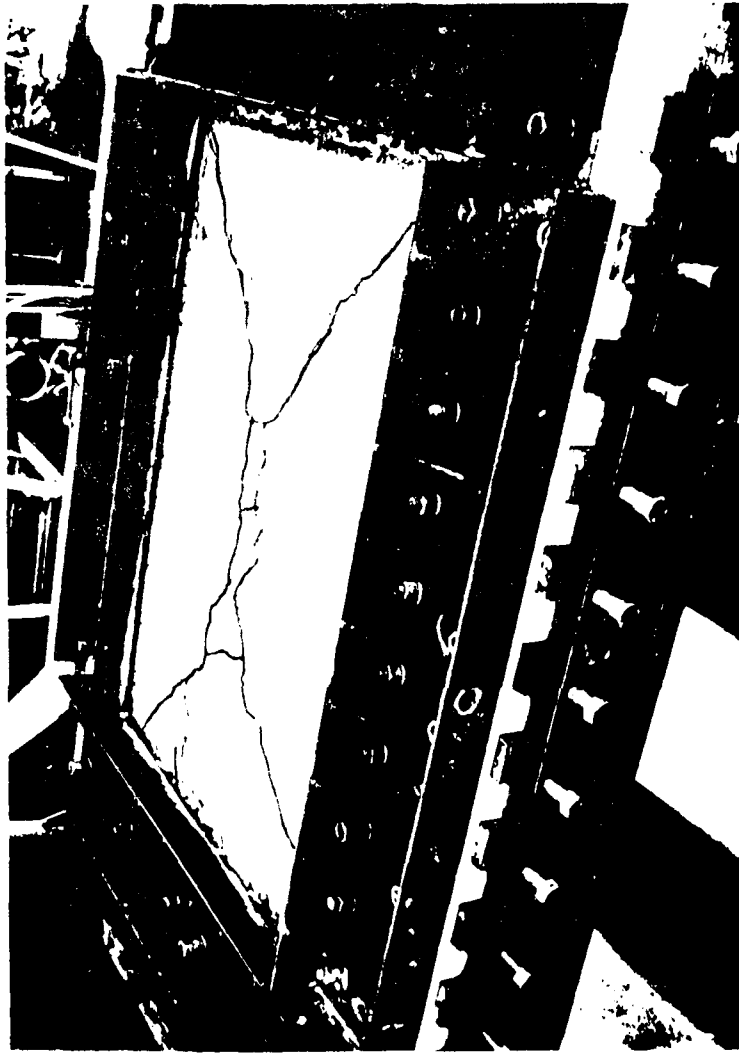
Fig. 11 Yield-Line Pattern and Surround of Uniformly Loaded Slab with Restraint Along All Edges - Park (from Ref. 22)
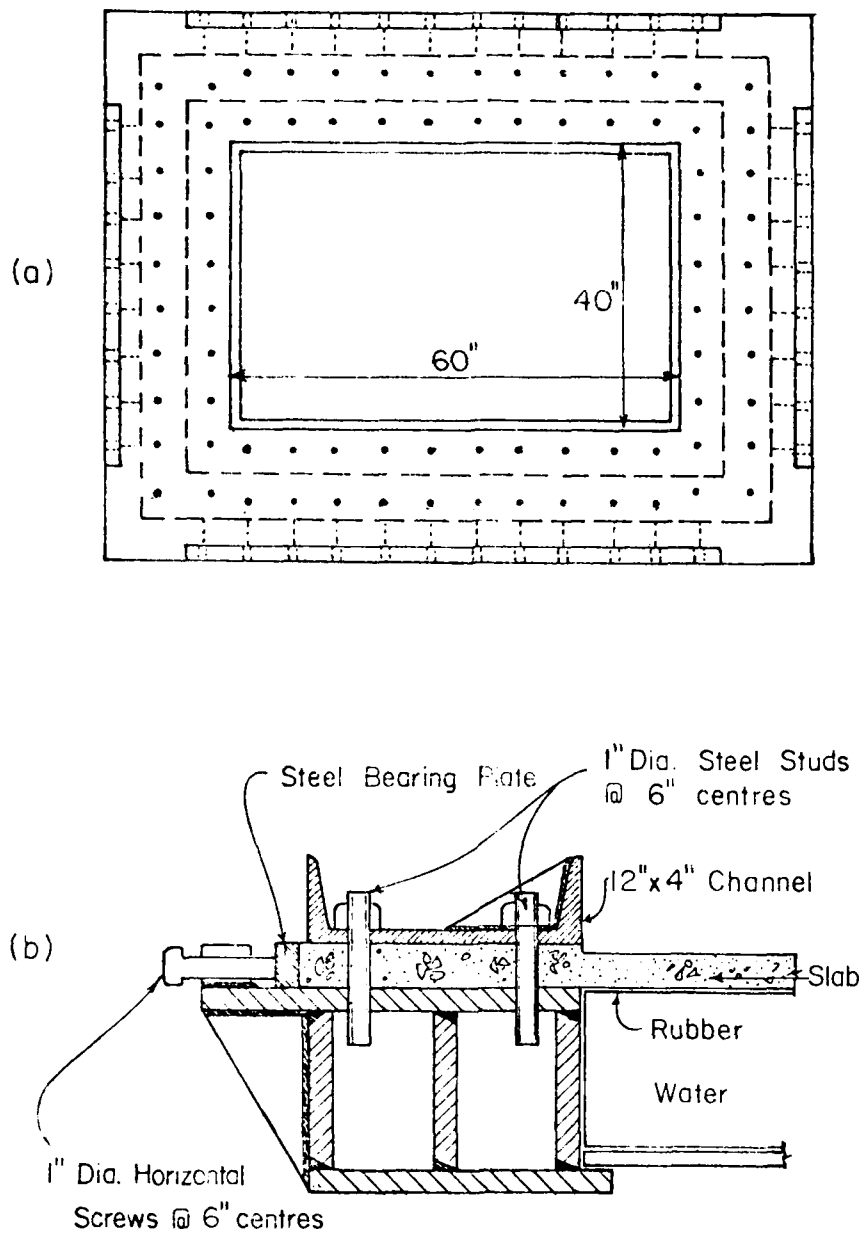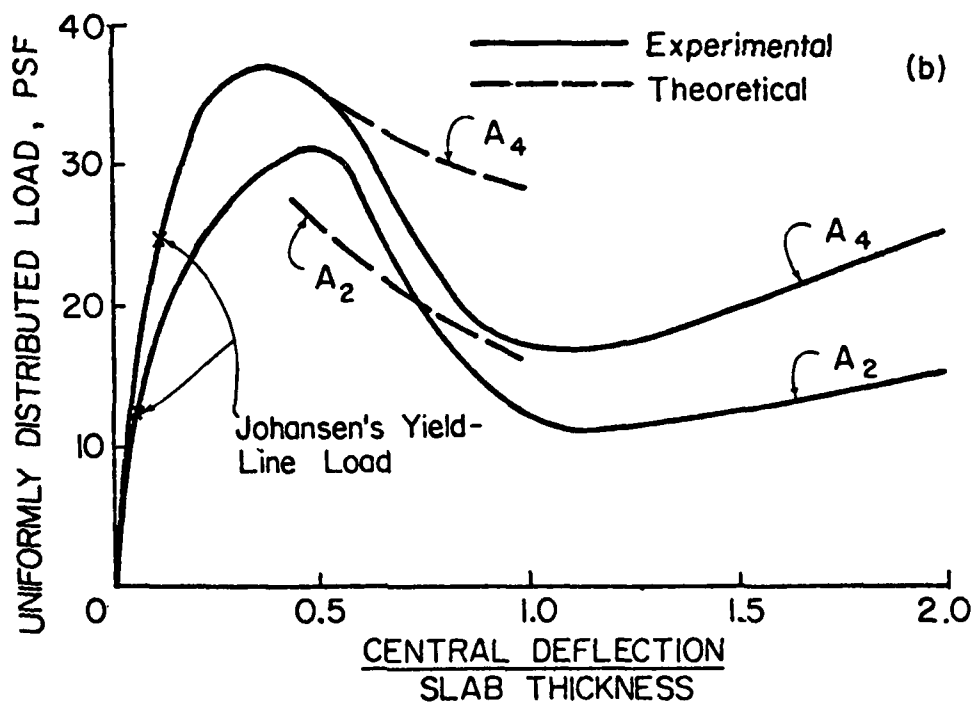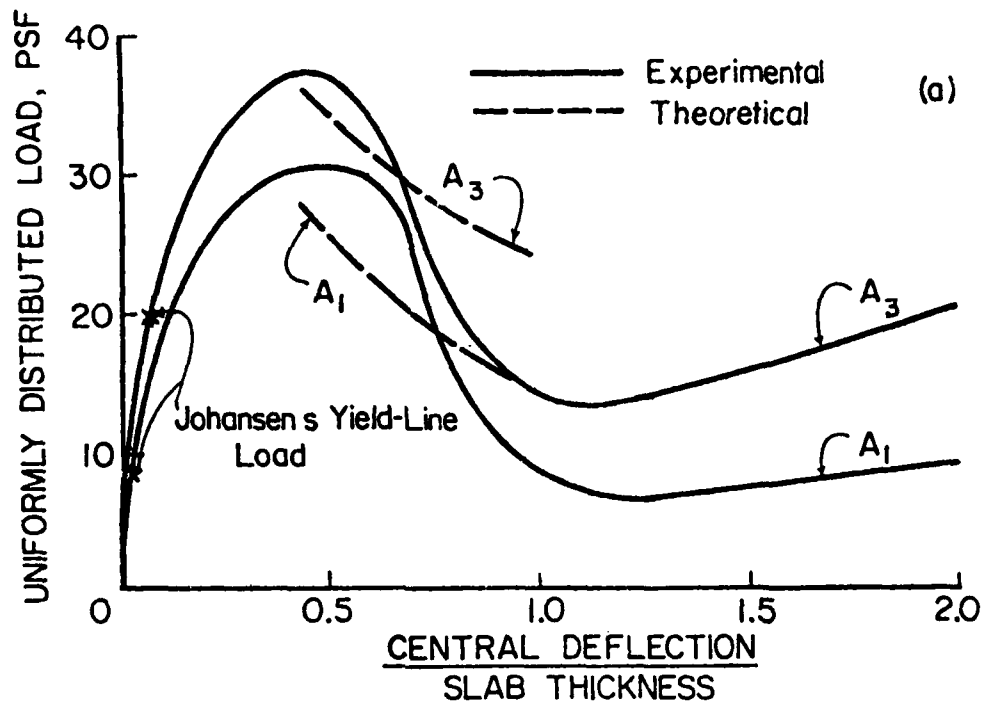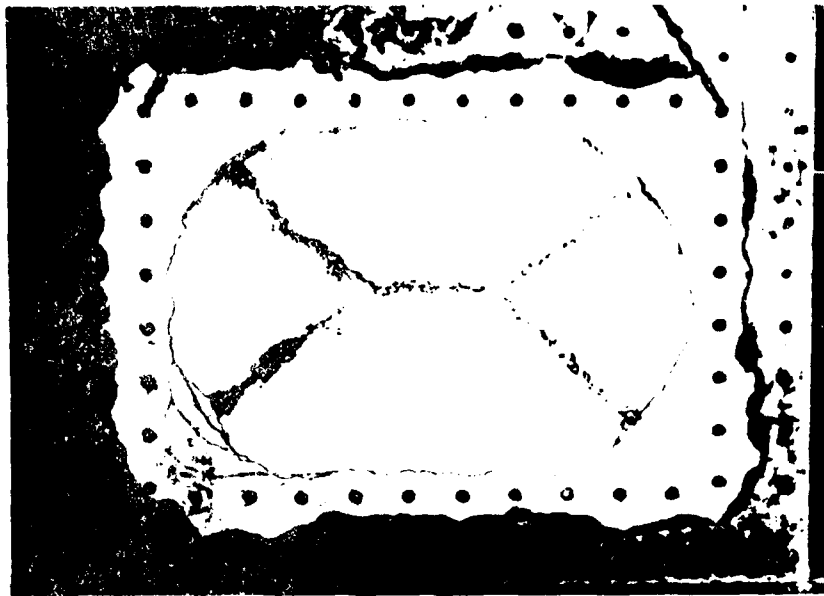
(a) Loaded Face
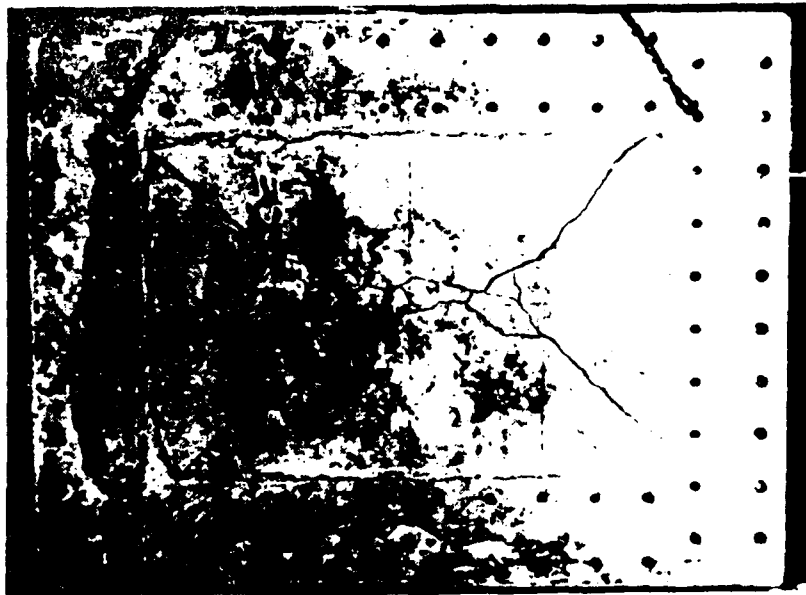
(b) Unloaded Face

Fig. 12   Yield Lines of a Restraining Slab at
Failure - Park (from Ref. 22)

-23-

tonic loading is considerably greater than the Johansen load. It was noted that the maximum slab deflection is never greater than 1/500 of the short span for loads within one-third of the measured slab capacity. Slab cracking did not become visible until at least 32% of the measured loading capacity, W_D, was attained for partially-hinged slabs and 42% for fully-clamped slabs.

On the basis of his own tests and those of others, Park made the following observations:

1. The load calculated for a central deflection equal to one-half the slab thickness can be taken as the maximum resistance of the slab, W_D.

2. Percentage of reinforcement plays an important role in the enhancement of strength beyond the yield-line load. Maximum enhancement of slab strength over that given by yield-line theory was obtained for the lowest percentage of steel. This was true for all support conditions.

3.5.2 <u>Analysis of Compressive Membrane Action</u>. In 1964, Park (20) presented an analysis of fully-restrained two-way rectangular slabs for compressive membrane action in the range DE of Fig. 3. He approximated the two-way slab by strips running along the short and long directions as shown in Fig. 13. Using rigid-plastic approximation, the extra compression at yield sections was obtained from the geometry and equilibrium of rigid strips as shown in Fig. 14. It was assumed that the sum of elastic, creep, and shrinkage axial strain was zero. A comparison of Park's theory and experimental work is shown in Figs. 10a and 10b.

Park's theory is quite simple and straightforward. The theoretical curve is similar to the region DE of the curve shown in Fig. 3. However, it does not correspond to the complete load-deflection curve (ADEF of Fig. 3) of a real two-way slab. In addition, an assumed value for deflection δ_D, such as 0.5 times the slab thickness, is necessary to estimate the slab strength, W_D. This assumption, based on limited test data, may not be applicable in all cases.

On the other hand, Park (24) argues that the assumption is conservative and that great precision in determining the deflection δ_D is unnecessary. Iwankiw and Longinow (25) compared results obtained by Park's method with those using a nonlinear finite element computer program. They concluded that Park's method is quite satisfactory. A special advantage is its relative simplicity. Recently, Park (24) extended his method to include effects of both lateral movements and slab axial strains. He derived coefficients for computing the reduction in compressive membrane action due to these effects.

-24-
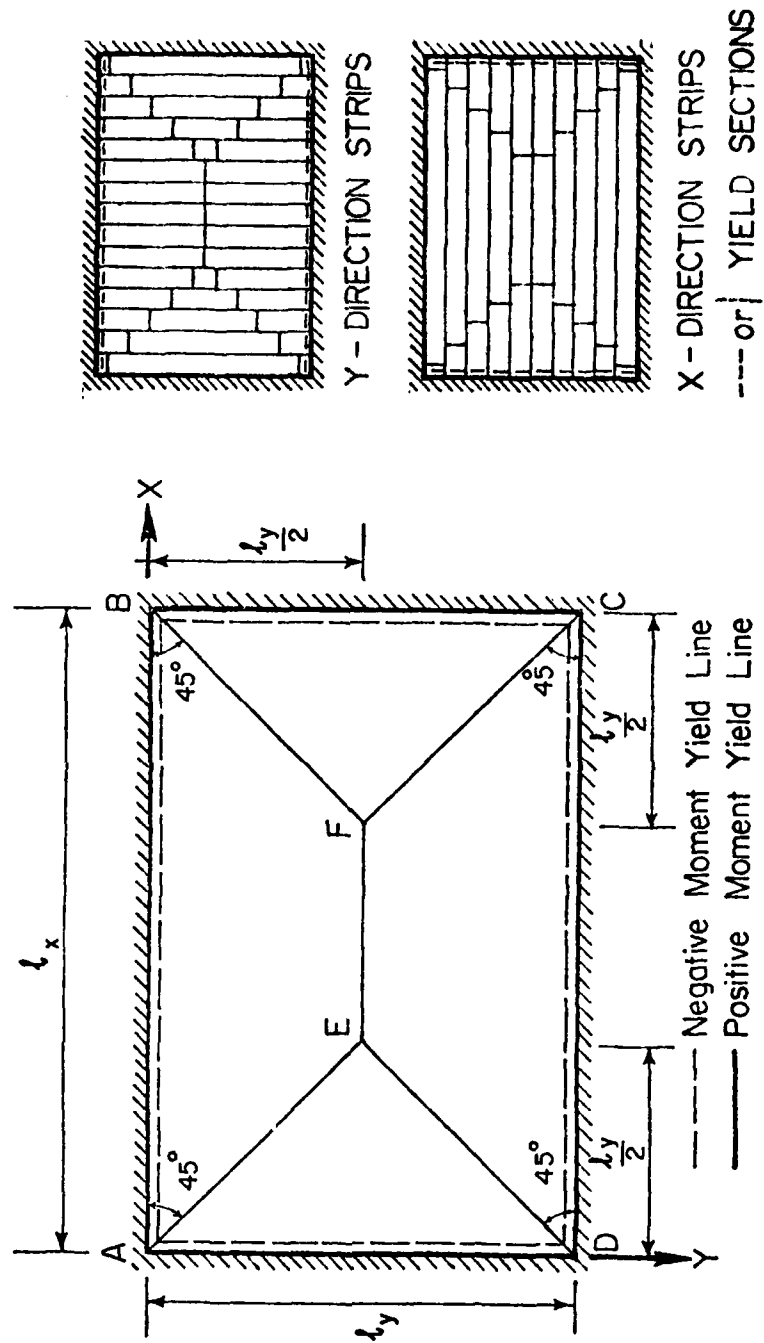
Fig. 13   Assumed Yield-Line Pattern for Uniformly Loaded Slab with Restrained
Edges - Park (from Ref. 20)
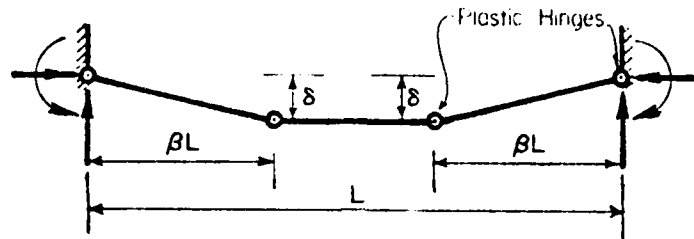
Fig. 14 Mechanism of Restrained Strip
(from Ref. 20)
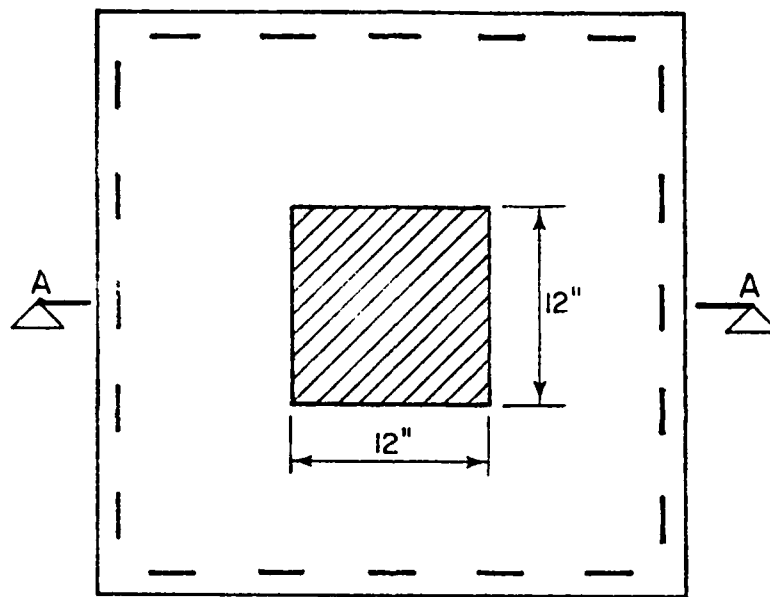
////// Loaded Area (Interior panel)
— — $\frac{1}{2}$" Diameter Roller Supports
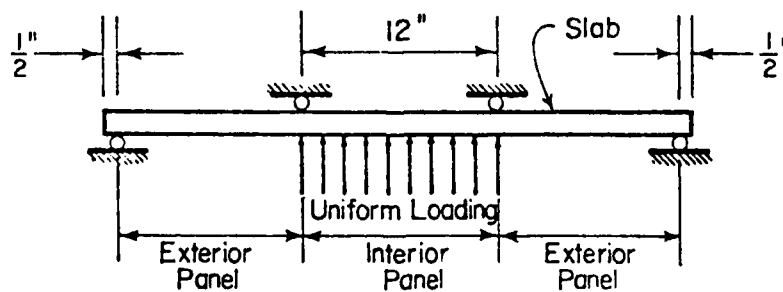
Fig. 15 Details of Loading and Supports of
Slabs Tested by Park (from Ref. 22)

-26-

Park (22) also investigated the degree of restraint stiffness required at the periphery of an individual panel of a multi-panel slab-beam system (Fig. 15) to ensure full enhancement in load-carrying capacity due to compressive membrane action. The following conclusions were drawn from the tests:

1. The surrounding panels should be almost square, for development of full membrane action.

2. Tie reinforcement continuous around the edges of the interior panel and around the outside edges of the floor, as shown in Fig. 16, is essential to develop compressive membrane action.

3. Stretching of the tie reinforcement results in outward displacement of the panel edges. This should be included in calculating the collapse load.

4. To mobilize compressive membrane action in a slab-and-beam floor system requires more steel as ties in the beams than that saved in the panels.

3.6 Hopkins and Park's Work

Hopkins and Park (27) tested a 1/4-scale, nine-panel reinforced concrete slab-beam floor system. This is shown in Fig. 17. The system was designed on the basis of equations developed by Park (22) for estimating the peak resistance of slab, W_D. The design load-carrying capacity was 800 psf. The design required an enhancement factor (W_D/W_j) of 2.00 for the interior panel, 1.35 for the center edge panels and 1.00 for the corner panels. The panels were lightly reinforced, the top and bottom steel of all panels being 0.16% and 0.15% of the gross concrete area, respectively. Steel had a yield strength of 52 ksi.

From the known steel quantities in the panels and the required slab strength, the maximum allowable lateral movements at the panel edges were estimated and the maximum compressive membrane forces in the panel were calculated. These membrane forces were then considered as uniformly distributed in-plane forces acting outward on the surrounding beams and panels. The beams were designed for the required strength for bending due to gravity loads and for tension due to membrane forces. Lateral deformations of the floor due to axial stretch of the beams under tension as well as bending and shear deformations of the edge panels under membrane forces were estimated. Beam sizes and reinforcement were then adjusted iteratively until the outward movement of the panel boundaries was approximately equal to the maximum allowed.

The floor behaved well both at service load and at the peak load levels. The load-versus-central deflection relationship

-27-

34 in. Square

Interior Panel

14 in. Square
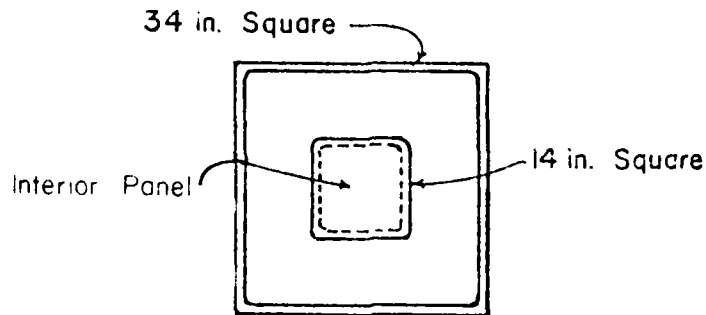
Fig. 16 Position of Two Ring Bars Essential
to Develop Compressive Membrane
Action in Interior Panel - Park
(from Ref. 22)

All Panels $1\frac{13}{16}$" Thick

Corner A Panel

B

A

Corner Edge Panel

Centre Panel

All Beams $3\frac{1}{2}$" wide

4'-0"

5'-6"

4'-0"

13'-9½"

4'-0"

5'-6"

4'-0"

Beam Centres
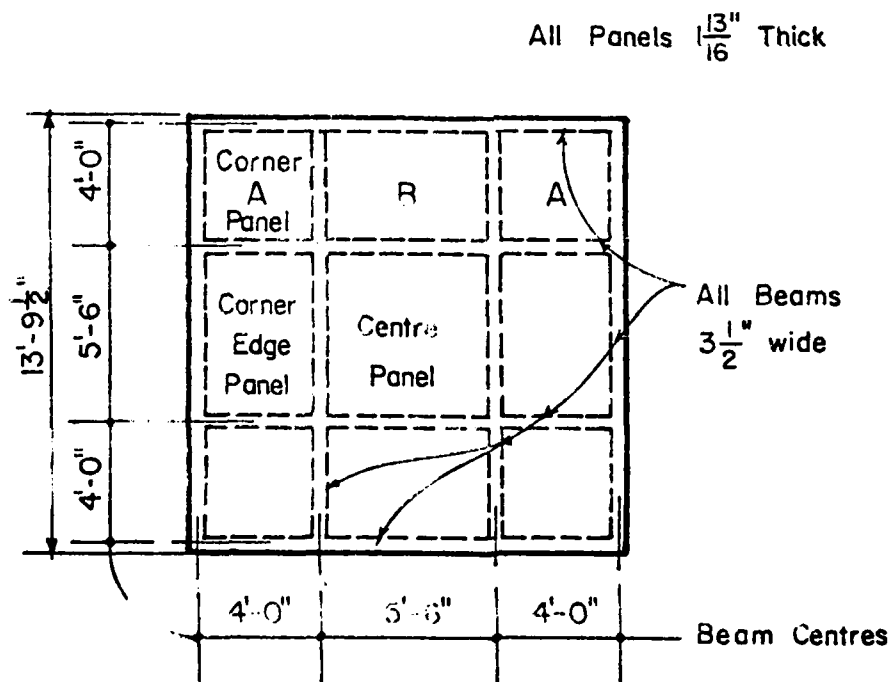
Fig. 17 A 1/4-Scale Beam-Slab System - Hopkins
and Park (from Ref. 27)
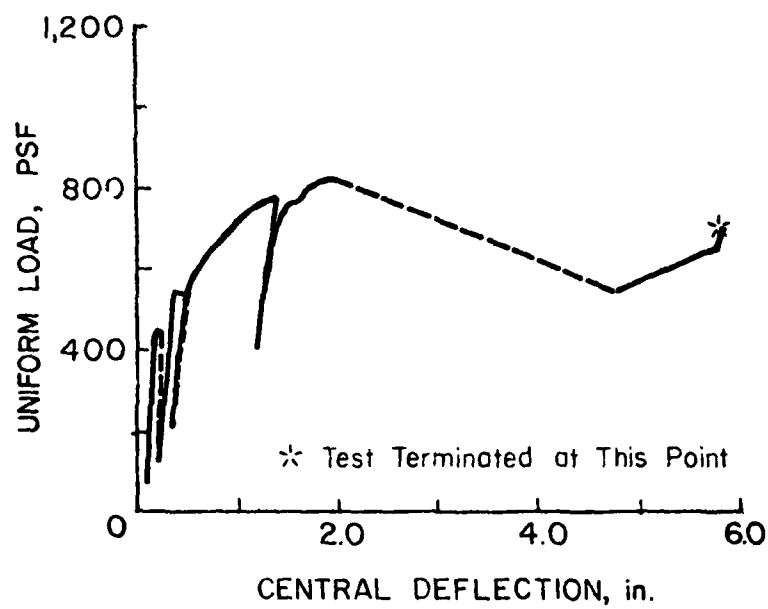
Fig. 18 Measured Load-Central Deflection Relationship
for Interior Panel of Nine-Panel Slab-Beam
System - Hopkins and Park (from Ref. 27

for the interior panel, shown in Fig. 13, indicates a peak load of 850 psf. The associated central deflection was almost equal to the panel thickness. Figure 19 shows top and bottom views of the floor after the test. The following conclusions were drawn from the test results:

1.   Designing to take advantage of the enhancement in load capacity due to compressive membrane action is possible provided an adequate safety margin is incorporated in the design procedure.

2.   Lack of information concerning the long-term behavior of the slab may limit the applicability of compressive membrane action in design.

3.7 Morley's Work

The conventional yield-line theory of two-way reinforced concrete slabs was extended by Morley (28) to allow for membrane action and moderately large deflections. In this approach, compressive membrane forces are calculated from a consideration of displacement rates in the assumed collapse mechanism and the in-plane equilibrium of compressive membrane forces. The load-deflection relationship is established by the principle of virtual work. This method is also based on the rigid-plastic approach and gives a load-deflection relation similar to that given by Wood (4) and Park (20). An empirical value for the deflection corresponding to the maximum load, δ_D, is necessary to estimate the collapse load. With an assumed value of deflection, δ_D, equal to 0.5 times the slab thickness, the results compared very well with those of Park (20). This theory is limited to isotropic slabs. Secondary effects like lateral movement or elastic shortening cannot be included easily.

3.8 Work at Rutgers University (Nawy and Associates)

Over 100 two-way slab specimens were tested by Nawy and his associates (18,29-31) at Rutgers University. The objective of these investigations was to gain better understanding of slabs with different boundary conditions and reinforcement ratios.

Of special interest are the twelve isotropic, fully restrained slab specimens tested under uniformly distributed load by Hung and Nawy (19). Geometric and material properties of these specimens are listed in Table 1. The loading system is shown in Fig. 20.

During early load stages, the deflected shape of the slab was that of a parabola. As the load increased, the center deflection increased more rapidly than elsewhere, and the deflected shape of the slab became more marked. All tests were terminated once a reduction in slab capacity was observed. The load-deflection relationship beyond this stage was not recorded. The

-30-
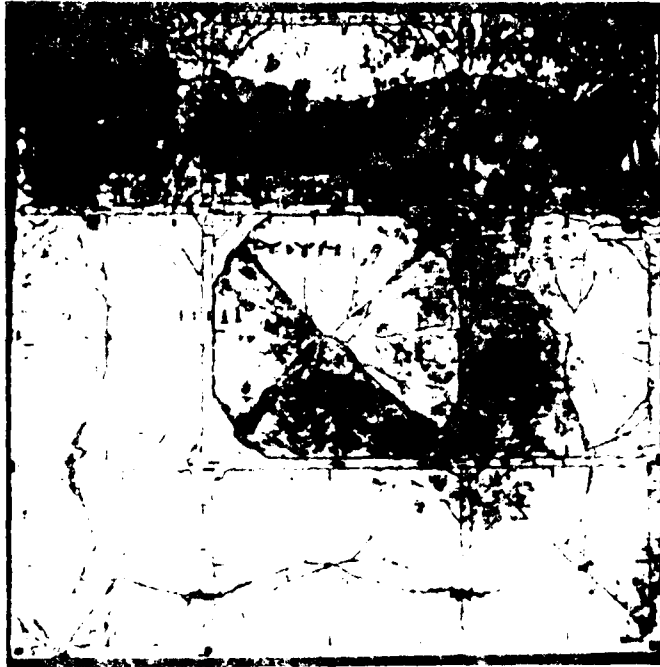
(a) Loaded Surface

(b) Unloaded Surface

Fig. 19 Slab and Beam Floor After Test - Hopkins
and Park (from Ref. 27)

-31-
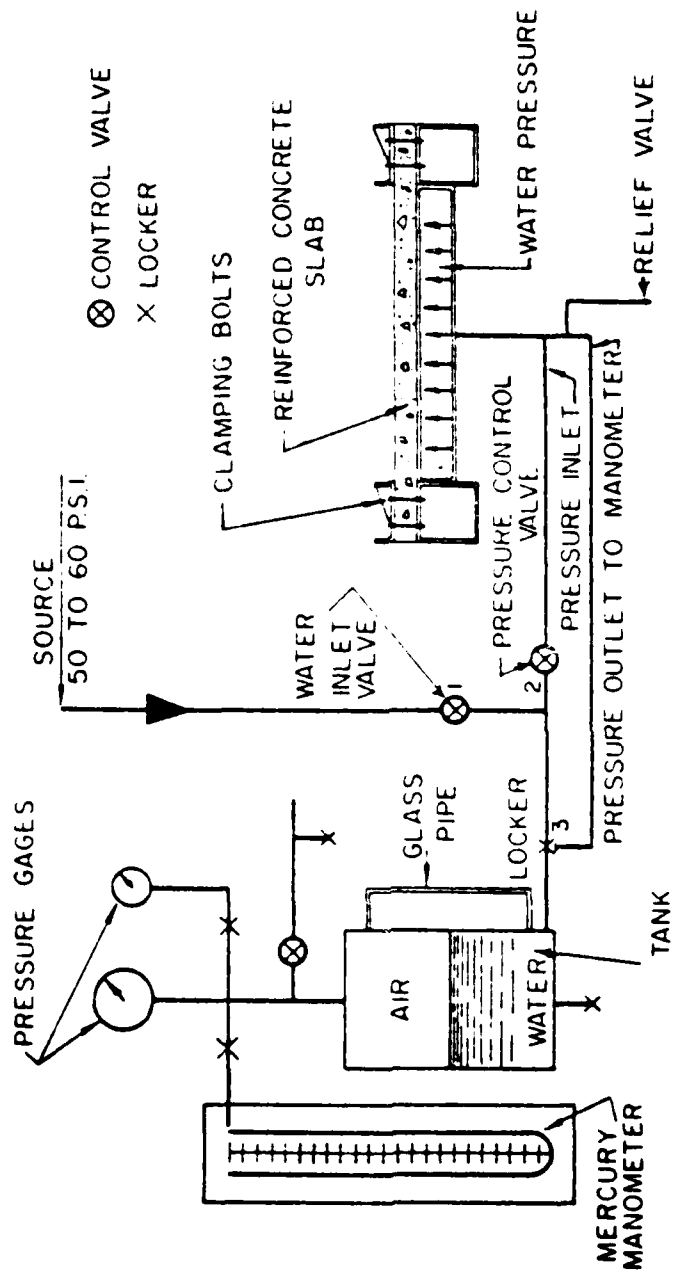
Fig. 20 Loading System Used in Rutgers University Tests   (from Ref. 19)

yield-line mechanism, shown in Figs. 21a through 21c, followed Johansen's yield lines. Load-deflection curves of the test slabs are shown in Fig. 22. In general, all curves have similar characteristics. The curves show that the value of deflection associated with the peak resistance, δ_D, is not constant at 0.5 times slab thickness as assumed by Park (20) but varies between 0.6 to 1.0 times the slab thickness. Park attributes this difference to the effect of restraint stiffness (21). A comparison of measured peak loads with those predicted by Johansen's yield-line theory is listed in Table 1. This indicates that the mean experimental load is 1.80 times that predicted by Johansen's yield-line theory.

Hung and Nawy (19) extended Sawczuk's (17) energy approach for computing the load-carrying capacity of restrained slabs. By idealizing the slab as shown in Fig. 23, the equation for the peak load of isotropically reinforced concrete slabs restrained on all four edges is obtained as follows:

$$W_D = \frac{1}{L_y^2} \left[C_1 M_1 + C_2 M_2 \left(\frac{\delta_D}{h} \right) + C_3 M_3 \left(\frac{\delta_D}{h} \right)^2 \right] \qquad \text{Eq. (5)}$$

where

$$C_1 = 48 \left[\frac{m}{3 - m(\lambda_1 + \lambda_2)} \right] \left\{ 1 + \frac{1}{8} \frac{1 - m(\lambda_1 + \lambda_2)}{\lambda_3(1 - \lambda_3)m} \right\}$$

$$C_2 = 48 \left[\frac{m}{3 - m(\lambda_1 + \lambda_2)} \right] \left\{ \frac{1}{2} + \frac{1}{8} \frac{1 - m(\lambda_1 + \lambda_2)}{\lambda_3(1 - \lambda_3)m} \right\}$$

$$C_3 = 48 \left[\frac{m}{3 - m(\lambda_1 + \lambda_2)} \right] \left\{ \frac{1}{3} + \frac{1}{8} \frac{1 - m(\lambda_1 + \lambda_2)}{\lambda_3(1 - \lambda_3)m} \right\}$$

$$M_1 = f_c' d^2 \left[0.24 \left(1 + \frac{d'}{d} \right) + q \left(1 - \frac{d'}{d} \right) - 0.07 \right]$$

$$M_2 = f_c' d^2 \left[q \left(1 + \frac{d'}{d} \right) - 0.35 \left(1 + \frac{d'}{d} \right) + 0.07 \right]$$

$$M_3 = f_c' d^2 \left[0.12 \left(1 + \frac{d'}{d} \right) - 0.02 \right]$$

A_s = area of tension reinforcement per unit width of slab

d = distance from extreme compression fiber to centroid of tension reinforcement

d' = distance from extreme tension fiber to centroid of reinforcement

(a)
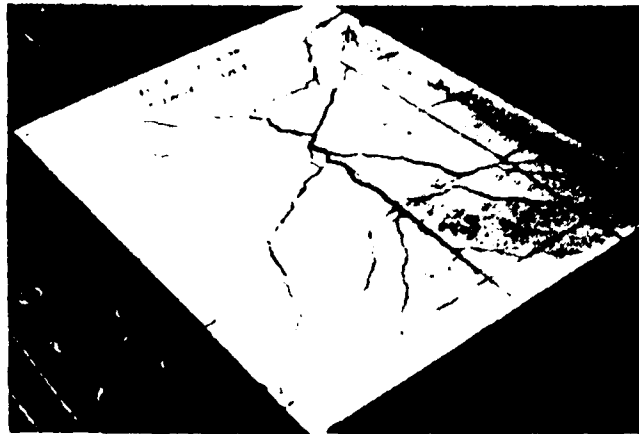
(b)
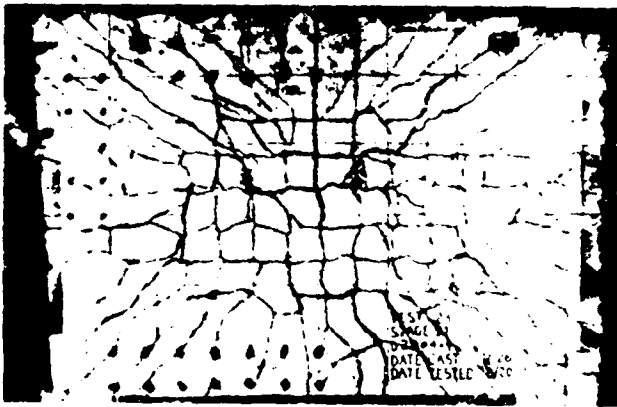
Fig. 21   Yield-Line Pattern
for   Rectangular
Slabs Tested   at
Rutgers University
(from Ref. 19)

(c)

-34-
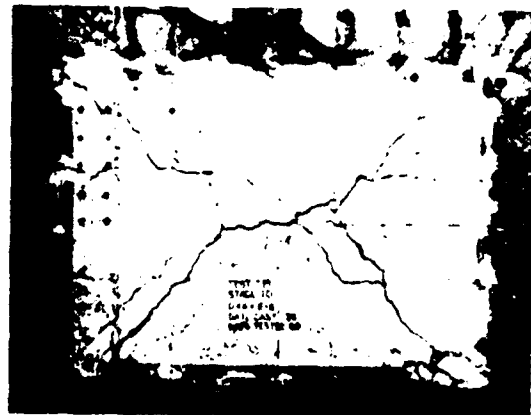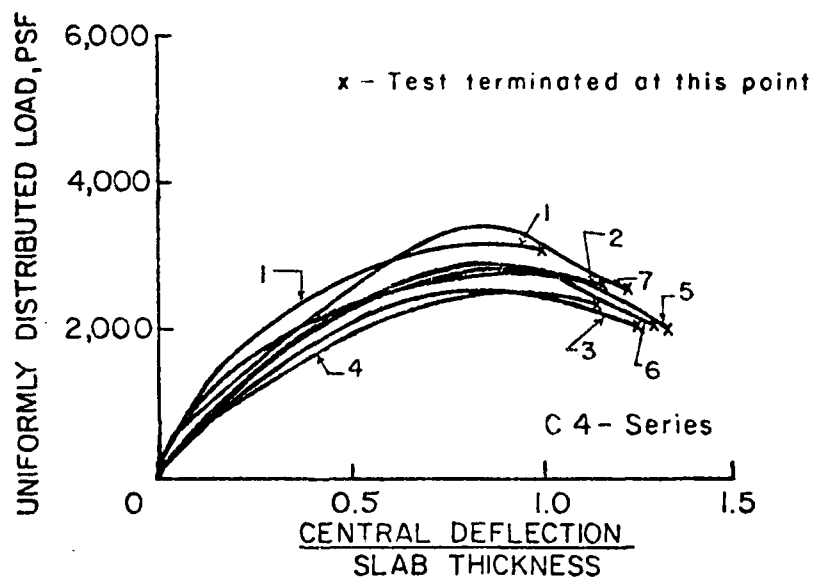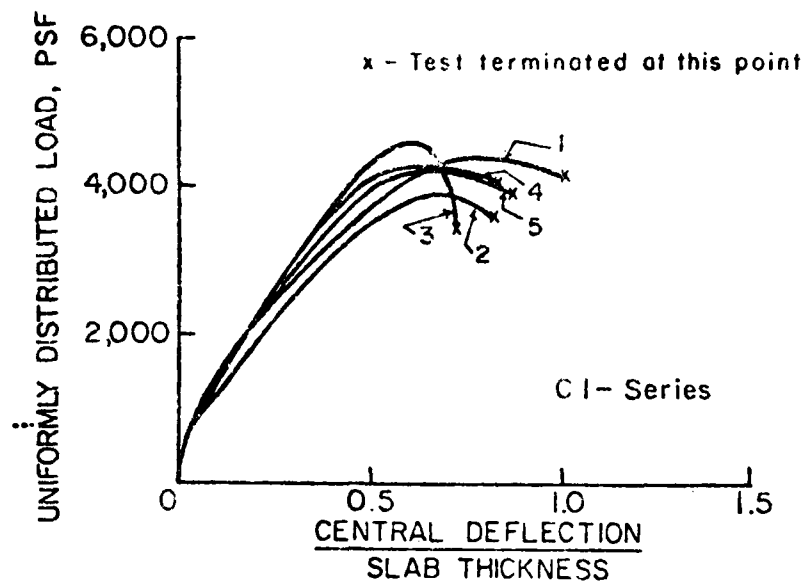
Fig. 22   Load-Deflection Relationships for Slab
Series C1 and C4 Tested at Rutgers
University (from Ref. 19)

-35-
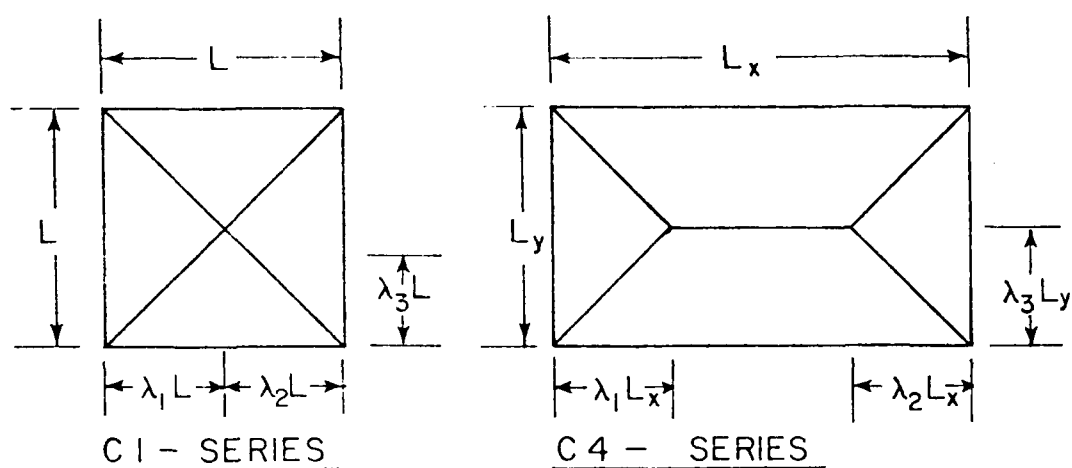
NOTE: λ_1, λ_2, λ_3 Define the Idealized Yield-line Geometry

Fig. 23   Idealized Segments of Slab Panels at Failure
- Hung and Nawy (from Ref. 19)

f'_c = compressive strength of concrete

f_y = yield strength of reinforcement

m = ratio of short span to long span for two-way action slabs

$q = A_s f_y / f'_c d$ = reinforcement index

h = total thickness of slab (in.)

W_D = load/unit area corresponding to point D in Fig. 3

$\lambda_1, \lambda_2, \lambda_3$ = parameters defining the yield-line geometry (Fig. 23)

δ_D = deflection corresponding to point D in Fig. 3

Hung and Nawy (19) further extended this approach to slabs with three edges fixed and one edge hinged as well as to slabs with two edges fixed and the other two hinged. As in the case of other methods, this method suffers from the drawback of having to assume a value of deflection, δ_D in order to determine the slab capacity, W_D.

Nawy and Blair (29) tested to failure ninety two-way slab specimens to investigate flexural cracking behavior of slabs. The geometric and material properties as well as test results for fifty-one slab specimens restrained along all four edges are listed in Table 1.

3.9 Work at the Massachusetts Institute of Technology (Jacobson, Brotchie and Holley)

Jacobson (32), and Brotchie and Holley (33) at M.I.T. tested forty-five 15-in. square two-way restrained slabs to investigate elasto-plastic behavior. The length-to-depth ratio was varied from 5 to 20 and the reinforcement ratio from 0 to 3%. Jacobson (32) was the first to measure the restraining force along the slab boundary. Typical plots of the experimental load-versus-central deflection, load-versus-average restraining force along the boundary, and crack patterns are given in Figs. 24a through 24c, respectively. In the first, elasto-plastic stage, the restraining force increases almost linearly with deflection. Gradually, both restraining force and load capacity approach a peak value. The slab subsequently fails either by instability or in compression. In the second, plastic stage, the slab capacity and the restraining force decrease as the deflection increases. The upper limit of deformation for this stage corresponds to point E in Fig. 3, just before the onset of tensile membrane action. In the tensile membrane stage, no compressive restraining force is provided by the support.

(a)

(b)

(c)

(A) SPREADING MECHANISM

(B) MECHANISM (PLASTIC)

(C) TENSILE MEMBRANE
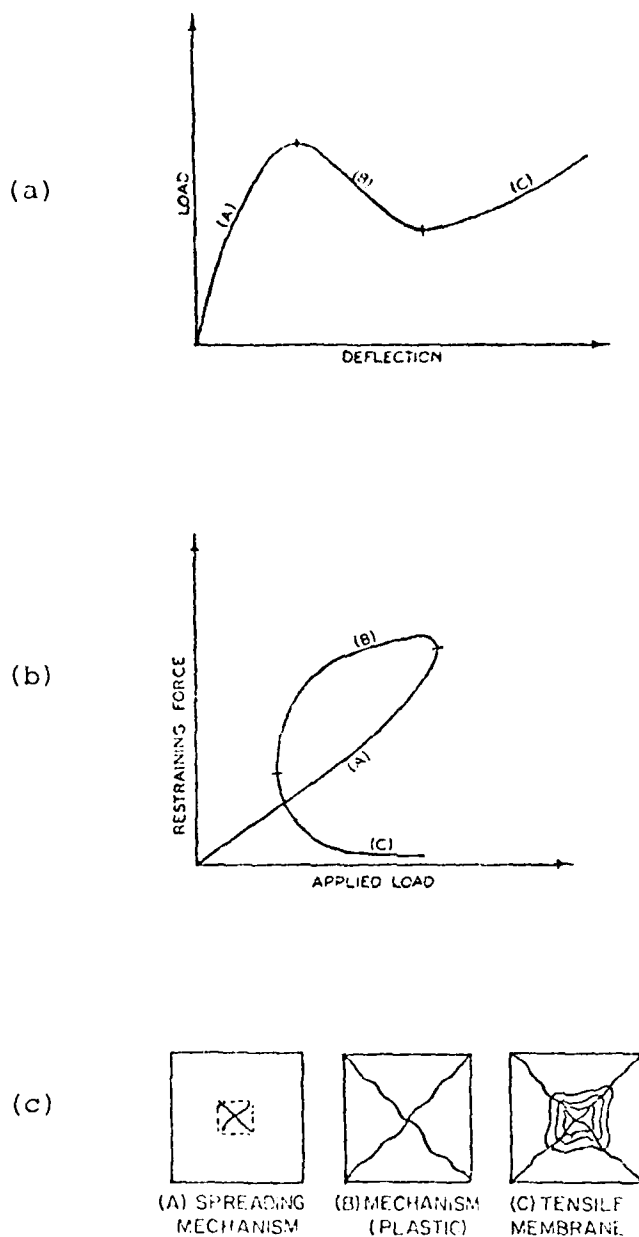
Fig. 24   Typical Load-versus-Deflection, Load-versus-
Restraining Force, and Cracking Pattern
(bottom of slabs)   for an Under-Reinforced
Slab with Edge Restraint Showing Three
Phases of Behavior:
(a) Loading Phase, Elastic or Elasto-Plastic,
(b) Unloading Phase, Elastic or Elastic-Plastic,
and
(c) Reloading Phase, Tensile Membrane
(from Refs. 32 and 33)

Results of Jacobson's and Brotchie and Holley's experiments are summarized below:

1. Load-deflection curves for restrained slabs with different reinforcement ratios and with span-depth ratios of 20 and 10 are shown in Figs. 25 and 26, respectively. For laterally restrained, unreinforced slabs with a span-to-depth ratio of 20, the peak load, W_D, was approximately 5,000 lbs/sq ft. For thicker slabs, i.e., slabs with lower span-to-depth ratio, the capacity increased more rapidly than the square of the thickness, e.g., for a span-depth ratio of 10, the peak load was 22,000 lb/sq ft.

   The increase in peak load with reinforcement ratio is less marked and added strength due to increased reinforcement is less than the initial capacity resulting from external restraint alone. Magnification of load capacity due to the restraining effect decreases as the reinforcement ratio increases.

2. The magnitude of the restraining force developed varies essentially linearly with thickness of the slab and with applied loading up to the maximum arching peak load.

3. Reinforcement ratio has only a slight effect on magnitude of the maximum restraining force. The effect of edge restraint differs from that of reinforcement in that it is sensitive to deflection.

4. Cracking is significantly reduced in restrained slabs, up to the peak arching load.

5. For thin slabs, with span-to-depth ratios of 10 or more, it is necessary to provide essentially full restraint against displacement if the full increase in load capacity is to be attained. For thicker slabs, the restraining force is still required, but additional edge and restraint displacement may be tolerated without significantly reducing load capacity.

6. Tensile membrane action is significant only at large deflections.

Jacobson (32) analyzed the test results for elastic, elasto-plastic and rigid-plastic cases. The rigid-plastic analysis provided an upper bound solution and is similar in approach to that of Morley.[28]

Based on the studies of Jacobson (32) and other work at M.I.T., Brotchie and Holley (33) presented an analysis for compressive membrane action. They gave the following simplified expressions for the maximum (peak) unit load carried by arching action,
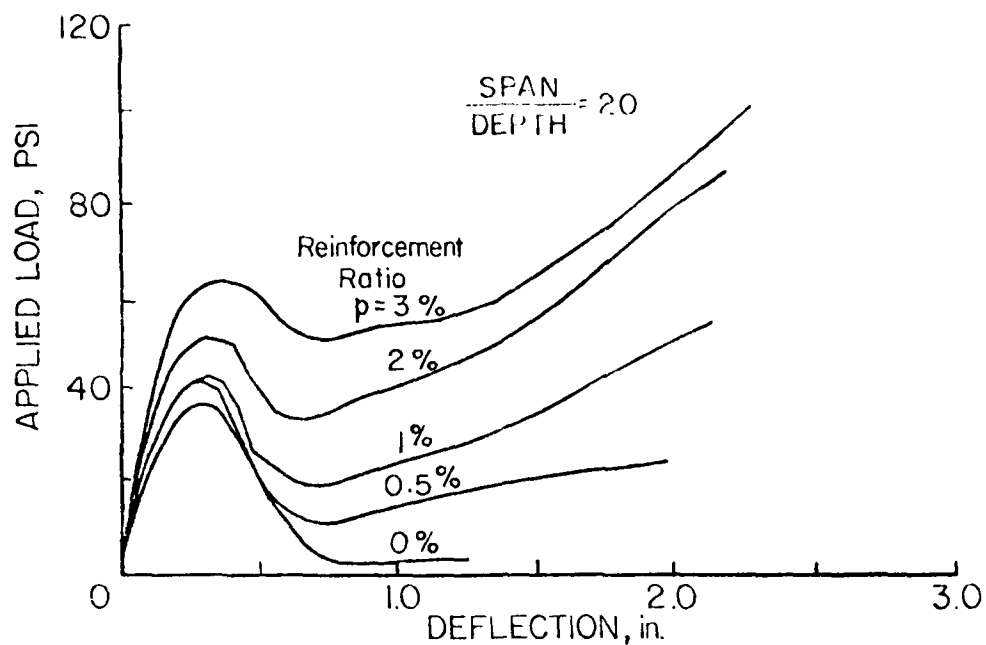
Fig. 25   Load-Deflection Relation for Restrained Slabs with
Various Reinforcement Ratios - Brotchie and Holley
(from Ref. 33)
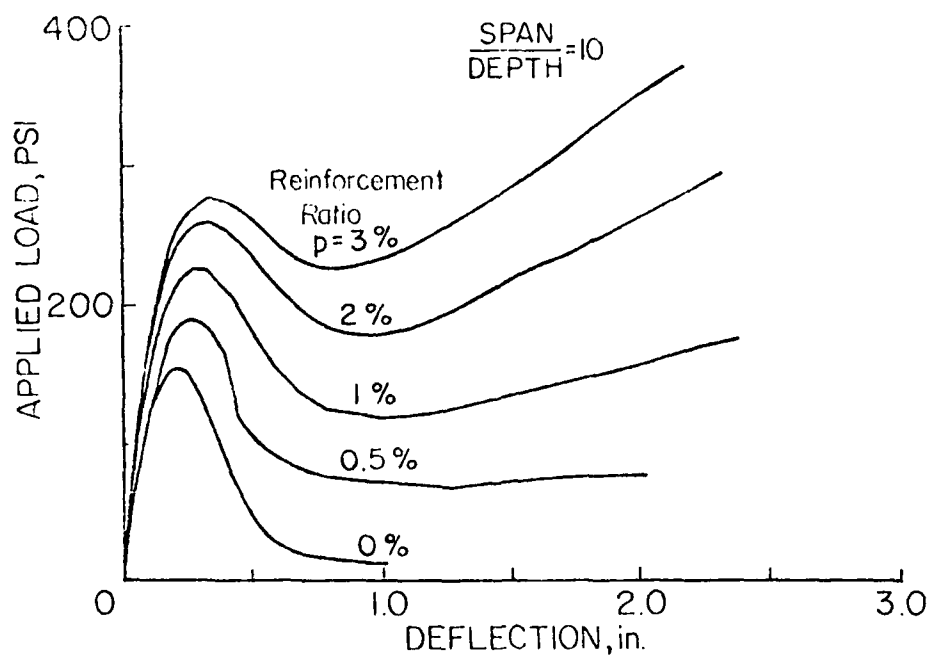
Fig. 26   Load-Deflection Relation for Restrained Slabs with
Various Reinforcement Ratios - Brotchie and Holley
(from Ref. 33)

-40-

$$W_D = 6\bar{f}_c \left[\left(\frac{L}{h} \right)^2 - 0.00133 \left(1 - \frac{p}{p'} \right) \right] \qquad \text{Eq. (6)}$$

The central deflection corresponding to W_D, and $\bar{f}_c$, is given by:

$$\delta_D = 0.001 \left(\frac{L^2}{h} \right)$$

And the maximum restraining force, C_{max}, is given by:

$$C_{max} = \left[\frac{1}{2} \bar{f}_c h \quad 1 - 0.00033 \left(\frac{L}{h} \right) \right]^2 \qquad \text{Eq. (7)}$$

where $\bar{f}_c = 0.85 f'_c + 16p \; d \; f_y \; \delta_D / L^2$

   d = effective depth to the steel

   L = side of the square slab

   h = slab thickness

   p = positive steel percentage

   p' = negative steel percentage

   f'_c = cylinder concrete strength

A comparison of experimental and theoretical load capacity, shown in Fig. 27, shows good agreement. However, the agreement between theoretical and experimental deflections and restraining forces, shown in Figs. 28 and 29 is, less satisfactory.

3.10 Moy and Mayfield's Work

Moy and Mayfield (34) applied Massonet's general elastic-plastic membrane theory (35), along with a proper yield criterion to determine the effect of membrane action in reinforced concrete slabs. They applied finite difference techniques to solve the equilibrium equations and the yield criterion curve for a restrained slab. The same investigators also conducted experiments to verify the analysis. However, comparison between theoretical and experimental results was unsatisfactory. This was primarily due to the fact that the analysis did not include the influence of concrete cracking, a mechanism that has a major effect on the load-deflection characteristics of slabs.

3.11 Datta and Ramesh's Work

Datta and Ramesh (36,37) investigated the effect of compressive membrane action on isolated slab-beam floors. Their analysis
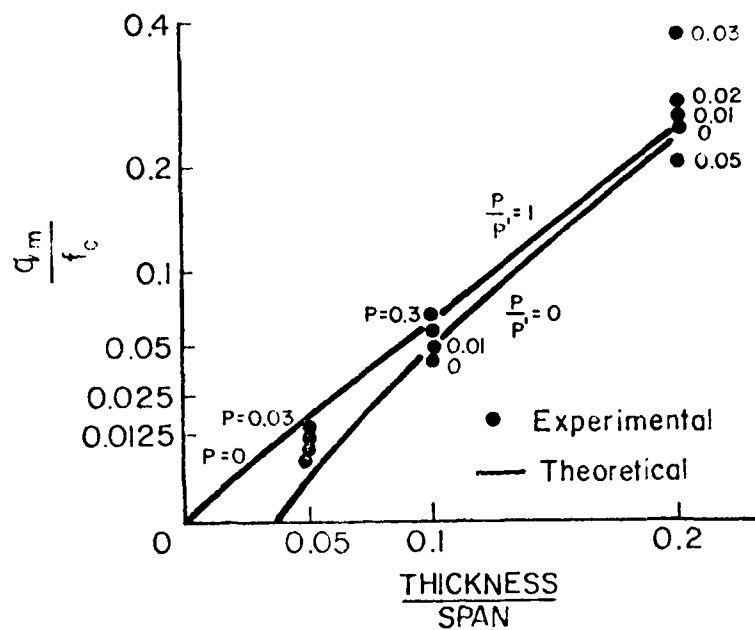
Fig. 27   Comparison of Experimental and Theoretical
Peak Load Capacities - Brotchie and Holley
(from Ref. 33)
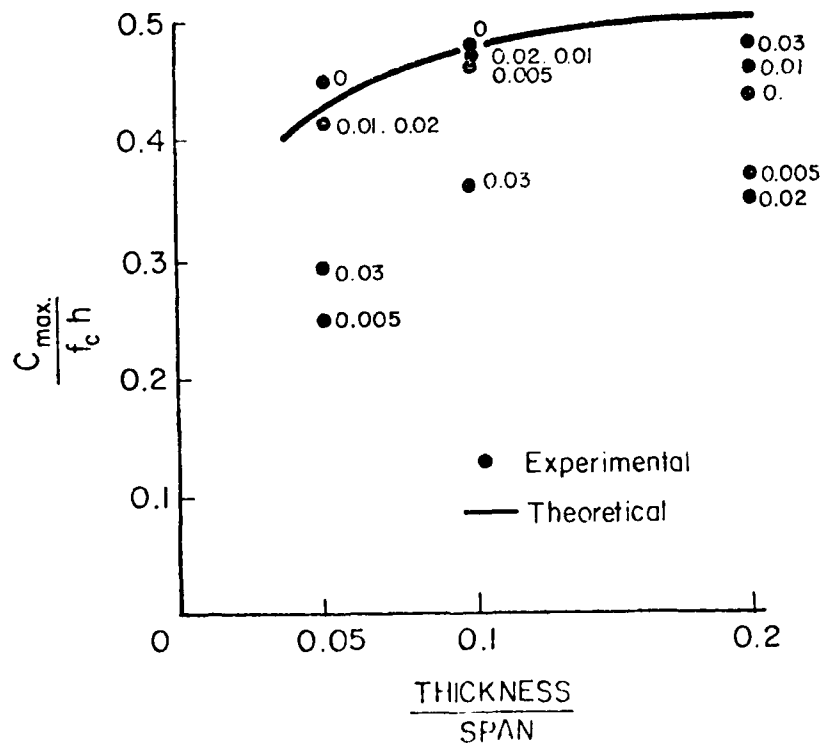
Fig. 28   Comparison of Experimental and Theoretical
Maximum Restraining Forces   - Brotchie and
Holley   (from Ref. 33)
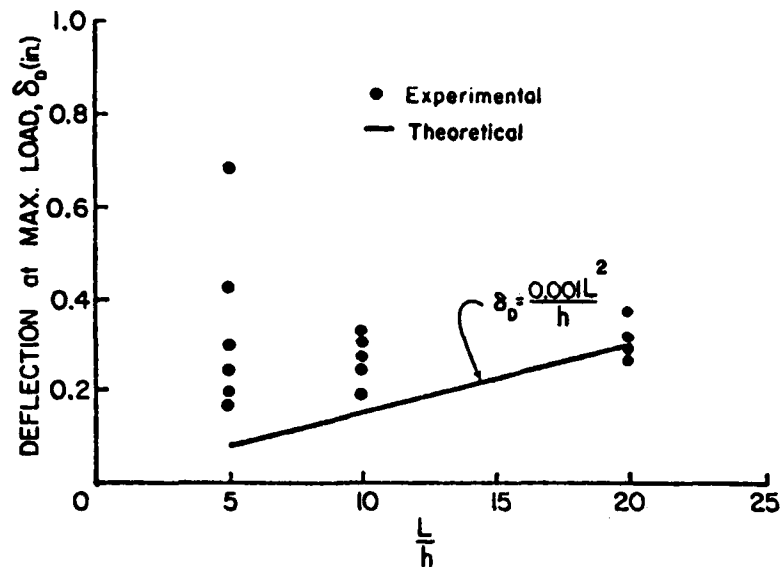
Fig. 29   Comparison of Experimental and Theoretical
Deflection at Peak Load - Brotchie
and Holley (from Ref. 33)
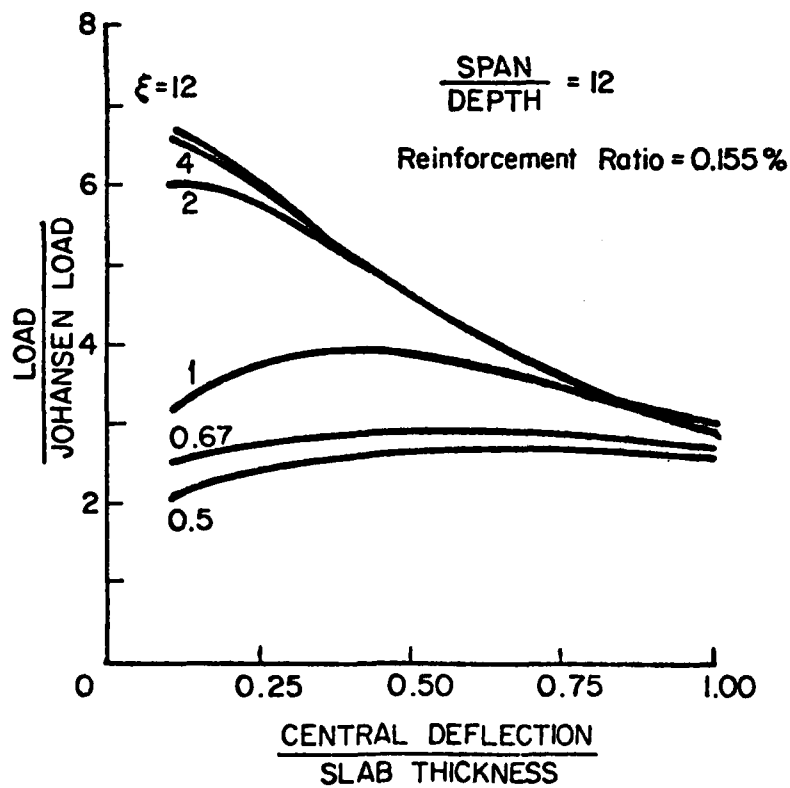
Fig. 30   Relation between δ_D/h and W_D/W_j for Various
Degrees of Edge Restraint ξ - Ramesh
and Datta (from Ref. 36)

-43-

considered the edge beam lateral displacement due to in-plane compressive forces in the slab. Using Park's (20) strip approach, Ramesh and Datta (36) developed an expression for the in-plane compressive force as a function of edge beam lateral displacement. The in-plane force was calculated by prescribing edge beam boundary conditions. Knowing the axial force, stress resultants on the yield lines were calculated. The load-deflection relationship was then established using the principle of virtual work.

Figure 30 shows the load-deflection curves obtained from the theory for different values of, ξ, the degree of edge restraint provided by the surround of an isotropically reinforced square slab. The parameter ξ is a non-dimensional quantity defined as

$$\xi = \left[\sqrt[4]{\frac{k\ f'_c\ L}{h\ I_b E_c}} \left(\frac{L}{4}\right) \right]^{-1}, \qquad \text{Eq. (8)}$$

where k = coefficient determining the compressive force in concrete in Hognestad (38) stress-block

L = sides of a square slab panel

I_b = moment of inertia of edge beam (for lateral deflection)

E_c = modulus of elasticity of concrete

h = slab thickness

f'_c = cylinder concrete strength

Figure 30 shows that, for degrees of edge restraint below $\xi = 0.67$, tensile membrane action predominates over compressive membrane action. For $\xi \geqslant 4$, a state of full compressive membrane action is attained.

Datta and Ramesh (37) also tested nineteen single-panel, square, isotropic slab-beam specimens. Figure 31 shows general details of the test specimens. Ten out of nineteen slabs were cast with the slab located at mid-depth of the beams to avoid T-beam action. The remaining specimens had the slab cast at the top of the beams. Load was applied equally at 64 points distributed uniformly on the slab surface. Variables included reinforcement ratio, degree of edge restraint, ξ, and influence of T-beam action.

The experimental load-deflection curves are similar to those shown in Fig. 22. The following conclusions were drawn from this study:

PLAN

SECTION

(a) SLAB AT THE END OF THE BEAM

(b) CENTRE OF SLAB COINCIDING WITH
CENTRE OF BEAM
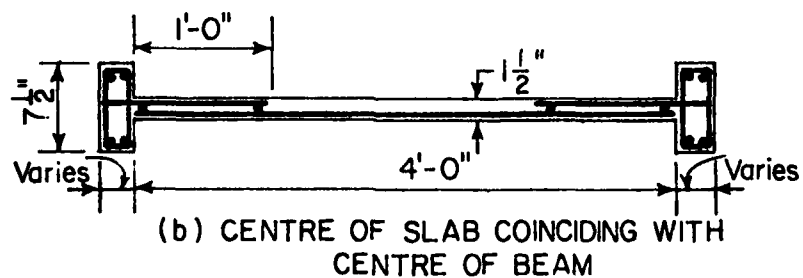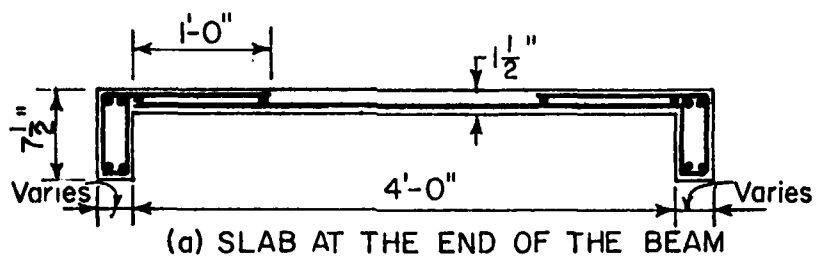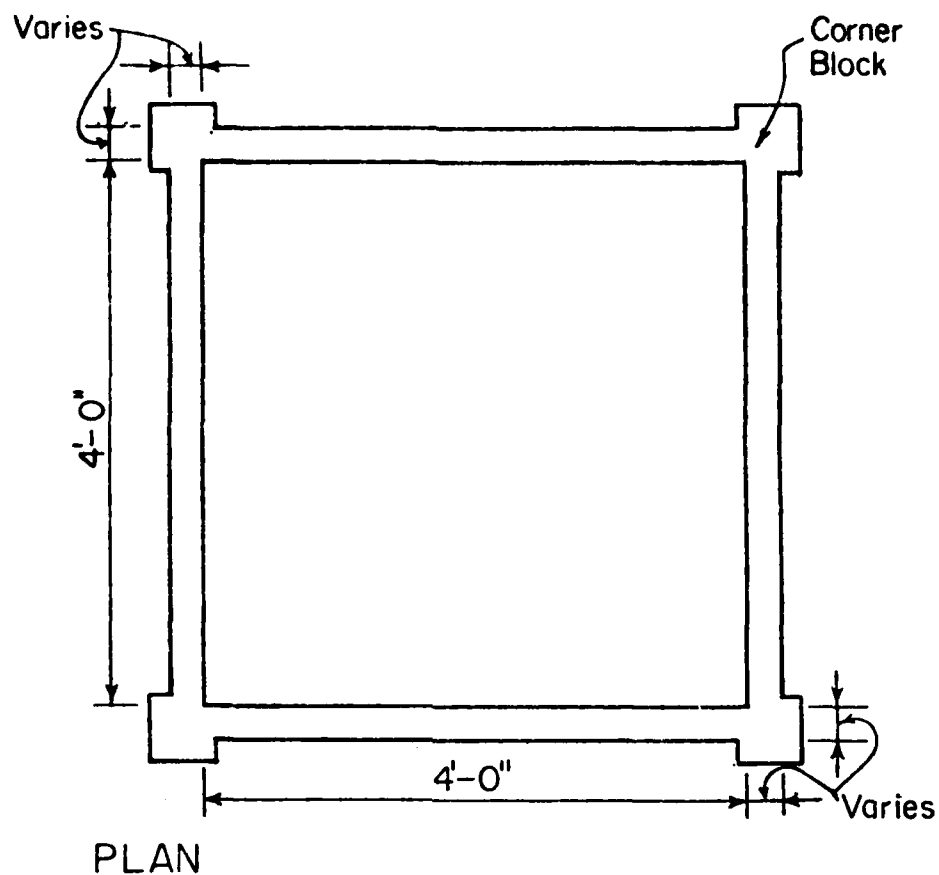
Fig. 31   General Details of Slab-Beam Specimen
Tested by Datta and Ramesh
(from Ref. 37)

1. The deflection corresponding to the peak load, δ_D, increases with a decrease in the degree of edge restraint.

2. Enhancement in slab capacity due to compressive membrane action decreases with increasing reinforcement ratio.

3. For slab-beam panels with partial horizontal restraint along their edges, i.e., with $\zeta \approx 0.67$, there was practically no enhancement in slab capacity and the slabs acted as tensile membranes.

4. Slab-beam panels with $\zeta \rightarrow 4$ behaved as if it they were fully restrained.

3.12 University of Illinois Tests (Girolami, Sozen, and Gamble)

Six reinforced concrete panels were tested at the University of Illinois by Girolami et al (39). All specimens were subjected to both transverse and in-plane loading. A number of point loads were applied over the panel surface to simulate uniform vertical loading. Equal horizontal loads were applied at five equally spaced points on each side of the slab to simulate membrane forces. For simplicity, membrane loads were held constant during the test.

Each panel was 6-ft square and 1.75-in. thick. The slab was cast monolithically with 6-in. deep by 3-in. wide doubly reinforced spandrel beams, as shown in Fig. 32. Vertical loads were also applied to cantilever extensions of the spandrel beams to maintain restraint at the corners. Two types of boundary conditions were considered. In the first three specimens, the panels were supported at the corners and the beams were permitted to deflect freely. In the remaining three cases, the specimens were supported at several points along the spandrel beams to simulate simple edge support conditions.

The three corner-supported structures initially developed diagonal yield-lines in the panel, but finally failed in the yield-lines parallel to the panel edges. The beams participated in the failure mechanism, as shown in Fig. 33. For the three specimens with nondeflecting beams, failure occurred within the panel. The measured panel load capacity, W_D, was 1.7 to 2.1 times the corresponding Johansen load, W_j. The corresponding deflection was approximately half the slab thickness.

For slabs with nondeflecting beams, the equilibrium equation at the peak load may be written as

$$\frac{W}{4} \frac{L}{6} = L(m + m') - \frac{2}{3} N \delta \qquad \text{Eq. (9)}$$

-46-

PLAN

SECTION

Fig. 32   Typical Geometry of Slab-Beam Specimens
Used in University of Illinois Tests
(from Ref. 39)
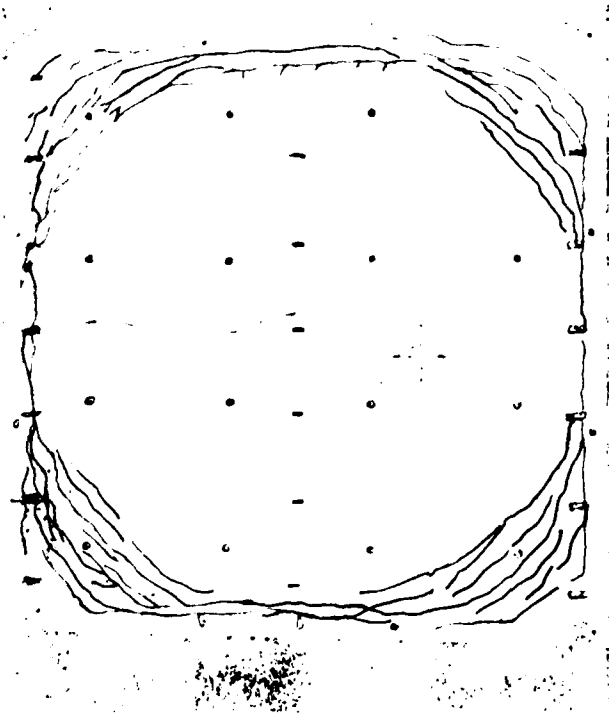
Fig. 33   Top View of a Slab After Test
at University of Illinois
(from Ref. 39)

where   W = total load on the panel

            L = panel span

     m, m' = positive and negative slab moments/unit width

            δ = slab central deflection

            N = total applied membrane force on one side of the
                panel

In Eq. 9, deflections were assumed to vary parabolically across
the slab so that the mean slab deflection along a positive yield
line is given by 2δ/3. Since both W and δ are unknown in Eq. 9,
an iterative procedure was used to calculate the theoretical
ultimate load. The effect of membrane forces was included.
Each step in this iterative procedure involved estimating and
then calculating W. The procedure was repeated until the load
giving the estimated deflection, calculated using elastic plate
theory with fully cracked sections, agreed with the load given
by Eq. 9. The ratio of experimental to theoretical load capac-
ities estimated by this procedure varied between 1.02 and 1.17.
This indicates that the load capacity of a panel can be esti-
mated accurately if the membrane forces acting on the panel are
known.

3.13 Desayi and Kulkarni's Work

Desayi and Kulkarni (40) presented a method to determine the
load-deflection relationship corresponding to the portion ADE
of the solid curve shown in Fig. 3. The analysis is carried
out in two stages. In the first stage, a semi-empirical method
is used to calculate deflections from zero load to Johansen's
yield-line load. In the second stage, an analysis considering
membrane action is used to find the load-deflection relationship
beyond Johansen's load.

In the first stage, results of classical plate theory are used.
Cracking of concrete and yielding of steel are accounted for by
suitably modifying flexural rigidity. Changes that occur in
support conditions due to possible yielding are also considered.
In the second stage of analysis, Park's (20) strip method is
used with some modifications. Desayi and Kulkarni compared
calculated ultimate loads and deflections with those obtained
from test results of sixty-seven slab specimens. Satisfactory
results were obtained. Load-deflection curves obtained by this
method are compared with Hung and Nawy's (19) experimental
curves in Fig. 34.
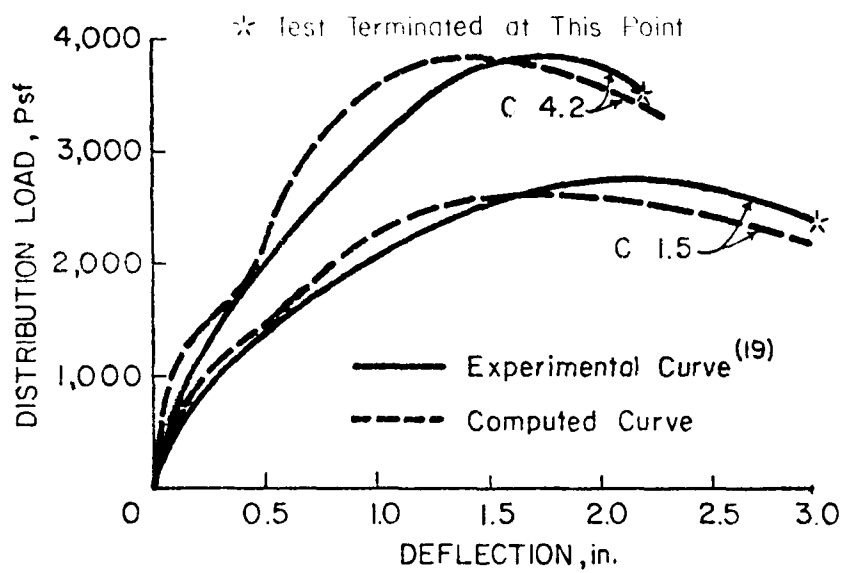
Fig. 34   Comparison of Experimental and Calculated
Load-Deflection Relationships
(from Ref. 50)

4. TENSILE MEMBRANE ACTION IN TWO-WAY RESTRAINED SLABS

For a slab with very stiff edge restraint, as point E in Fig. 3 is approached, the membrane forces change from compression to tension in the central region of the slab. At this point, the boundary restraints begin to resist inward movement of the slab edges. Initially, the outer regions of the slab act with the restraint as part of the compression ring supporting the tension membrane action in the inner region of the slab. With further deflection beyond point E, the region of tensile membrane action gradually spreads throughout the slab. As this occurs, load carried by the yielding reinforcement acting as a tensile membrane (with full depth concrete cracking) increases until the steel starts to fracture at point F. For restrained slabs, point F represents the condition of incipient collapse.

4.1 Park's Work on Tensile Membrane Action

In analyzing tensile membrane action in orthotropic, restrained slabs, Park (41) made the following assumptions:

1. All the concrete has cracked throughout its depth and is incapable of carrying any load,

2. All reinforcement has reached the yield strength and acts as a plastic membrane,

3. No strain hardening of steel occurs,

4. Only reinforcement that extends over the whole area of the slab contributes to membrane action.

Using standard membrane theory (4), Park (41) presented the following load-deflection relationship of the plastic tensile membrane:

$$\frac{wL_y^2}{T_y \delta} = \frac{\pi^3}{4 \sum_{n=1,3,5} \frac{1}{n^3}(-1)^{\frac{n-1}{2}} \left[1 - \frac{1}{\cosh \frac{n\pi L_x}{2L_y}\sqrt{\frac{T_y}{T_x}}}\right]}, \quad \text{Eq. (10)}$$

where w = uniform load/unit area

δ = central deflection of membrane

T_x, T_y = yield force of the reinforcement/unit width in x and y direction, respectively

L_x, L_y = slab side length in x and y direction ($L_x \gg L_y$)

-51-

To simplify the use of Eq. 10, values of wL_y^2/T_y for various values of L_x/L_y and T_y/T_x have been plotted in Fig. 35. Only $T_y \not> T_x$ for slabs with $L_x \not> L_y$ was considered since more steel will generally be required in the direction of the short span than in that of the long span.

A comparison of Eq. 10 with experimental data is shown in Fig. 36. It may be noted that Eq. 10 gives a linear relationship between w and δ. It provides a conservative estimate for portion EF of the experimental curve due to the following reasons:

1. A pure plastic tensile membrane did not develop over the whole slab. In lightly reinforced slabs, the load is carried mostly by a combined bending and tensile membrane action.

2. The assumption of no strain hardening of steel also makes the theory conservative.

Based on his own work and that of Powell (15), Park concluded that a conservative value of the central deflection that can be associated with the development of full tensile membrane action would be 0.1 of the short span. Any greater deflection may result in bar fracture. The associated loading can exceed Johansen's load when the amount of reinforcement is large enough.

For a square slab, Eq. 10 becomes:

$$w = k(p + p') \frac{hf_s}{L^2} \qquad \text{Eq. (11)}$$

where f_s = steel stress

   p, p' = positive and negative steel ratios, respectively

   $k = 13.5$, determined from Fig. 35

Equation 11 was derived assuming a pure tensile membrane action ($T_x = T_y$). However, tests (41) showed that pure tensile membrane action did not develop. Keenan (42) allowed for this discrepancy in Eq. 11 by modifying the value of k.

4.2 Keenan's Work

Keenan (42) tested six fully clamped slabs under uniform pressure. All slab specimens were square, with a clear span of 72 in. The slab thickness ranged from 3 to 6 in. and reinforcement from zero to 1.33%, as shown in Table 1. In all six specimens, tension cracks first became visible at a load corresponding to over 70% of the Johansen load. The slabs hinged initially in
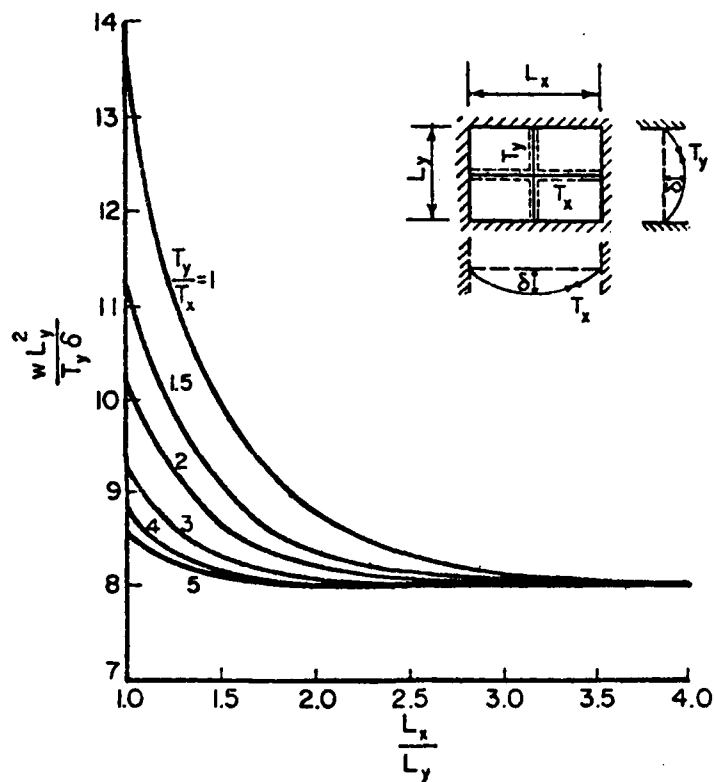
Fig. 35 Load-Deflection Relations from Eq. 10
for Uniformly-Loaded Plastic Tensile
Membranes with Rigid Rectangular
Boundaries - Park (from Ref. 41)
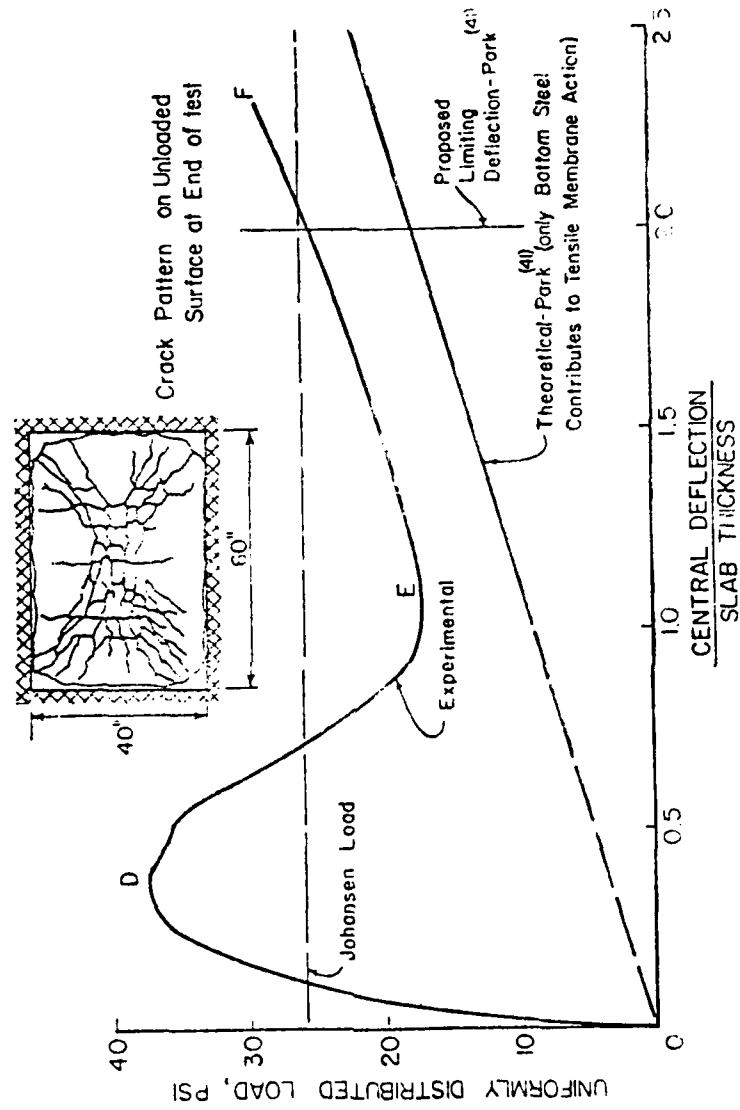
Fig. 36   Load-Deflection Curves and Cracking Pattern for Slab A4 Tested by Park (from Ref. 41)

flexure, followed by total collapse at a much greater deflection. Complete load-deflection relationships for the specimens are shown in Figs. 37 through 39.

The shapes of the load-deflection curves are similar for all slabs. However, the loss of resistance in transition from compressive to tensile membrane action is least for the slab with highest reinforcement ratio, as shown in Fig. 39. This finding agrees with the M.I.T. (32,33) test results shown in Figs. 25 and 26.

Collapse corresponded to rupture of the reinforcement in tension, with the slab acting as a membrane. The central deflection at collapse was more than 2.5 times the slab thickness for the thinner slabs.

Based on his and other's work, Keenan (42) developed a semi-empirical method to determine the load-deflection relationship for square, full restrained slabs. The method involves solution of eight equations covering different ranges of slab behavior from elastic through tensile membrane action.

To obtain better agreement with his test results, Keenan modified the factor k in Park's pure membrane formulation (Eq. 11). He determined that a value of k equal to 20 yielded a better correlation with the measured value of the deflection at secondary resistance, δ_s. It was assumed that the associated secondary resistance, W_s, is equal to Johansen load, W_j. By setting k equal to 20, the ratio T_x/T_y becomes less than unity. This implies that reinforcement in the two directions do not yield simultaneously.

Keenan further determined that a safe maximum value for the central deflection associated with tensile membrane action is one-tenth of the span. This confirms Park's (40) recommendation mentioned earlier. No attempt was made to extend his method to rectangular slabs.

4.3 Work at U.S. Army Engineer Waterways Experiment Station

Denton (43) and Black (44) tested small-scale slabs at the U.S. Army Engineer Waterways Experiment Station. Both simply-supported and restrained slab specimens were subjected to uniform pressure.

Geometric and material properties of four restrained slabs tested by Black (44) are listed in Table 1. The specimens, square in shape, were tested in a Small Blast Load Generator (SBLG), shown in Fig. 40.

The load-deflection relationships, shown in Figs. 41 through 44 indicate behavior similar to that observed by earlier investigators. The dual peak shape of the load-deflection curves
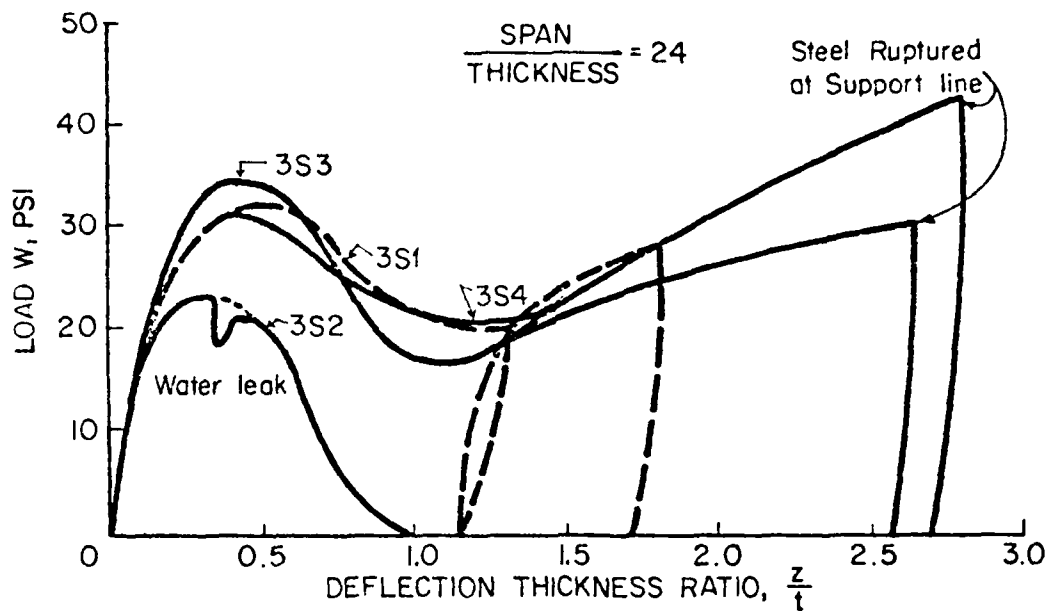
Fig. 37   Load-Deflection Relationship for 3-in. Thick Slabs
Tested by Keenan   (from Ref. 42)
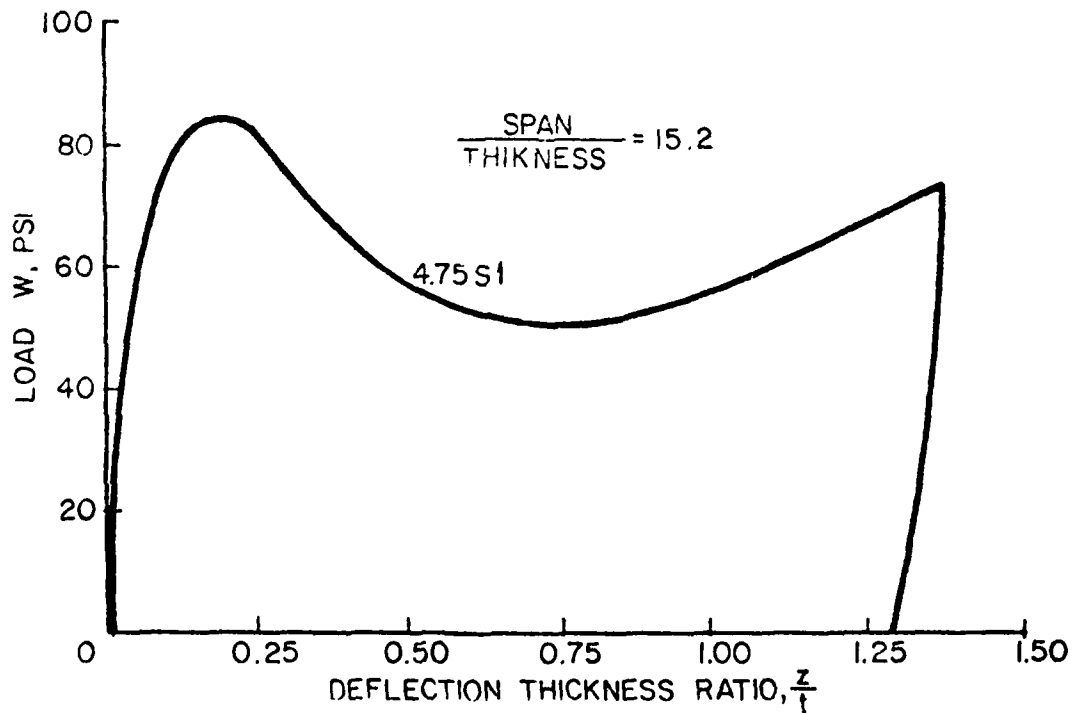
Fig. 38   Load-Deflection Relationship for 4.75-in. Thick Slab
Tested by Keenan   (from Ref. 42)
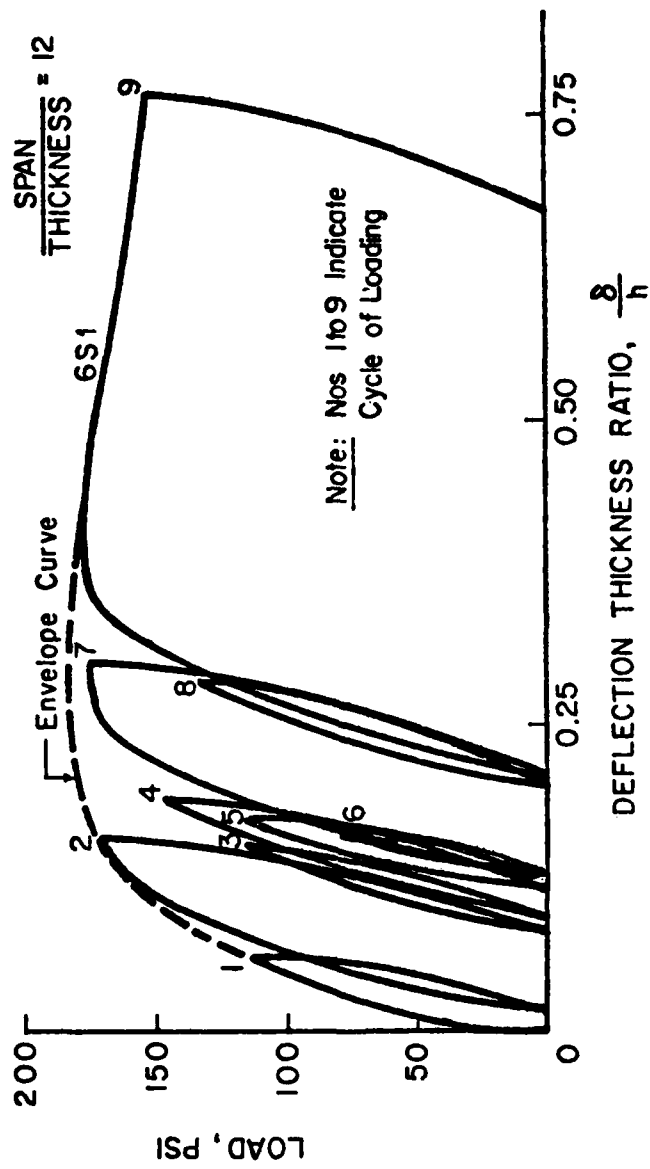
Fig. 39 Load-Deflection Relationship for 6-in. Slab Tested by Keenan
(from Ref. 42)

-57-
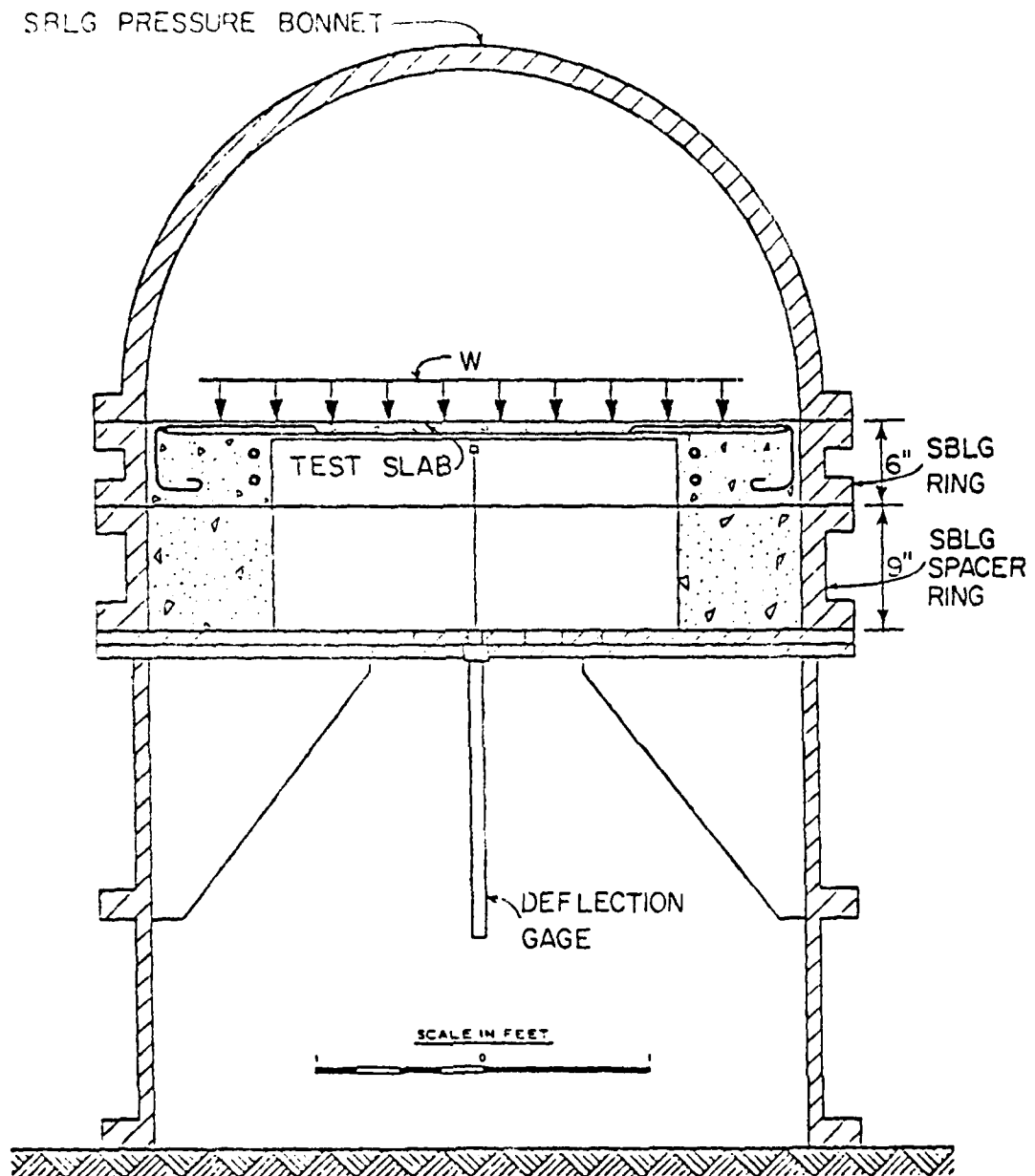
Fig. 40   SBLG Test Set-Up for Slabs Tested by Black
(from Ref. 44)
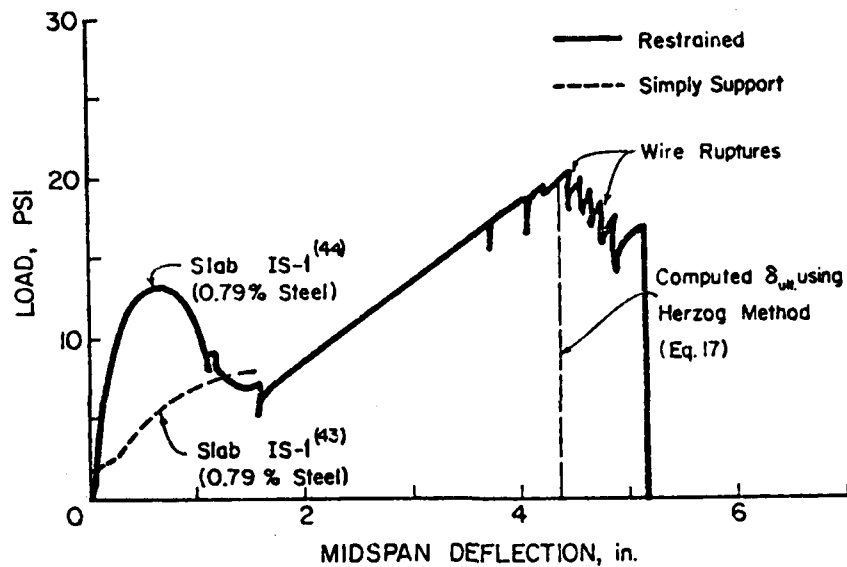
Fig. 41   Load-Deflection Relationship for Slab IS-1
Tested by Black (from Ref. 44)
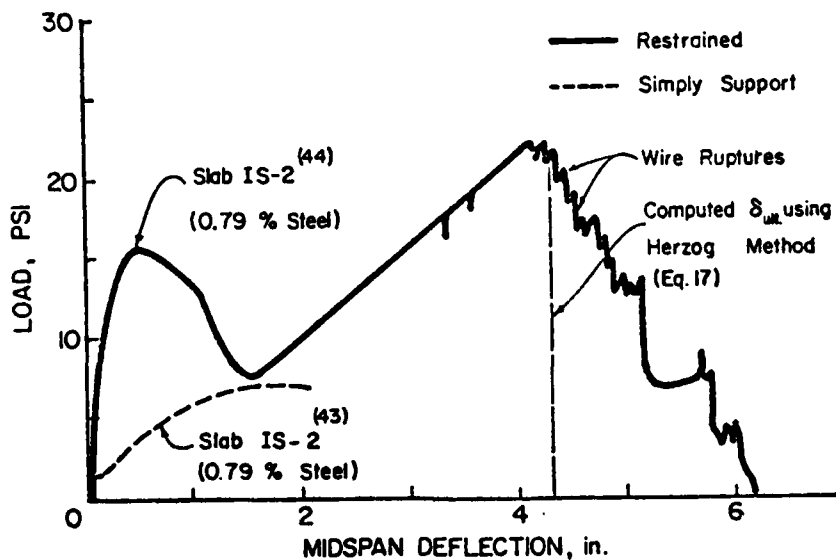
Fig. 42   Load-Deflection Relationship for Slab IS-2
Tested by Black (from Ref. 44)

-59-
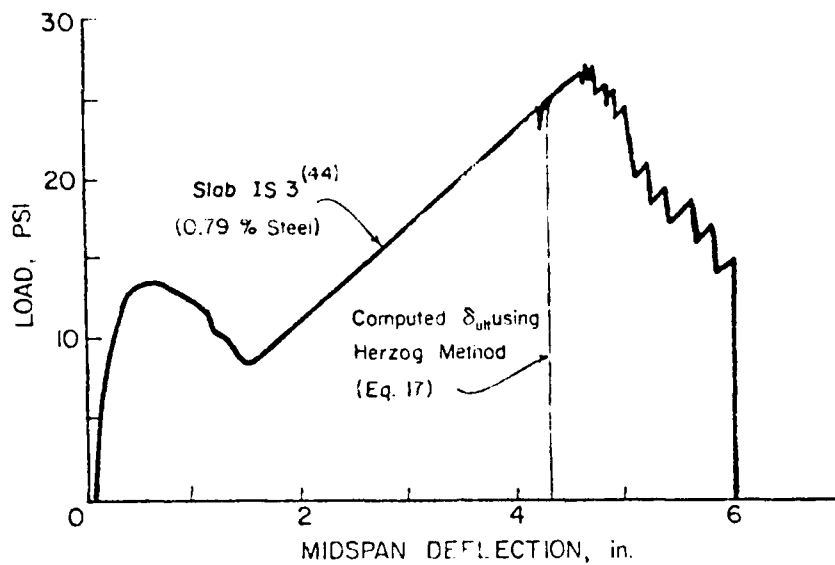
Fig. 43   Load-Deflection Relationship for
Restrained Slab IS-3 Tested
by Black (from Ref. 44)
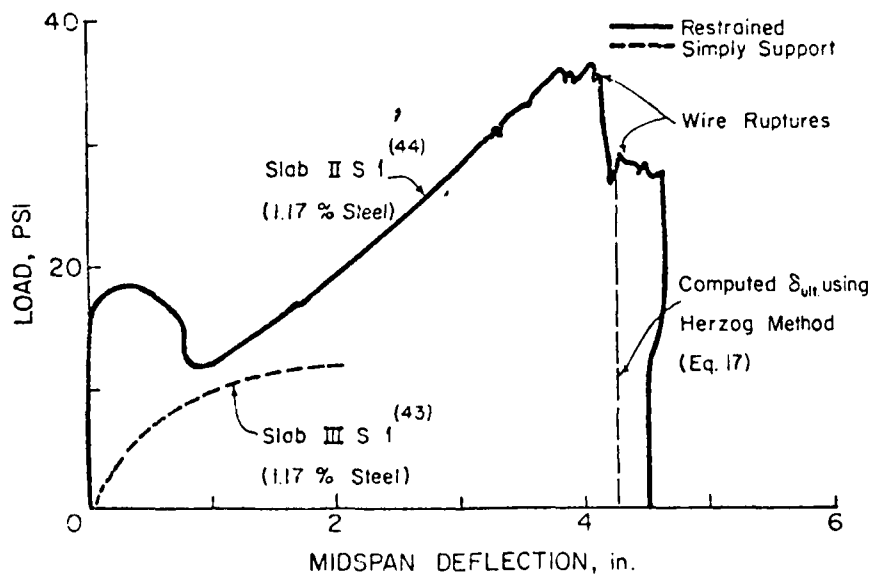
Fig. 44 Load-Deflection Relationship for
Slab IIS-1 Tested by Black
(from Ref. 44)

characterizes two failure mechanisms: compressive membrane and tensile membrane. Maximum deflection at the end of tensile membrane action, δ_{ult}, was approximately one-fifth of the span length for the first series of slabs. Deflection δ_{ult} for the second series was about one-sixth of the span length. Slab IIS1, which had 50 percent more reinforcement than the Series I slabs, showed considerable increased strength. It was noted that the increased steel percentage made the slab stiffer. Cracking patterns for Slabs IS2 and IIS1 are shown in Figs. 45 and 46.

Black determined that the use of k = 20 in Eq. 11 is justified. He noted that Park's (41) and Keenan's (42) estimates of the maximum value for central deflection at the end of tensile membrane action, δ_{ult}, are conservative. Based on his tests, Black proposed the following relationship for δ_{ult}:

$$\delta_{ult} = 0.15L \qquad \text{Eq. (12)}$$

Equation 12, in conjunction with Eq. 11, yielded results in good agreement with Black's tests.

4.4 Herzog's Work

Herzog (45) presented approximate procedures for calculating incipient collapse deflection capacity, $_{ult}$, of restrained two-way slabs. He determined that $_{ult}$ depends on two parameters: slab span and reinforcement elongation at rupture. Herzog derived his equation using a one-way tension member in the following manner.

Consider a cable of horizontal length, L, under a load uniformly distributed in the horizontal direction, as in Fig. 47. From a consideration of cable equilibrium, it can be readily shown that the length of the stretched cable, L_1, to a first approximation, is given by:

$$L_1 = L + \frac{8}{3}\frac{\delta^2}{L} \qquad \text{Eq. (13)}$$

In other words, the cable elongation,

$$\epsilon L = L_1 - L = \frac{8}{3}\frac{\delta^2}{L} \qquad \text{Eq. (14)}$$

In limiting case, when the cable is at the point of rupture,

$$\epsilon_u L = \frac{8}{3}\frac{\delta^2_{ult}}{L} \qquad \text{Eq. (15)}$$

$$\delta_{ult} = L\sqrt{\frac{3}{8}\epsilon_u} \qquad \text{Eq. (16)}$$

(a) Top Face
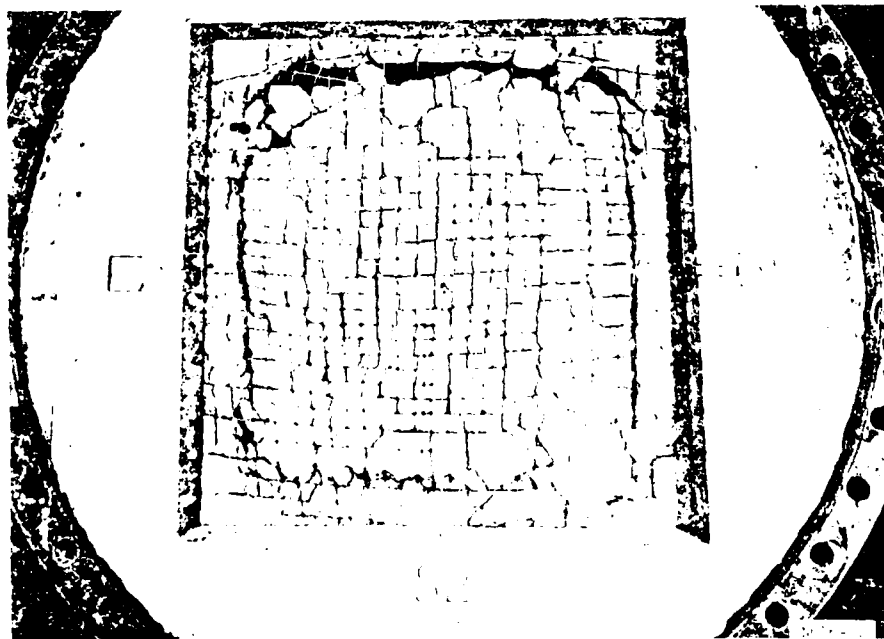
(b) Bottom Face

Fig. 45 Cracking Pattern for Slab IS2 Tested by Black
(from Ref. 44)
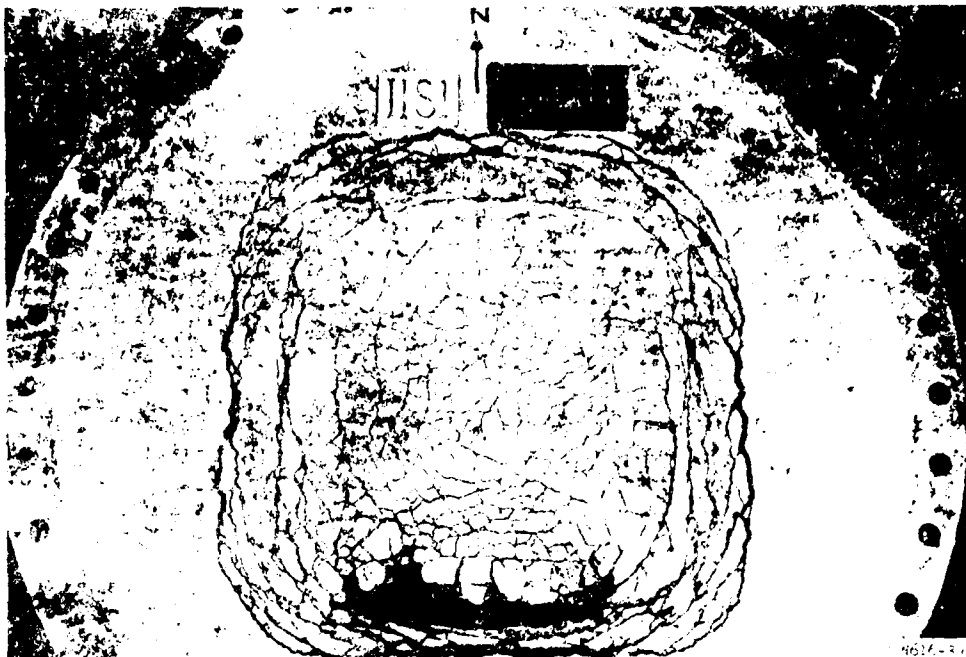
(a) Top Face
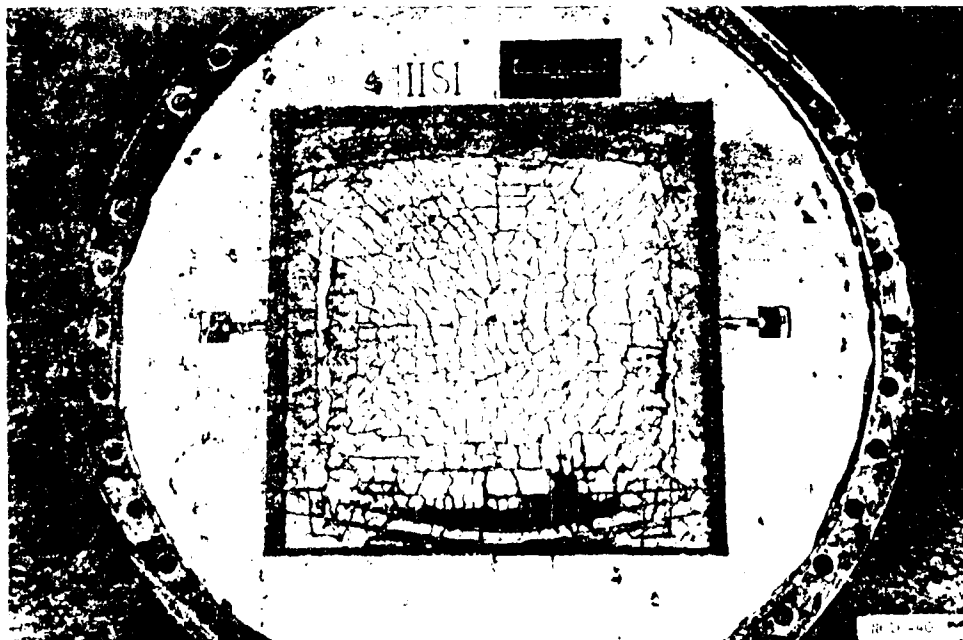
(b) Bottom Face

Fig. 45 Cracking Pattern for Slab IISl Tested by Black
(from Ref. 44)
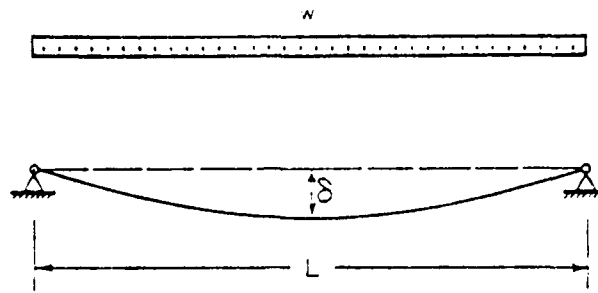
Fig. 47 Parabolic Deflected Profile of a Cable
Under a Uniformly Distributed Load
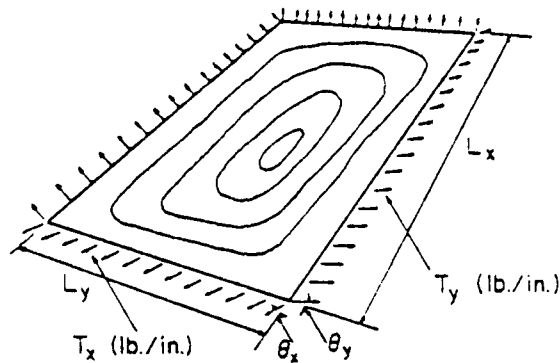
Fig. 48 Equilibrium of Rectangular Tensile Membrane
Hawkins and Mitchell (from Ref. 49)
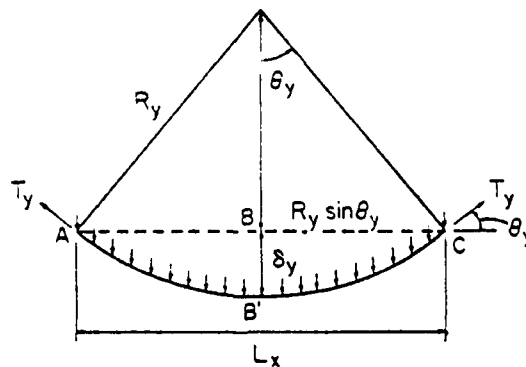
Fig. 49 Assumed Circular Profile of Deformed Slab
in Y Direction - Hawkins and Mitchell
(from Ref. 49)

Herzog accounted for the difference between the uniform strain distribution associated with pure tensile membrane action and the irregular strain distribution in the slab reinforcement by assuming as average ultimate strain equal to one-fourth ε_u. The assumption appears reasonable in view of the nonuniform strain distribution along the bar length (46). Thus, Herzog obtained for the midspan ultimate deflection after tensile membrane action,

$$\delta_{ult} = L_y \sqrt{\frac{3}{32} \varepsilon_u}, \qquad \text{Eq. (17)}$$

where L_y = short span of slab

ε_u = steel strain at rupture

4.5   Hawkins-Mitchell Method

Most recently, Hawkins and Mitchell (47) developed simplified expressions for tensile membrane action in two-way flat slabs. Assuming that the membrane takes a circular deformed shape, they developed the load-deflection equation in the following manner.

Consider a rectangular slab shown in Fig. 48. The slab is subjected to a uniform load w, resisted by edge tensions per unit length of T_x in the x-direction and T_y in the y-direction. The deformed shape assumed for the slab in x-direction is shown in Fig. 49.

Vertical equilibrium gives

$$WL_x L_y = 2T_x \sin \theta_x + 2T_y L_x \sin \theta_y \qquad \text{Eq. (18)}$$

and geometry gives:

$$L_x = 2R_x \sin \theta_x \qquad \text{Eq. (19)}$$

$$L_y = 2R_y \sin \theta_y \qquad \text{Eq. (20)}$$

Substituting Eqs. 19 and 20 in Eq. 8 yields

$$w = \frac{T_x}{R_x} + \frac{T_y}{R_y} \qquad \text{Eq. (21)}$$

The loading lengthens the membrane from the straight line ABC in Fig. 49 of length $2R_x \sin \theta_y$ to a circular arc AB'C of length $2R_y \theta_y$. By approximating $\sin \theta_y$ by the first two terms of the corresponding Taylor series expansion,

-65-

$$\epsilon\phi_y = \frac{AB'C - ABC}{ABC} = \frac{\theta_y^2}{6} \qquad \text{Eq. (22)}$$

Similarly, $\epsilon_x = \theta_y^2/6$

Thus the deflections δ_x and δ_y are

$$\delta_x = \frac{R_y}{2} \theta_x^2 = 3R_x \epsilon_x \qquad \text{Eq. (23)}$$

and

$$\delta_y = \frac{R_y}{2} \theta_y^2 = 3R_y \epsilon_y . \qquad \text{Eq. (24)}$$

Since $\delta_y = \delta_x$ at the center of the membrane,

$$\epsilon_x = \epsilon_y (L_y/L_x)^2 \qquad \text{Eq. (25)}$$

Substituting Eq. 25 into Eq. 21,

$$w = \frac{2T_x \sin\left(\frac{L_y}{L_x}\sqrt{6\,\epsilon_y}\right)}{L_x} + \frac{2T_y \sin\sqrt{6\,\epsilon_y}}{L_y} \qquad \text{Eq. (26)}$$

For a rectangular slab with length L_x greater than L_y, the short span elongation ϵ_y increases faster than ϵ_x. At the incipient collapse deflection, ϵ_y equals ϵ_u and thus Equation 14 becomes:

$$\delta_{ult} = 3R_y \epsilon_u \qquad \text{Eq. (27)}$$

Expressing R_y in terms of L_y and $_u$,

$$\delta_{ult} = \frac{1.5L_y \epsilon_u}{\sin\sqrt{6\epsilon_u}} \qquad \text{Eq. (28)}$$

It should be noted that the properties of the short span steel are sufficient to compute the incipient collapse deflection capacity of a slab.

5. MEMBRANE ACTION IN TWO-WAY SIMPLY-SUPPORTED SLABS

In the case of simply-supported reinforced concrete slabs, membrane action develops as the slab deflects. This occurs in uniformly loaded slabs at relatively large deflections, when the slab regions at the edges tend to move inward but are restrained from doing so by the adjacent outer regions. The result is an outer ring of compression supporting tensile membrane forces in the inner (central) region of the slab. The compressive forces have a beneficial effect on the yield strength of the concrete, resulting in an increase in slab resistance as the deflection increases.

The effect of membrane action on the load-deflection characteristics of simply-supported slabs has been investigated by several researchers. A summary of these works is given below.

5.1 Wood's Work

Wood (4) tested three simply-supported slab specimens. Two specimens, denoted by G5 and G6 were large-size models, while a third specimen, L2, was a small-scale one. The specimen properties are given in Table 2.

Specimens G5 and G6 were identical in all respects except for their boundary conditions. Specimen G5, shown in Fig. 50, was simply-supported but had encased steel beams along its edges. Specimen G6, also simply-supported, had no edge beams. The beams in Specimen G5 were sufficiently strong to prevent combined beam-slab type collapse. Also, beam deflections were negligible.

Figures 50 and 51 show the yield-line pattern for Specimen G5 under 16-point loading. Slab G6 exhibited similar behavior during testing. In both cases, cracking initiated at 56% of the load predicted by Johansen's theory. For Slab G5, the reinforcement yielded at 1.15 times Johansen's load. The corresponding value for G6 was 1.0. There was no definite yield load for either specimen. The slab load increased continuously due to tensile membrane action. The tests were suspended when slab loads for both specimens were at least 50% higher than Johansen's load, as shown in Table 2.

The behavior of small-scale Specimen L2 was very similar to that of the large-scale Specimens G5 and G6.

For simply-supported reinforced two-way slabs, compressive membrane action is non-existent and tensile membrane action comes into play at large deflections, as shown by the experimental curve in Fig. 52. Also shown in Fig. 52 is the theoretical load-deflection curve suggested by Wood.

Fig. 50   Underside of a Square Slab G5, Supported on
          Four Encased Steel Beams, After Collapsing
          Under 16-Point Loading. The beams were suf-
          ficiently strong to prevent the composite
          beam-and-slab mode of collapse.   - Wood
                          (from Ref. 4)
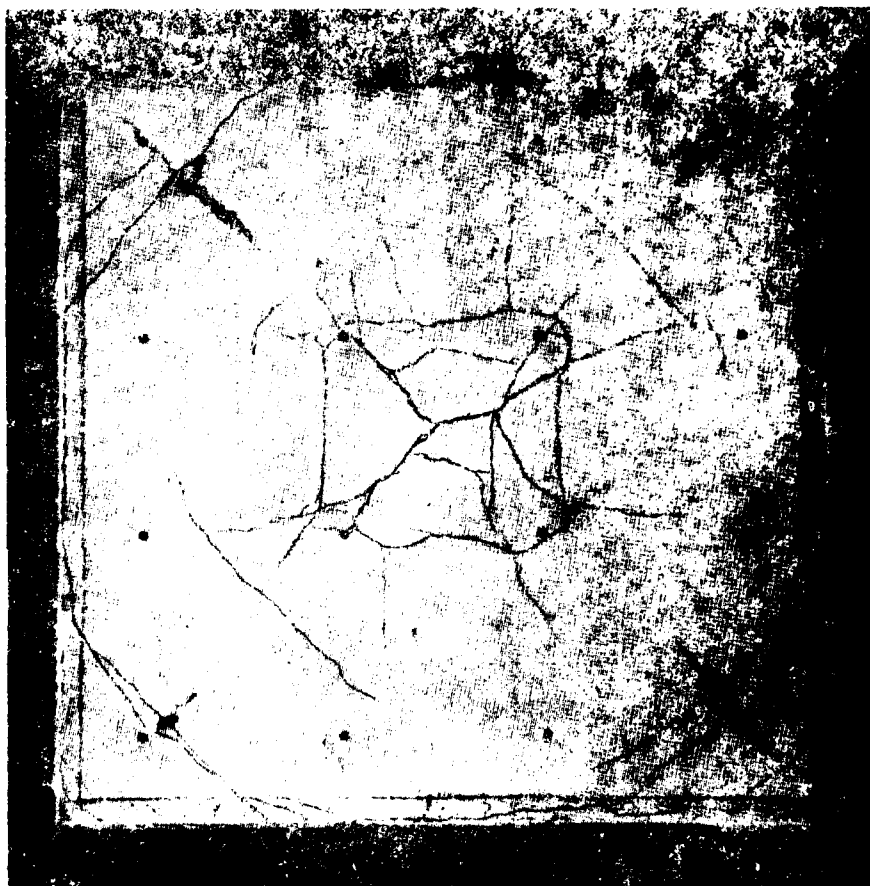
Fig. 51 Upper Surface of Slab G5 Shown in Fig. 50.
Note the torsional effects in the corner
giving rise to crushing and cracking at
right angles.   As the center of the slab
is approached the crushing on the diago-
nals changes to tensile cracks which cut
through the slab. This is strong evidence
of membrane action   — Wood (from Ref. 4)
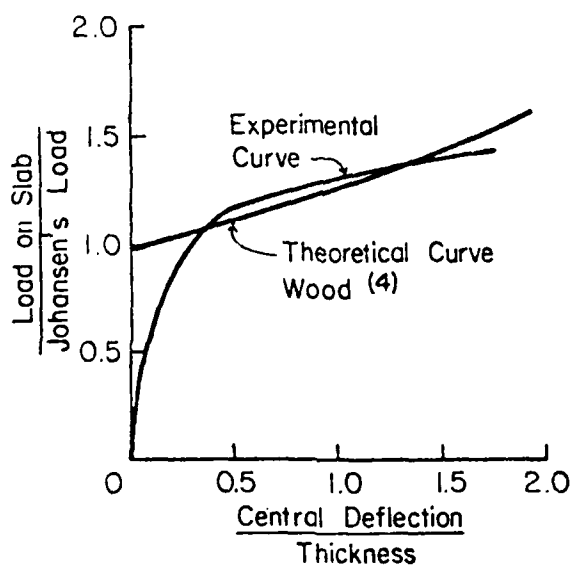
Fig. 52   Typical Theoretical and Experimental
Load-Deflection Curves for a Simply-
Supported Two-Way Slab
(from   Ref. 4)

There is a discrepancy between the initial portions of the experimental and theoretical curves. This is primarily due to the fact that the analysis neglects curvatures that occur prior to Johansen's load. In addition, the theoretical curve shows a continuous increase in load with deflection. In practice, rupture of the reinforcement and/or the loss of its bond with concrete will result in loss of slab capacity.

Wood suggested that compressive membrane action can be induced in simply-supported slabs by using prestressing. This leads to design of slightly thinner slabs. However, excessive compression may lead to violent collapse.

5.2 Taylor, Maher, Hayes and Morley's Work

Taylor, et al (48), suggested a possible basis for incorporating membrane action into the design of simply-supported slabs. Figure 53 illustrates a uniformly loaded simply-supported square slab with large deflections after the yield-line pattern has formed. In the central region of the slab the cracks will have penetrated the entire slab depth at this stage.

From the equilibrium condition of Segment A (see Fig. 53), it is evident that the total tension in the reinforcement shown in elevation must be balanced by the total compression in the compression zones at each end of the segment. These forces will balance each other if the entire system of yield-lines is considered. However, they will not be in equilibrium along each part of the yield-line as assumed in Johansen's yield-line theory. In other words, the lower region of the yield-line is in tension and the upper, outer region in compression. The effect of the change of geometry due to deflections is simply to increase the effective lever arm of the internal forces.

Consider a square slab of side L carrying a uniformly distributed load of w per unit area. If the equilibrium of Segment A is considered by taking moments about the support line, the following equation can be written for a particular slab deflection:

$$\frac{wL^2}{24} = y \sum T \qquad\qquad \text{Eq. (29)}$$

where   T = total tensile force in reinforcing steel

y = distance from centroid of steel to centroid of concrete compression

Taylor obtained load-deflection curves from calculations based on Eq. 29. These agree well with experimental data after the development of the yield-line pattern, as shown in Fig. 54. The figure shows the theoretical curve starting from the Johansen load. This is because the method is based on a rigid-plastic approach and curvatures prior to Johansen's load are
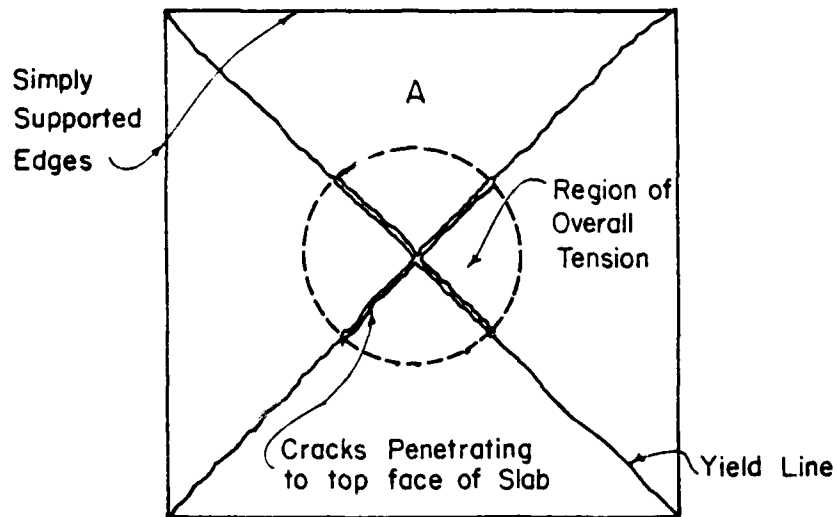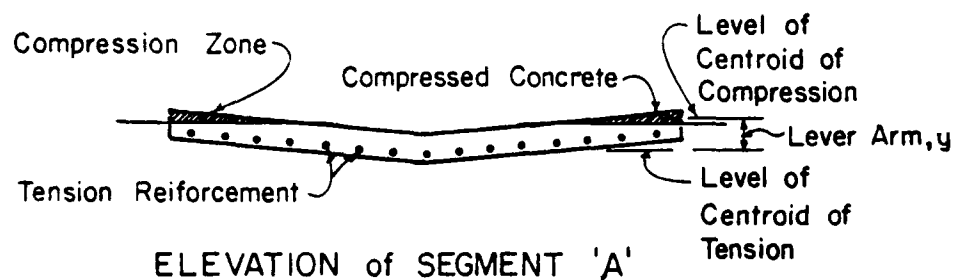
Fig. 53   Tensile Membrane Action in Uniformly Loaded
Simply-Supported Slab   - Taylor
(from Ref. 49)

-72-
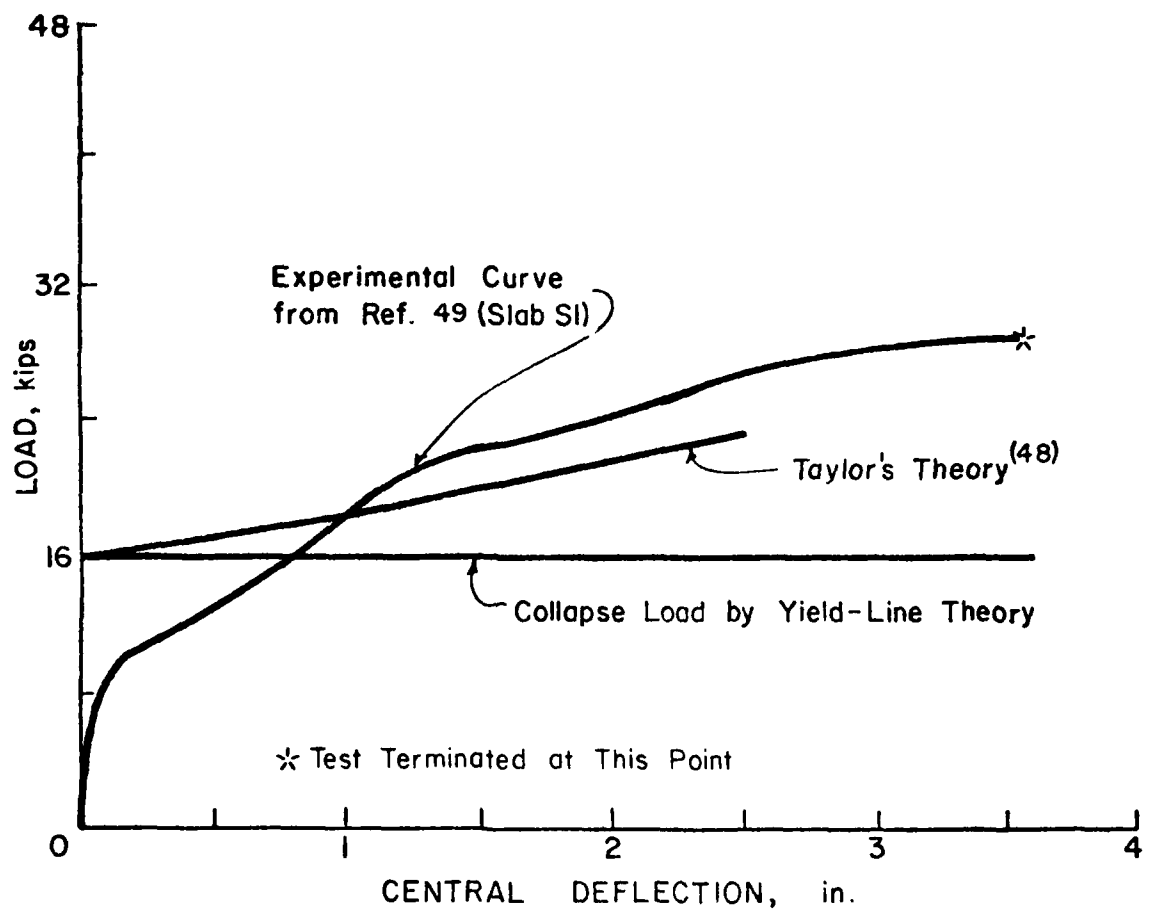
Fig. 54 Comparison of Theoretical and Experimental
Relationships for a Simply-Supported
Square Slab — Taylor (from Ref. 48)

neglected. Also, for the most part, the experimental curves give a higher load carrying capacity, due largely to the strain hardening of the reinforcement at large deflections.

Taylor, Maher and Hayes tested ten two-way, simply-supported slabs to investigate the effects of reinforcement arrangement and slab-depth ratio on slab behavior. The slabs were designed to have the same maximum flexural resistance under uniform loading. Slab properties are given in Table 2. As Fig. 55 shows, Slabs S1, S7, and S9 had uniformly spaced reinforcement parallel to the slab edges. Slab S6 had reinforcement placed diagonally and the remaining six slabs had variable reinforcement.

The slabs were loaded at sixteen uniformly spaced points by means of small hydraulic jacks. The loading of specimens was terminated because of excessive deflections at the center and rotation of the supports. As the load-deflection curves in Fig. 56 indicate, the specimens withstood appreciable deflection without any noticeable decrease in slab capacity. The tests were terminated because of excessive deflections at the center and rotations at the supports. Often there was no fall-off in load-carrying capacity of the slab specimen. The incipient collapse deflection capacity was not recorded. Associated cracking patterns are shown in Fig. 57.

In the 2-in. thick slab specimens, S1-S6, deflections remained small up to initiation of cracking. The deflections then increased more rapidly. The variably reinforced slabs were slightly stiffer than the uniformly reinforced slabs. However, the stiffness of slabs with stopped-off bars deteriorated rapidly after formation of a square yield pattern following approximately the line of the ends of the stopped-off bars. This is pattern C shown in Fig. 57. In the 1-1/2-in. thick Specimens S7 and S8, deflections increased more rapidly than in the 2-in. thick slabs, S1-S6. Again, the variably reinforced Slab S8 was also observed to be slightly stiffer than the uniformly reinforced Slab S7.

In the two 3-in. thick slabs, the cracks did not occur until the design capacity had been exceeded. Because of the low percentage of reinforcement, the cracks widened very rapidly and extended to the top surface in the central region. Load-deflection curves for the two slabs were very similar and the maximum loads recorded were the same, as shown in Fig. 56.

Taylor, Maher and Hayes drew the following conclusions for simply-supported square slabs:

1. In slabs designed by the yield-line method, the use of variable spaced bars will lead to minimal economy, if any, compared with uniformly-spaced bars. Stopping-off bars, however, will effect some economy.
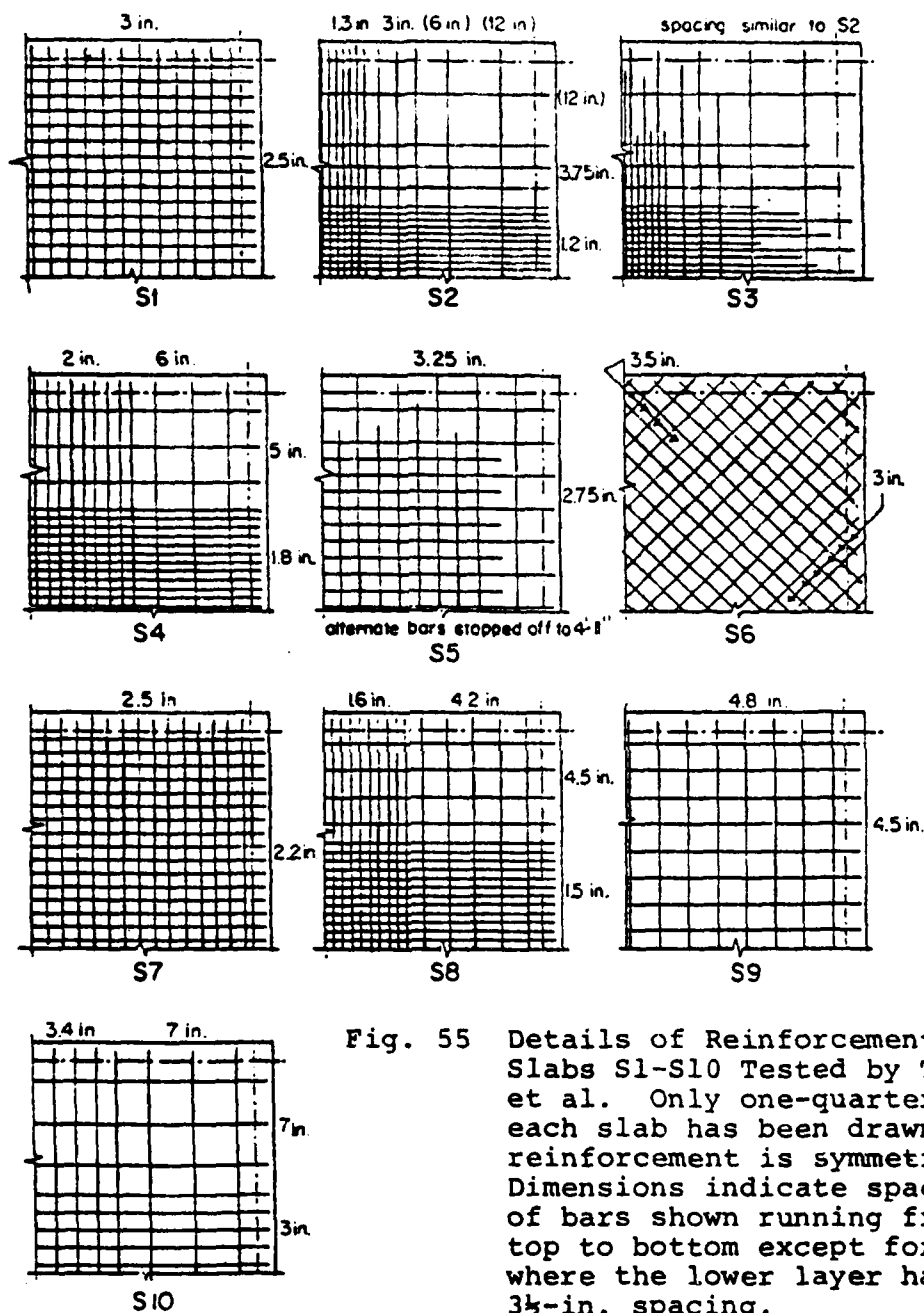
Fig. 55 Details of Reinforcement for Slabs S1-S10 Tested by Taylor, et al. Only one-quarter of each slab has been drawn, as reinforcement is symmetrical. Dimensions indicate spacing of bars shown running from top to bottom except for S6 where the lower layer has the 3½-in. spacing.

(from Ref. 49)
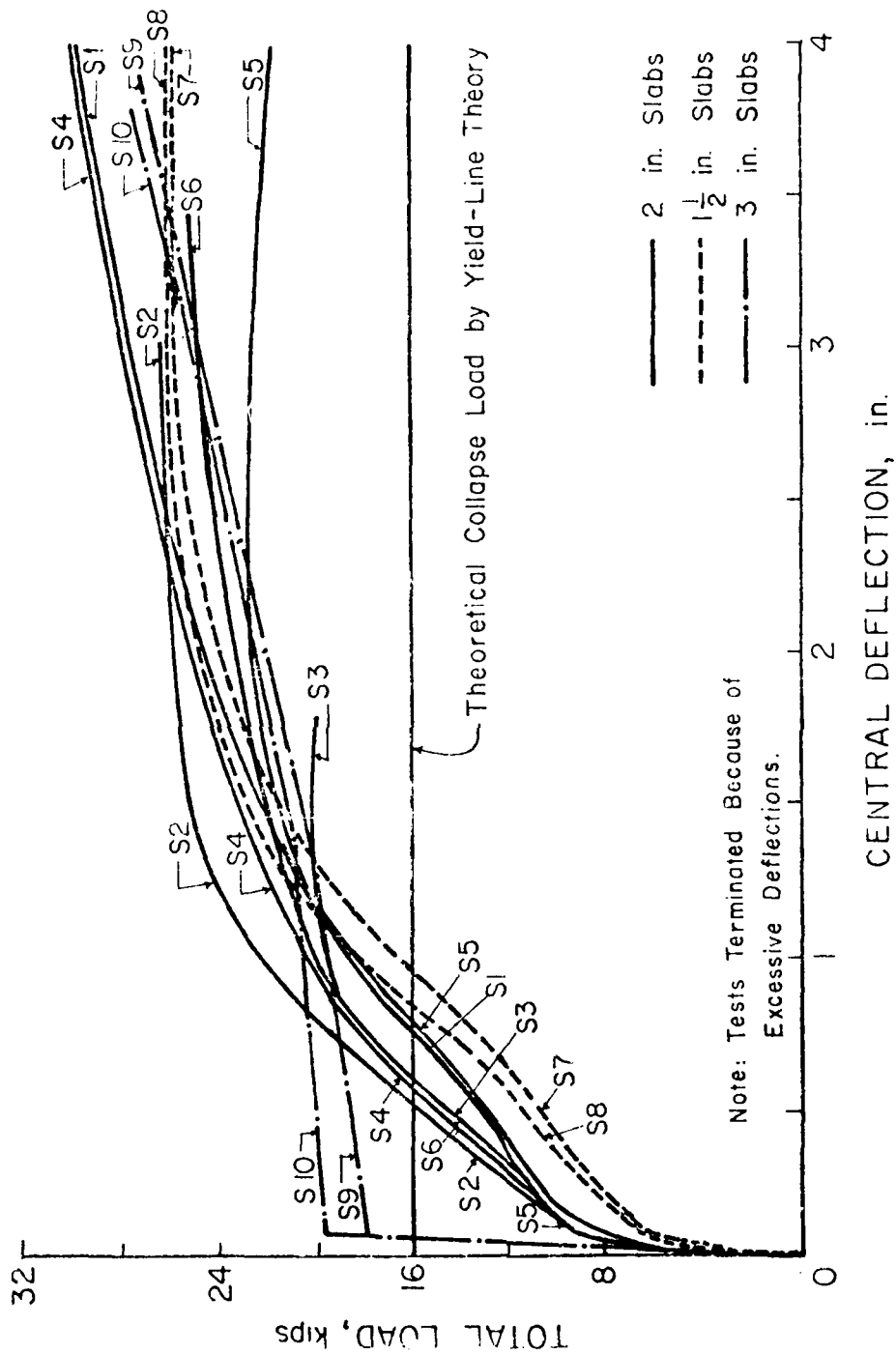
Fig. 56 Load-Deflection Curves for Slabs S1-S10 Tested by Taylor, Maher and Hayes (from Ref. 49)
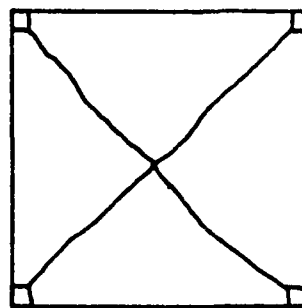
S1, S9, S10

(a)
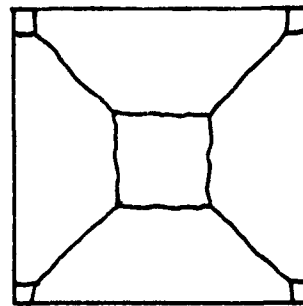
S2, S4, S7, S9

(b)
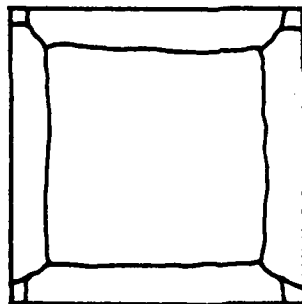
S3, S5

(c)
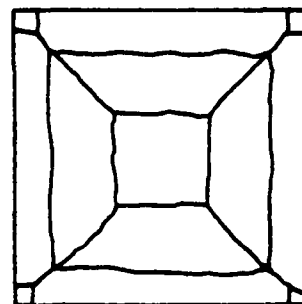
S6

(d)

Fig. 57   Different Yield-Line Patterns for
Slabs S1-S10 Tested by Taylor,
Maher and Hayes (from Ref. 49)

2.   Variably-reinforced slabs are slightly stiffer than uniformly-reinforced slabs over the initial load range up to the Johansen load.

3.   All slabs sustained loads higher than that predicted by yield-line theory, partly because of tensile membrane action. The enhancement depends on the particular yield-line pattern by which the slab achieves the Johansen load. For slabs with stopped-off bars, the enhancement is small.

4.   The use of variable reinforcement does not lead to higher enhancement of load-carrying capacity.

5.   The use of variable reinforcement reduces crack width in the central region of slabs, but increases the crack widths in the corner regions.

5.3 Work at U.S. Army Engineer Waterways Experiment Station

Geymayer and McDonald (51) at the U.S. Army Engineer Waterways Experiment Station tested seven simply-supported, thin, square, slab specimens under uniformly distributed loading. The objective of this investigation was to determine the influence of reinforcing details on the yield-line pattern and load-carrying capacity of the slabs. Variables selected were geometry and number of bent or terminated bars, corner reinforcement, and column strip width. Specimens had a clear span of 60 inches and a uniform overall thickness of 1 inch. The mid-span reinforcement ratio was 0.8%. The specimen properties are listed in Table 2.

The tests were stopped well before the incipient collapse deflection capacity of the specimens was reached. Maximum deflection recorded was about 4 in., i.e., 4 times the slab thickness, as shown in Fig. 58. The corresponding maximum edge rotation was about 8 degrees. The following conclusions were drawn:

1.   Small variations in reinforcing details, although normally not considered in analysis, may significantly affect the load-carrying capacity and yield-line pattern of reinforced concrete slabs. In general, corner reinforcement increases and bent bars decrease slab capacity.

2.   Formation of a yield-line system does not result in immediate collapse.

3.   Variations in reinforcing details within the range of the ACI recommendations (26) do not significantly affect slab deflections under working loads.
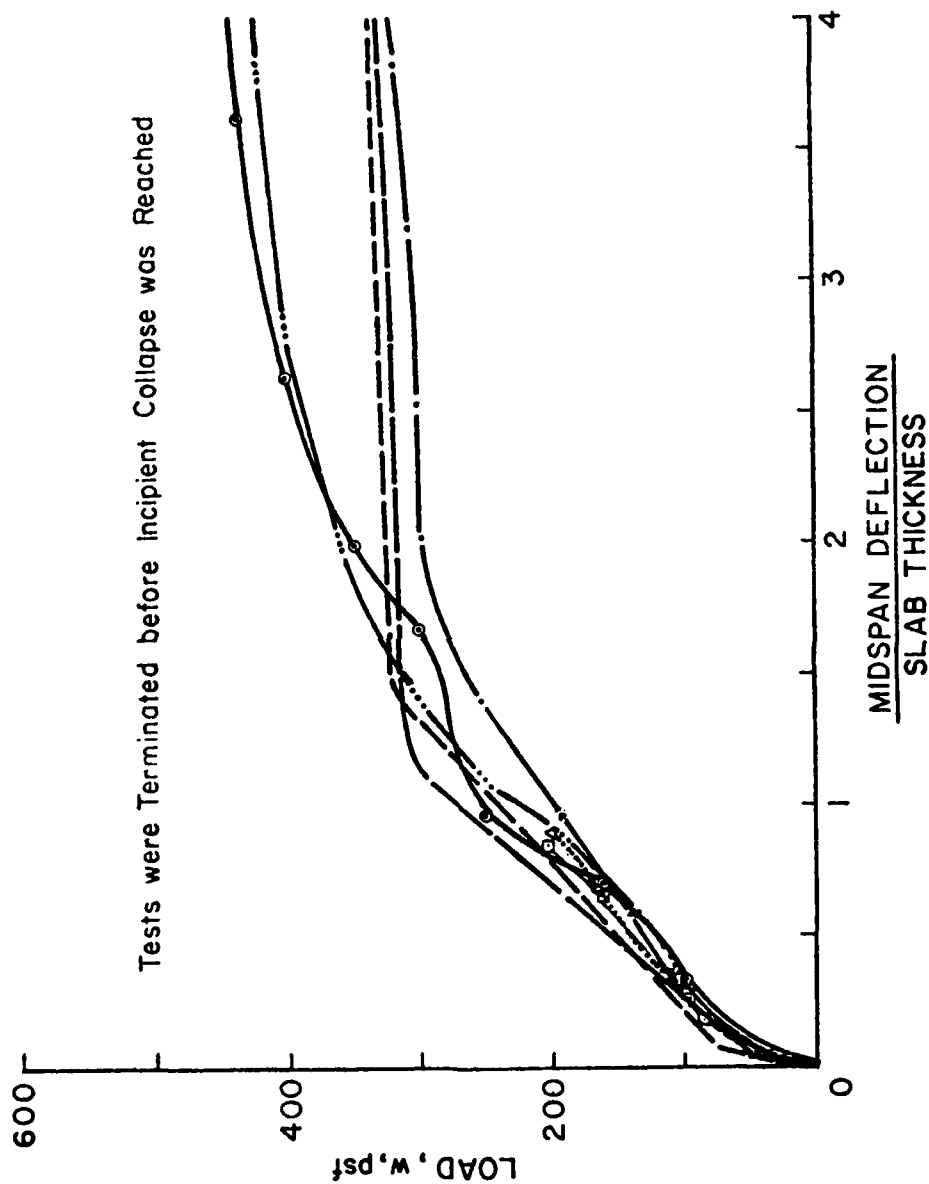
Fig. 58 Load-Deflection for Simply-Supported Slabs with
Various Reinforcing Details Tested by Geymayer
and McDonald (from Ref. 51)

5.4   Sawczuk and Winnicki

Sawczuk and Winnicki (18) tested three types of two-way simply-supported slabs, using two identical specimens for each type. Reinforcement and aspect ratio were the two variables investigated. Geometric and material properties of the slab specimens and some test results are listed in Table 2. The load-deflection relationship, Figs. 59 through 61, show the significant influence of tensile membrane action on both strength and deformation capacity of slabs. The tests were stopped before the incipient collapse deflection capacity was reached. Membrane action is accompanied by large permanent deflections, as shown in Fig. 62.

Sawczuk and Winnicki observed that tensile membrane action is localized in yield-line zones. Membrane action causes steel to go into the strain-hardening range. This enhances the load-carrying capacity of slab. The influence of strain-hardening on slab capacity is relatively easy to calculate by using the breaking strength in place of the yield strength in the calculations.

To determine the complete load-deflection relationship of slab specimens, Sawczuk and Winnicki presented a kinematical approach for the analysis of membrane action in simply-supported slabs. Based on kinematically admissible collapse modes, dissipation functions were established. Axial forces and moments at the yield sections were considered dependent on deflections. The resulting load-deflection relationships were linear, as shown by the dashed curves in Figs. 59 through 61.

In computing total deflection, elastic deflections were added to post-yield deflections. This method of simple addition is not fully justified and represents an approximation. In computing elastic deflection, it was assumed that up to the yield limit, W_j, a slab is linearly elastic. Beyond this stage the slab was assumed to be perfectly plastic. The upper theoretical curve corresponds to the ultimate steel stress, f_u, while the lower theoretical curve corresponds to the steel yield stress, f_y. As Figs. 59 through 61 show, there is good agreement between the theoretical and experimental curves.

5.5   Kemp's Work

Kemp (14) suggested that the increase in strength in simply-supported slabs arises partly from tensile membrane action produced in the central region of the slab and partly from the increased yield moment in the outer regions where compressive membrane action occurs. Kemp presented an upper bound solution for simply-supported slabs that accounts for the effect of membrane action. The approach follows Wood's (4) method for circular isotropic slabs and is limited to square isotropic slabs.
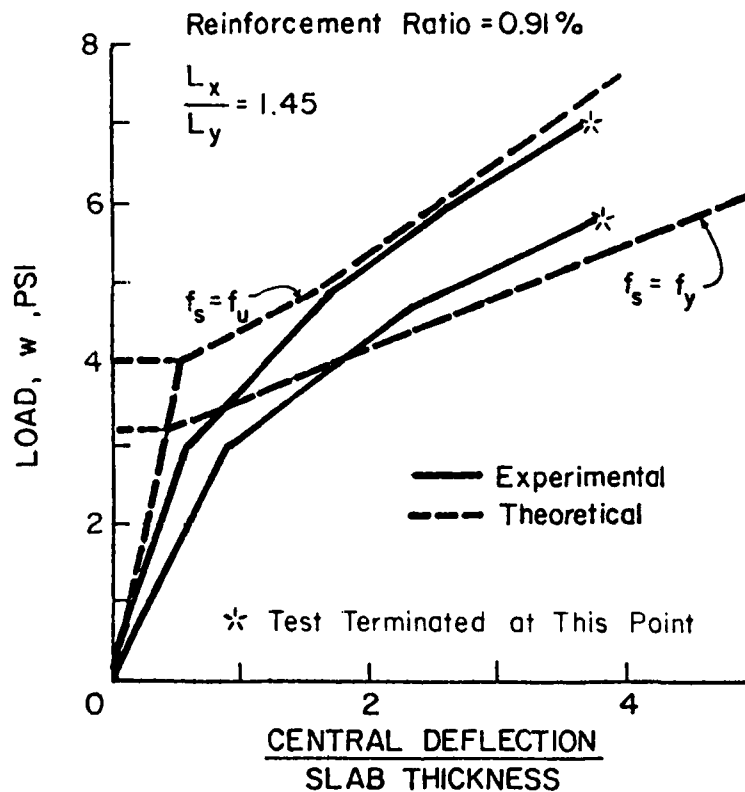
Fig. 59 Comparison of Experimental and Theoretical
Load-Deflection Relationships for Slabs I2,
with L_x/L_y = 1.45 and Reinforcement
Ratio = 0.91%   (from Ref. 18)
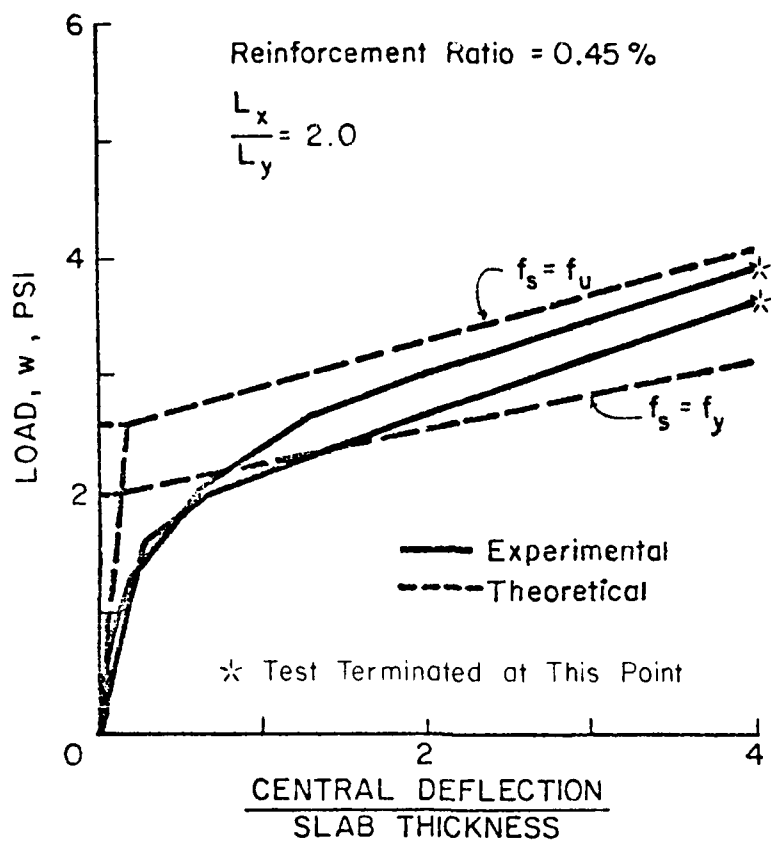
Fig. 60   Comparison of Experimental and Theoretical
Load-Deflection Relationships for Slabs I1,
with L_x/L_y = 2.0 and Reinforcement
Ratio = 0.45% (from Ref. 18)
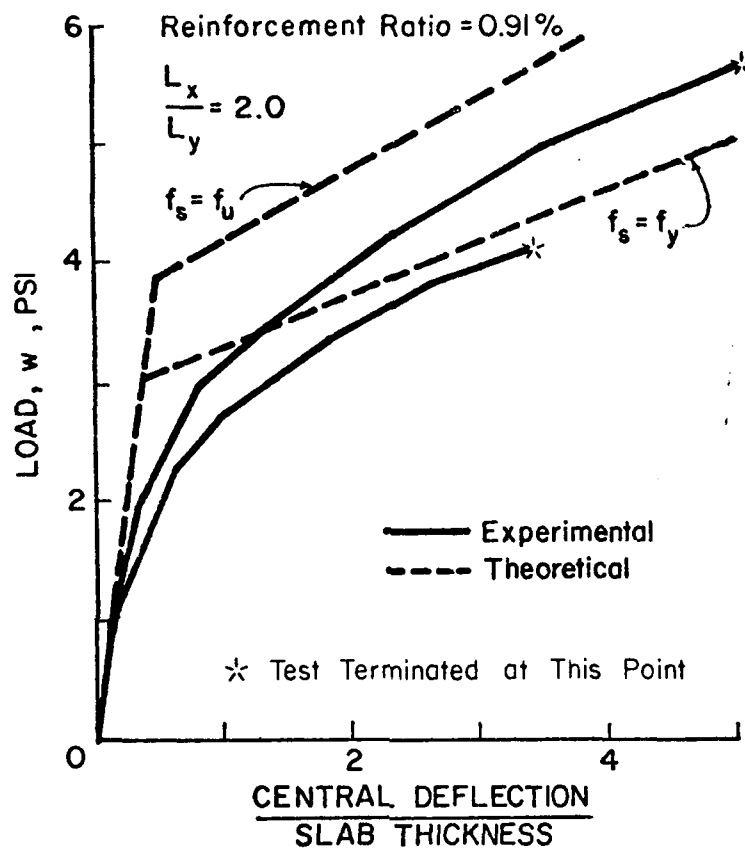
Fig. 61   Comparison of Experimental and Theoretical
Load-Deflection Relationships for
Slabs IT1, with L_x/L_y = 2.0 and
Reinforcement Ratio = 0.91% (from Ref. 18)
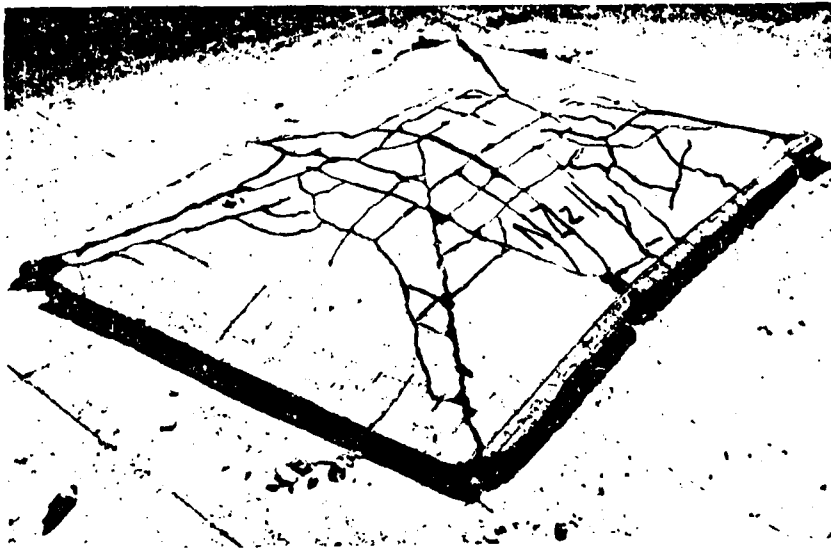
Fig. 62   Permanent Deflection of a Slab Due to
Membrane Action and Bending - Sawczuk
and Winnicki (from Ref. 18)

Assuming the slab to be made up of rigid-plastic material, stress resultants were obtained from the geometry of rigid regions and their horizontal equilibrium under membrane forces. It was concluded that for low percentages of reinforcement, enhancement in slab strength was pronounced and that a saving in reinforcement was possible by allowing for membrane action.

5.6 Brotchie and Holley's Work

Brotchie and Holley (33) tested four simply-supported slabs. All slabs were square, spanned 15 in., and were uniformly loaded. Slab specimens were reinforced near the bottom only with smooth steel wire uniformly and equally distributed in each direction. Material and geometric properties of the specimens are listed in Table 2. Reinforcement ratio and span-depth ratio were the two variables investigated.

Measured load-deflection relationships are shown in Figs. 63 and 64. The figures show that reinforcement ratio has an important effect on slab behavior. As Fig. 63 illustrates, the 'fully reinforced' slab (p = 0.03) shows a peak in resistance followed by instability. With further increase in slab deflection, the slab resistance increases as a result of tensile membrane action. The lightly reinforced slab (p = 0.01), on the other hand, exhibits a relatively flat post-yield slope with no strength increase.

The question of the applicability of the results of these small-scale slab tests to full-scale slab systems was considered. Brotchie maintained that the results should apply to full-scale slabs provided that the same geometric proportions, reinforcement ratios, and material strengths are used.

Hayes (50) presented an equilibrium approach to allow for the membrane action in reinforced concrete slabs. The method is quite similar to that of Sawczuk and Winnicki (18) except that Hayes used an equilibrium approach instead of an energy approach. He assumed that in-plane plastic hinges are formed on the long side, and that in-plane forces exist along the yield lines. The magnitudes of axial and shear forces were calculated by using in-plane equilibrium of the rigid portions between the yield-lines. Moments of the forces were taken about the in-plane plastic hinges. The load-deflection relationship thus obtained was linear and similar to that shown in Fig. 52. Analysis showed that the membrane forces were independent of deflection, a conclusion that does not appear to be reasonable.

Hayes (50) also tested slabs to verify the analytical work. However, no details are available on the geometry or material properties of the slab specimens.
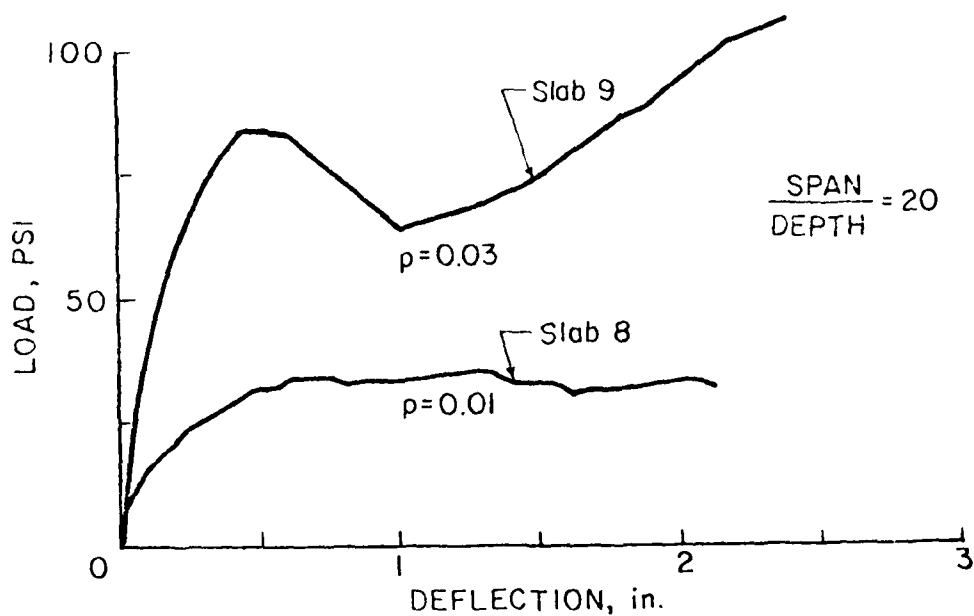
Fig. 63 Load-Deflection Relation for Simply-Supported
Slabs Tested by Brotchie and Holley
(from Ref. 33)
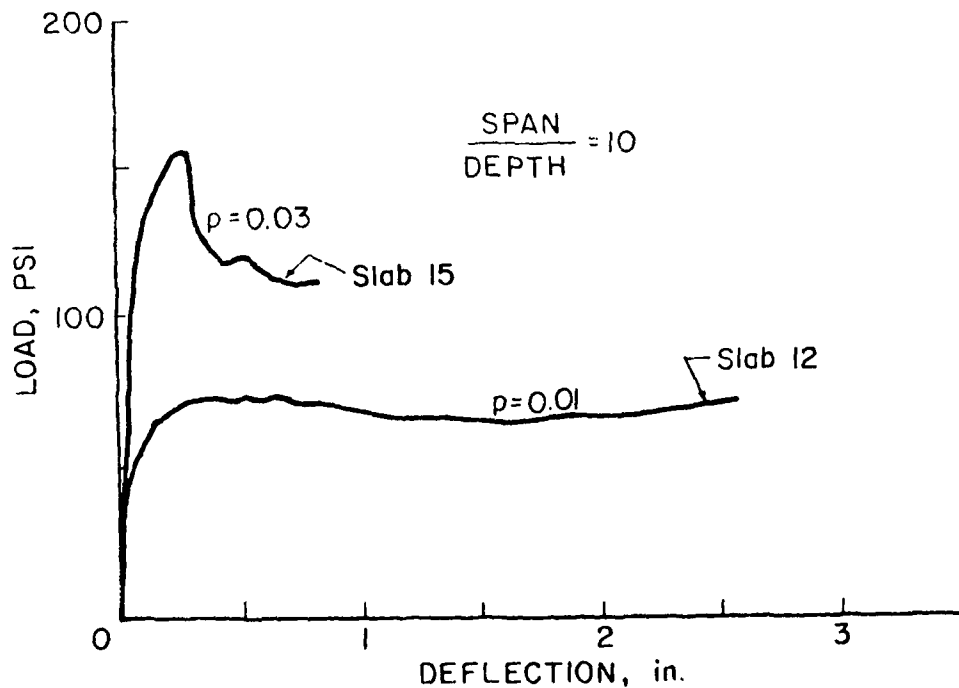
Fig. 64 Load-Deflection Relation for Simply Supported
Slabs Tested by Brotchie and Holley
(from Ref. 33)

5.7 Desayi and Kulkarni's Work

Desayi and Kulkarni (52) presented the most notable work on the load-deflection behavior of simply-supported reinforced concrete slabs. Their investigation included both analytical and experimental work. The analysis to determine the load-deflection characteristics was carried out in two stages. In the first stage, a semi-empirical method was used for calculating deflection up to the Johansen load. In the second stage, membrane action was taken into consideration in predicting load-deflection behavior beyond Johansen's load.

Desayi and Kulkarni followed the CEB method (53) for calculating the load-deflection relationship up to the Johansen load. Figure 65 shows the three-segment idealized load-deflection curve used in the analysis. The reduction in flexural rigidity with increasing load signifies concrete cracking and steel yielding in the slab. Empirical constants were introduced to determine the efective flexural rigidity in Segments 2 and 3 in Fig. 65.

To calculate load-deflection behavior beyond Johansen load, Kemp's approach (14) for square slabs was used with two modifications. First, the method was generalized for rectangular orthotropic slabs. Second, effects of deflection prior to the Johansen load on the neutral axis depth and the membrane forces were considered. To simplify the analysis, yield lines were assumed to make a 45° angle with the edges, as shown in Fig. 66.

Twelve slabs were tested by Desayi and Kulkarni to verify their analytical approach. The three variables investigated were aspect ratio, span-depth ratio, and coefficient of orthotropy. The coefficient of orthotropy represents the ratio of the design yield moments along the two principal directions. Details of slab properties are listed in Table 2.

The experiments were stopped before reaching incipient collapse deflection capacity of the specimens. The main reason was the excessive slab deflection and instability of loading system at the large deflection levels. Computed and experimental load-deflection curves for Specimen S4 are shown in Fig. 67. The two computed curves shown in the figure correspond to the two assumed values of steel stress at the Johansen load, namely, yield stress, f_y, and breaking stress, f_u. The figure also shows the theoretical load-deflection relationships obtained by Morley (28) and Hayes (49).

It was concluded in this investigation that the use of steel breaking stress instead of yield stress provided better agreement between analytical and experimental curves. No data is available on experimental load deflection relationship at the incipient collapse deflection capacity.
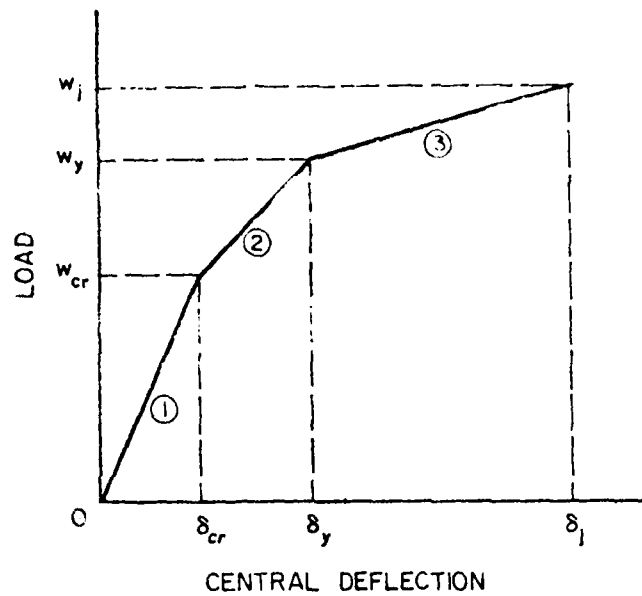
Fig. 65   Assumed Load-Deflection Behavior for
Simply-Supported Slabs Up to Johanser
Load - Desayi and Kulkarni
(from Ref. 52)
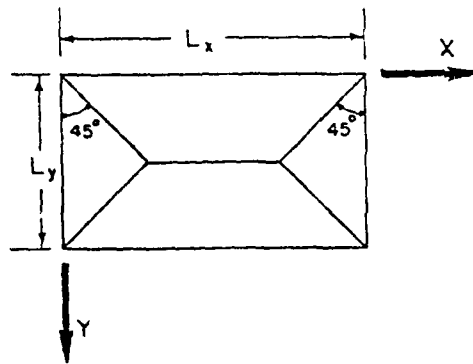
Fig. 66   Assumed Collapse Mechanism at Yield-Line
Load - Desayi and Kulkarni
(from Ref. 52)
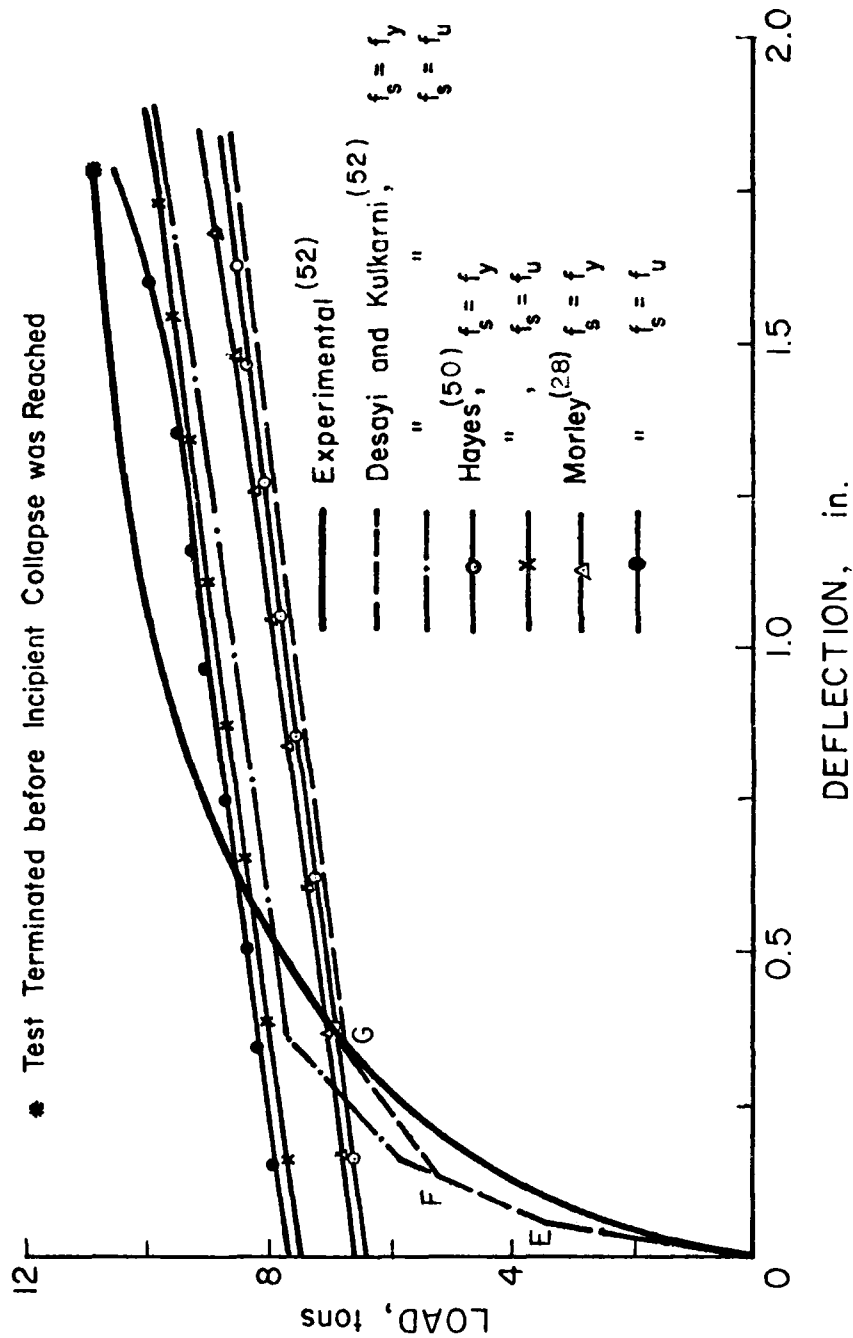
Fig. 67 Comparison of Theoretical and Experimental Results for One-Way
Slab Specimen (from Ref. 52)

6.   MEMBRANE ACTION IN ONE-WAY SLABS

6.1 Christiansen's Work

Christiansen (54) tested four one-way slabs restrained along parallel edges. The strips were 3-in. thick, 6 in. wide, had a clear span of 5 ft, and were loaded with a concentrated load at their midspan. Also tested was an identical set of four slab strips that were simply-supported. The purpose of these tests was to gain greater understanding of arching action in two-way slabs.

The ratio of slab capacity, W_D, to Johansen's yield-line load varied between 1.42 and 3.83. To show the effect of arching action on slab strips, Christiansen calculated load-deflection curves for simply-supported slabs of identical dimension using bending theory. Experimental load-deflection curves for a pair of restrained and unrestrained slab specimens are shown in Fig. 68. The vertical distance between the two curves represents the load carried by arching.

By considering the outward support movement, slab shortening due to axial force, and slab lengthening due to hinge rotation, Christiansen determined the depth of concrete in compression. The resultant compressive forces at the support and midspan were assumed to induce arch action in the slab. Maximum load that could be carried by the arching action was calculated by maximizing the moment due to arching forces. Using this approach, a good comparison between experimental and theoretical results was obtained. However, analysis was not generalized for two-way slabs.

Since the tests were not carried into the tensile membrane regime, no information on the incipient collapse deflection capacity of one-way strips can be derived from this experimental investigation.

6.2 Roberts' Work

Roberts (55) tested 36 strips representing one-way slabs. The purpose here was to gain an understanding of strip action as a basis for explaining compressive membrane action in two-way slabs. The strips were restrained against longitudinal expansion in a specially designed frame, shown in Fig. 69. The strips were loaded by several point forces to simulate uniformly distributed loading. Properties and test results of all thirty-six strips are listed in Table 3. A representative load-deflection curve is shown in Fig. 70. The following conclusions were drawn from the test results:

1.   The ratio of peak load to that given by Johansen's yield-line theory varies from approximately 17 for strips with high concrete strength and a low percentage
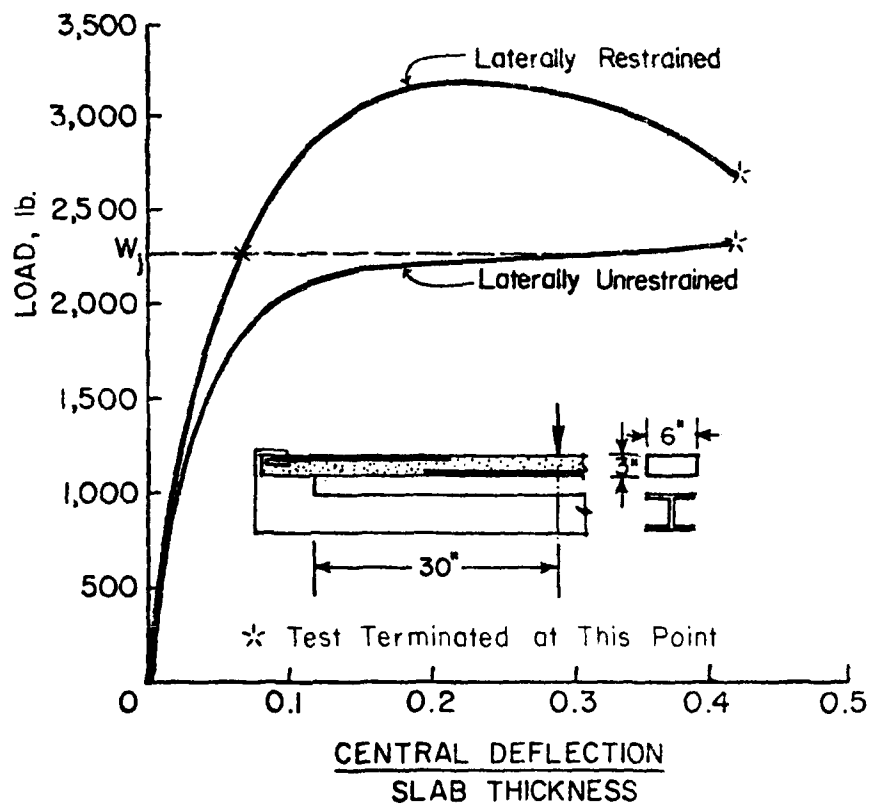
Fig. 68   Details and Load-Deflection Curves for
One-Way Slab Strips Tested
by Christiansen
(from Ref. 54)
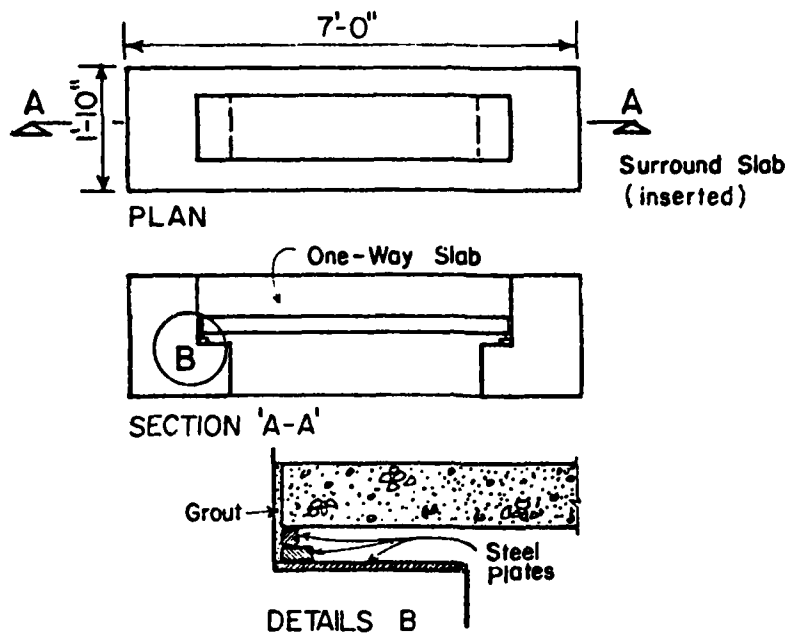
Fig. 69   Details of Surrounded and Strip
Support - Roberts (from Ref. 55)
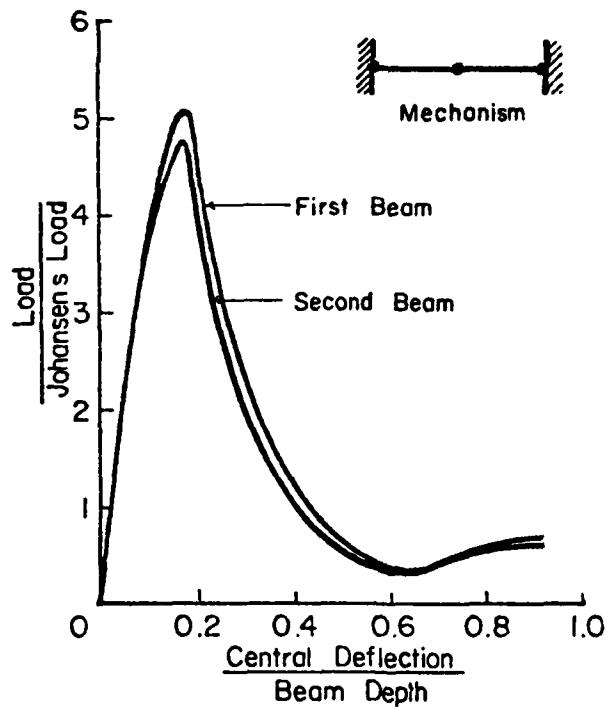
Fig. 70   Experimental Load-Deflection Curves
for Beams RB23 Tested by Roberts
(from Ref. 55)

of reinforcement, to 3 for beams with low concrete strength and a high percentage of reinforcement.

2. Deflection at maximum load is not a fixed proportion of the strip thickness. The average value of δ_D/h was 0.27 for 2-in. thick strips and 0.16 for the 3-in. thick beams.

3. It is not necessary for the restraint to have enormous stiffness to develop enhanced peak loads. Theoretically, the load is increased by 10% when the restraint stiffness, initially equal to that of the beam, is increased eleven times.

4. Comparison between theoretical and experimental deflections was not satisfactory due to the neglect of elastic curvatures in the analytical model.

6.3 Park's Work

Park (24) calculated load-deflection curves corresponding to the strips tested by Roberts (55). One such comparison, shown in Fig. 71, indicates the peak load predicted by the theory to be conservative. It will be noted in Fig. 71 that the load on the actual slab decreases more rapidly than that predicted by the theory. Also, deflection at Johansen's yield-line load is zero. Park explained these discrepancies as follows:

1. The theory assumes concrete strength to be the uniaxial value. In the test, the concrete at the strip ends was confined transversely by the friction between the strip end and the restraining frame. Roberts (18) showed experimentally that concrete strength at the strip ends was about 2,000 psi greater than the cylinder strength.

2. The theory assumes that the concrete compressive stress block parameters remain at the ACI (26) values. However, at high strains the stress block parameters will change and concrete cracking will occur.

3. The theory assumes that concrete stress-strain properties are reversible as the neutral axis decreases. In reality, permanent set occurs on reversal of strain.

4. Initial strip behavior is mostly elastic. Plastic theory neglects this portion of the test.

6.4 Other Investigations

Geymayer and McDonald (51) at the U.S. Army Engineer Waterways Experiment Station tested two one-way slab strips. The strips were simply-supported and loaded equally at the middle-third
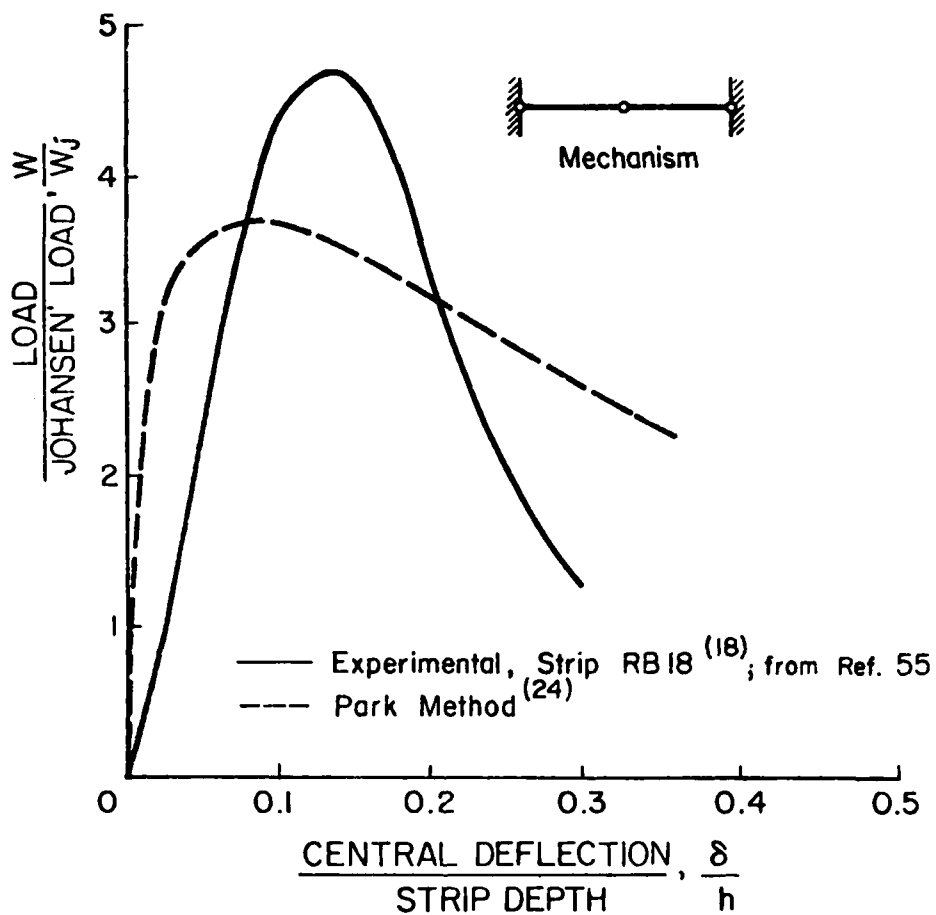
Fig. 71   Comparison of Experimental and Theoretical
Load-Deflection Relationships for One-Way
Slab Strip   (from Ref. 24)

points. The strips were quite slender, with a span-depth ratio of 60. Material and geometric properties are given in Table 3.

The experimental load-deflection curves, shown in Fig. 72, indicate a considerable loss of slab stiffness first at the onset of cracking and then at steel yield. Observed slab strength was higher than that predicted by Johansen's yield-line theory, as indicated in Table 3. The loading was stopped when the strip deflected 2 to 2.5 times the strip thickness.

Iqbal (54) investigated the effect of steel properties on load-deflection behavior of one-way slabs. Two strips were tested. One was reinforced with hot-rolled steel having a definite yield plateau and the other with cold-rolled steel with no definite yield point or plateau. The strips were loaded symmetrically at their middle-third points. The strip properties are given in Table 3.

Observed load-deflection curves are shown in Fig. 73. Both specimens showed a resistance slightly greater than that predicted by Johansen's yield-line theory. In the post-yield range, the strip reinforced with steel having a definite yield plateau sustained the ultimate load with large deflections. However, the resistance of the other strip dropped due to loss of bond between the steel and surrounding concrete. Permanent deflection of one strip after unloading is shown in Fig. 74.

Birke (57) developed a relationship between ultimate moment due to compressive membrane action and the span-to-thickness ratio. The relationship is applicable to slabs with a single load at midspan. The edge restraint may be full or partial.

Komoro (58) developed a method to compute the load-deflection relationship of one-way reinforced concrete slabs under a single load at midspan. Sixteen slabs were tested to confirm the accuracy of the approach. The main conclusions from the tests are as follows:

1. Magnitude of the compressive membrane force at supports changes with slab deflection.

2. Arching effect due to the compressive membrane force increases as span-depth ratio decreases.

3. The load-deflection curve for one-way slabs loaded at midspan, from zero load to the onset of tensile membrane action (point E in Fig. 3), can be calculated using Komoro's method.
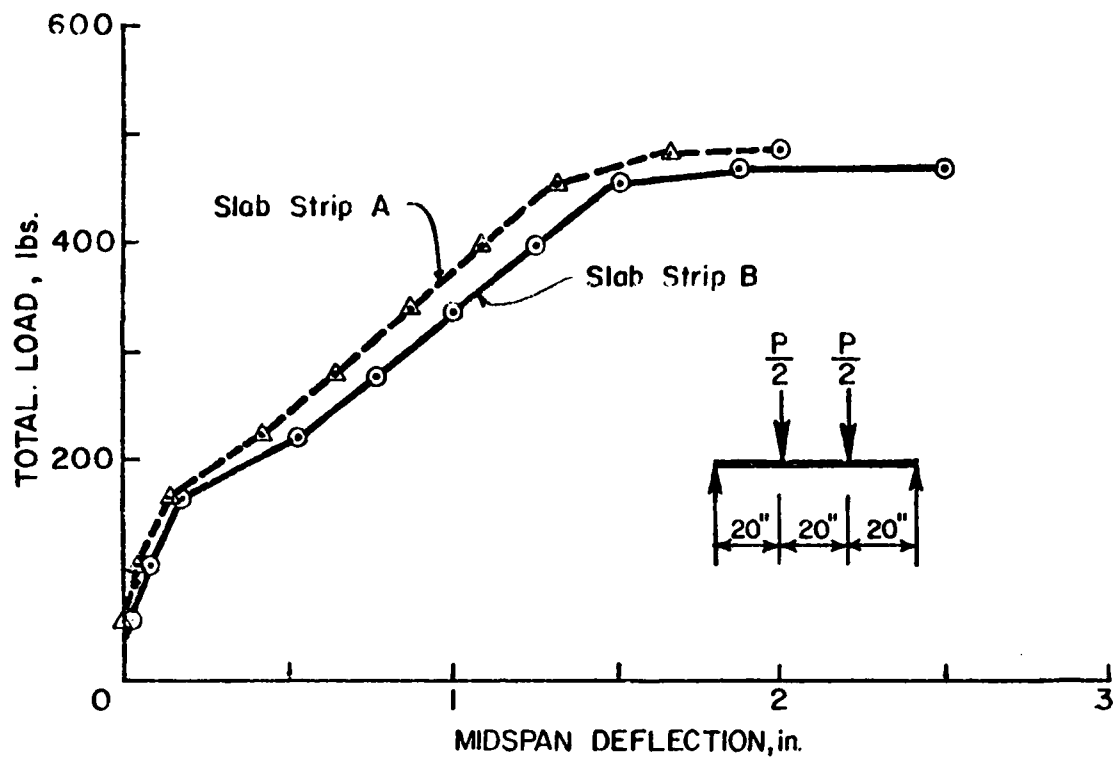
Fig. 72   Load-Deflection Relationship of One-Way
Simply-Supported Slab Strips Tested by
Geymayer and McDonald (from Ref. 51)
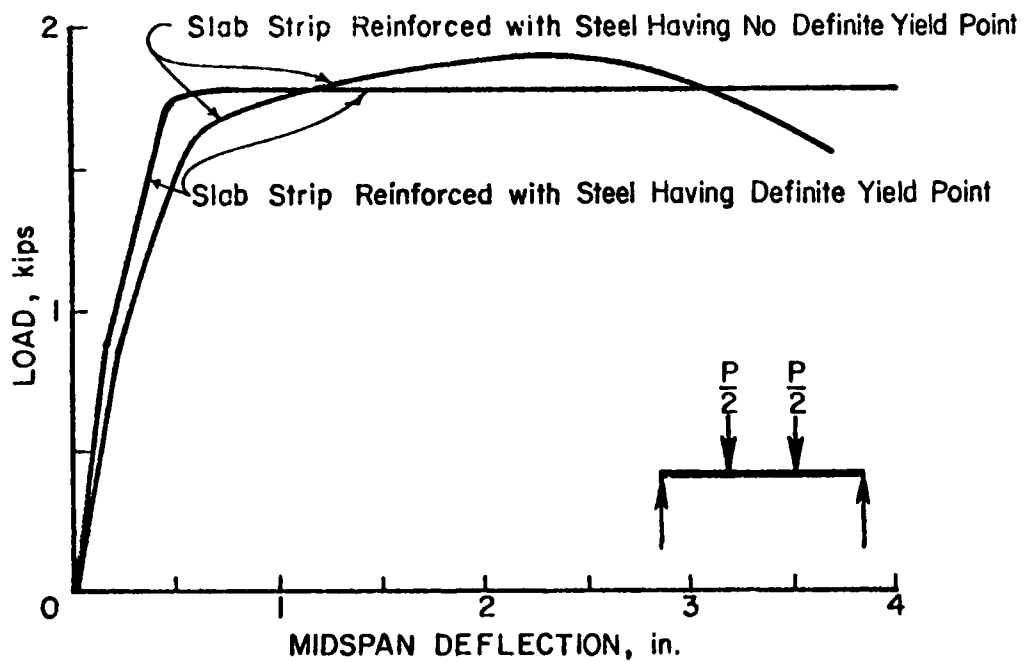
Fig. 73   Load-Deflection Relationship for One-Way
Slab Strips Tested by Iqbal
(from Ref. 56)

-96-

Fig. 74 Permanent Deflection and Cracking Pattern
of Simply-Supported Slab Strip at
Termination of Test - Iqbal (from Ref. 56)

7. NONLINEAR FINITE ELEMENT MODELS FOR REINFORCED CONCRETE SLABS

7.1 Review of Finite Element Models

With recent advances in computational methods, the finite element technique has become a powerful analytical tool. Several approaches have been used in modelling reinforced concrete. Bazant, Schnobrich and Scordelis (59) provide an excellent summary of work in this area.

Analysis of the behavior of reinforced concrete beams and slabs have received considerable attention from investigators (60-85). Two basic approaches have been used. These are the modified stiffness approach and the layered element approach.

An early application of the finite element method to reinforced concrete was carried out by Ngo and Scordelis (60). They developed an elastic two-dimensional model of reinforced concrete beams with defined crack patterns. Bond slip between concrete and steel bars was modeled by finite spring elements designated as bond links spaced along the bar length. Cracking was modeled by separation of nodal points and a redefinition of structural topology.

Nilson (61) extended Ngo and Scordelis' work by including nonlinear properties. This approach has not achieved popularity due to the difficulties encountered in redefining the structural topology after each load increment. Mufti, Mirza, McCutcheon and Houde (62) used the same model, but without modifying the topology. They deleted the cracked element from the overall stiffness. Forces in the cracked element were redistributed during the next cycle.

Rashid (63) introduced another approach in which the cracked concrete was treated as an orthotropic material. Steel elements were assumed to be elastic/perfectly plastic. The von Mises yield criterion and the Prandtl-Reuss flow equations were used to define the behavior of the steel in the range of plastic deformation. This approach proved to be more popular and many investigators have used it with variations in material properties and modes of failure.

Isenberg and Adham (64) introduced a nonlinear orthotropic model and demonstrated its use on tunnel problems. The nonlinear stress-strain behavior of concrete and steel was idealized with bilinear stress-strain curves. Bond and the effect of lateral confinement on compressive and tensile strength were considered.

Valliappan and Doolan (65) studied the stress distribution in reinforced concrete beams, haunches, and hinges using an elasto-

plastic model for steel and concrete. The concrete was represented as a brittle material in tension.

Nam and Salmon (66) compared the constant stiffness and the variable stiffness approaches for nonlinear problems. Using a combination of isoparametric elements and bar elements, they found the variable stiffness approach to be far superior for problems involving the prediction of cracking in reinforced concrete structures.

Bell and Elms (67) presented a method for computing deflections and crack patterns of reinforced concrete slabs for the entire range of loading, i.e., from zero to ultimate. Triangular bending elements and the method of successive approximations were used. Cracking normal to the principal moment direction was accounted for by using a reduced stiffness. However, their analytically derived displacement curves did not agree well with selected experimental data. They also developed a partially cracked element, but found that analysis using this element was neither as accurate nor as well behaved as one based on either an elastic or a totally cracked element.

Jofriet (68,69) used a quadrilateral plate bending element with four corner nodes and three degrees of freedom at each node. Cracking on normals to the principal moment directions was accounted for by using a reduced stiffness for beams. Their research did not take into account load history or post-yield behavior.

Scanlon (70) presented a finite element analysis to determine the effects of cracking, creep, and shrinkage on reinforced concrete slabs. The finite elements consisted of a series of layers, each with a different plane stress constitutive relationship. Cracks progressed through the thickness of the element, layer by layer, parallel or perpendicular to the orthogonal reinforcement. The concrete was modeled as a linear elastic material in compression and an elastic brittle material in tension. The modulus in tension, after cracking, was obtained using a stepped stress-strain diagram. Stiffness of a layer was evaluated by superposing the stiffnesses of steel and concrete. The shear modulus of a layer, whether cracked or uncracked, was taken to be that of an uncracked plain concrete layer. It was found that tensile stiffening of concrete between cracked zones resulted in a significant redistribution of moments. Comparison made with the experimental data and theoretical results of Jofriet (68) showed good agreement, as indicated in Fig. 75. It will be noted that the range of slab deflection shown in Fig. 75 has a maximum value equal to 1% of slab span. This is considerably less than the experimental incipient collapse deflection capacity which ranges between 10 and 15 percent of the slab span.

Lin and Scordelis (71) extended the work of Scanlon to include elasto-plastic behavior for the steel in tension and compression
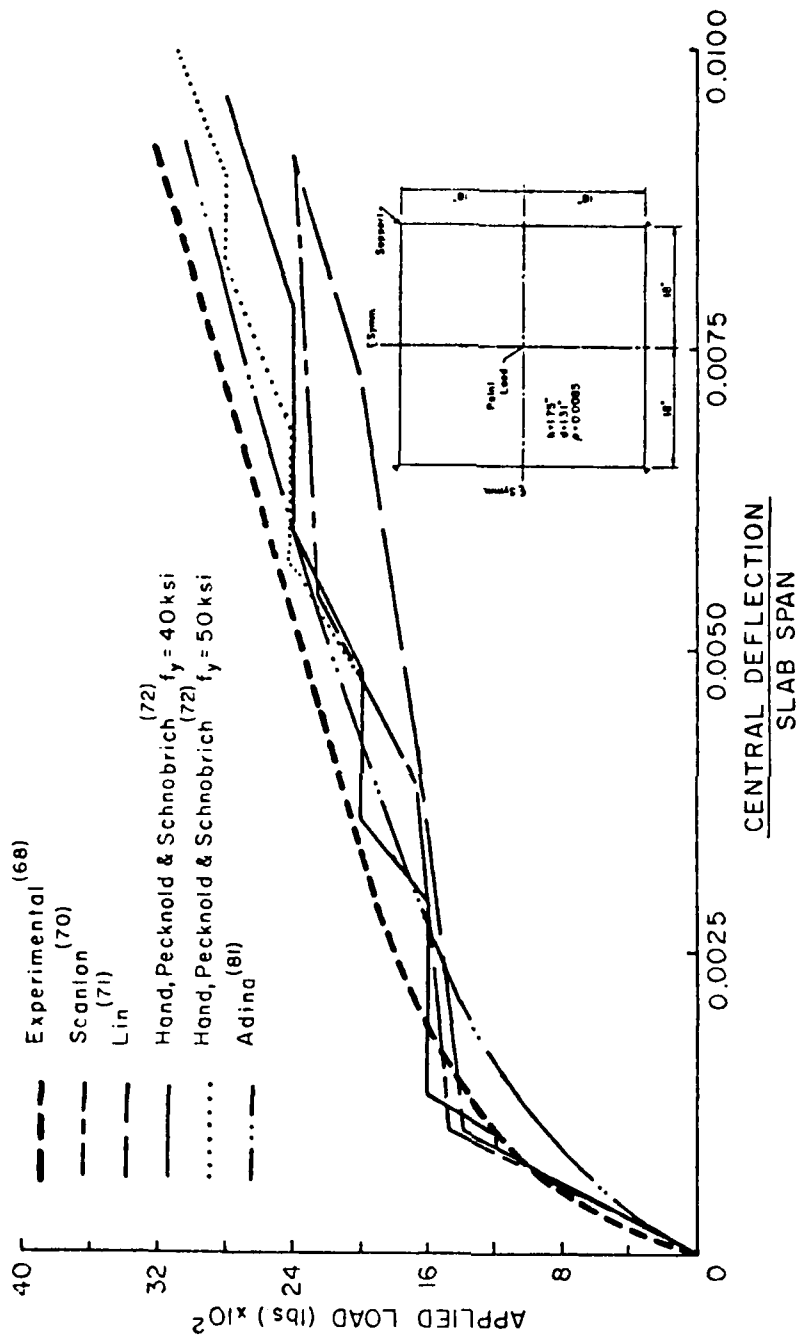
Fig. 75   Comparison of Experimental and Theoretical Load-Deflection
Curves for Corner-Supported Slab Tested by Jofriet (Ref. 68)

and for the concrete in compression. For tension in concrete, they replaced the actual curve by a triangular-shaped curve with a descending slope after initial tensile failure. The post-yield behavior was defined by von Mises' yield criterion. Incremental loading was used with iteration within each increment. A comparison of analytical results with Joffriet's (68) experimental load-deflection curve is shown in Fig. 75.

Hand, Pecknold and Schnobrich (72) used a layered element to determine the load-deflection history of reinforced concrete plates and shells of uniform thickness. The nonlinear behavior of steel and concrete was considered in the analysis. Steel was modeled as elasto-plastic; concrete was assumed to be elastic brittle in tension and to have a bilinear stress-strain relationship up to yield in biaxial compression. They used the strength envelope obtained by Kupfer, Hilsdorf and Rusch (73) as a yield criterion. A shear retention factor was introduced to provide torsional and shear stiffness after cracking. The layered finite element allowed the material properties to vary through the element depth. Bending and membrane forces were considered and a doubly curved rectangular shallow shell element with twenty degrees of freedom was used in the analysis. The authors stated that their numerical results were as good or better than the modified stiffness approaches, as shown in Fig. 75.

Wanchoo and May (74) introduced a layered model with concrete in compression and steel following the von Mises criterion. Concrete was elastic-brittle in tension. A rectangular finite element was used. Fig. 75 shows a comparison of the theoretical relationship with an experimental curve taken from Taylor, Maher and Hayes (49). The experimental slab was simply-supported and had a reinforcement ratio of p = 0.005 and an aspect ratio of 36. It is seen that the agreement is excellent both in linear elastic range and in the subsequent cracking range. However, the comparison is limited to a maximum deflection equal to 1.4% of the slab span and does not include larger deflection levels where effects of membrane forces are notable.

Wanchoo and May also obtained theoretical load-deflection relationships for clamped slabs. These relationships pertained to small deflections (range AD in Fig. 3) and did not cover the range where tensile membrane action is predominant. Also, no comparison was made with experimental results.

Kabir (79-80) modeled the reinforced composite section as a layered system of concrete and "equivalent smeared" steel layers. Perfect bond is assumed to exist between concrete and steel layers. Stiffness properties of an element are then obtained by integrating the contributions from all the layers across the section. Concrete behavior under the biaxial state of stress is represented by a nonlinear constitutive relationship that incorporates tensile cracking at a limiting stress,

tensile stiffening between cracks, and strain-softening phenomenon beyond the maximum compressive stress. Reinforcement is represented by a bilinear, strain-hardening model exhibiting the Bauschinger effect. The constitutive relations are based on small displacement theory. This may represent a serious shortcoming when applying the method to the analysis of slab behavior in the tensile membrane range.

Most recently, Bathe and Ramaswamy (81) developed a three-dimensional concrete model and incorporated it in the computer program ADINA (82). In this model, concrete is treated as a hypoelastic material based on a uniaxial stress-strain relationship that is generalized to take biaxial and triaxial stress conditions into account. Tensile cracking and compression crushing conditions are identified using failure surfaces. Figure 75 shows the load-displacement relationship predicted by ADINA for Jofriet's (68) test slab. It is seen that the analytical and experimental displacements compare reasonably well, particularly at the higher load levels. No results using ADINA are available for slabs tested to the point of incipient collapse. Bathe and Ramaswamy (81) point out that significant further studies, evaluations and improvements of the model are needed.

Another difficulty in using a finite element model to compute the entire load-deflection relationship of a restrained slab arises due to presence of an unstable region (DE in Fig. 3) in the load-deflection relationship. In this region, the load decreases, with increasing deflections. No finite element study is available which attempts to predict the behavior in this unstable region.

Analysis of reinforced concrete systems including cracking, nonlinear geometric and material properties involves complex problems of finite element modeling. Because of the nature of such nonlinear problems, even the speed and storage capacities of today's large digital computers are sometimes insufficient to provide solutions at reasonable costs. Despite some notable breakthroughs in the use of nonlinear finite element methods, no computer program is available that can be used to calculate the entire load-deflection relationship up to incipient collapse. In fact, no computer program has been found to adequately reproduce the load-deflection curve for a restrained slab even up to point E in Fig. 3.

Before the finite element method can be expected to predict with reasonable accuracy the actual response of reinforced concrete slabs at large deflections, additional basic experimental research must be conducted to develop the necessary stress-strain and load-deflection relations to be used with the finite element model. The required information relates to the following:

    1.   constitutive relations and failure criteria for concrete under combined stresses

b. bond stress-slip relationship

c. tension stiffening effect of concrete between cracks

d. aggregate interlock, and

e. dowel shear.

7.2 Use of Program ADINA

It is mentioned earlier in the text that *no computer program is
available that can be used to calculate the entire load-deflec-
tion relationship up to the incipient collapse.* The main reason
for this is the presence of an unstable region (DE in Fig. 3)
in the load-deflection relationship of restrained slabs. Since
the primary concern in this study is the behavior in the ten-
sile membrane range, it was thought that with the use of appro-
priate boundary conditions, it might be possible to bypass the
portion of the curve to the left of point E in Fig. 3. The
intent was to remove any restraint to horizontal edge displace-
ment during the early part of the response and thus prevent the
development of compressive membrane action. It was hoped that
this could be accomplished without significantly affecting the
calculated incipient collapse deflection. With this rationale
in mind, the computer program ADINA was implemented on North-
western University's Computer Center. However, further efforts
to employ the program ADINA were abandoned in view of dissatis-
faction of other users with ADINA. It was learned that equi-
librium problems arise when the concrete model in ADINA is used
to analyze reinforced concrete systems where cracks transverse
an embedded reinforcing bar (86). Since this project *is con-*
cerned with slab behavior under conditions where cracks pene-
trate the entire slab thickness, the program ADINA in its pres-
ent form does not appear to be a useful tool.

8. PLASTIC HINGE METHOD TO DETERMINE DEFLECTION CAPACITY

Since no computer program considering both geometric and material nonlinearities is available to reasonably determine the effect of various parameters on deflection capacity, an approximate analytical approach was developed. The method considers end conditions, force equilibrium, strain compatibility and the deflected shape of a slab strip. The approach follows closely the procedure used by Park (20) and Keenan (42) and extends this to take into consideration spalling in the hinging regions.

This chapter describes a step-by-step development of the approach and examines the analytical results obtained.

8.1 Idealized Load-Deflection Behavior of a Restrained Strip

A fixed-end slab strip with flexural mechanism developed is shown in Fig. 76. The strip is initially of length L and is fully restrained against rotation and translation at the ends. The strip is considered to have symmetrically positioned plastic hinges as shown in the figure. The following assumptions are made:

1. At each plastic hinge, the tensile steel has yielded.

2. The compressed concrete has reached its strength with the stress distribution idealized as an equivalent rectangular concrete stress block as defined by ACI 318-77 (26).

3. The tensile strength of concrete can be neglected.

4. Top steel areas (per unit width) at opposite supports are equal.

5. Bottom steel is constant across the strip span, but the amount of top and bottom steel may be different.

6. Segments of the top strip between critical (plastic hinges) sections are assumed to remain straight.

7. The axial tensile strain, ε, is constant along the strip span, corresponding to a constant membrane force along the length.

8. Cover concrete has spalled off.

Portion AB of the strip ABCD has been enlarged in Fig. 77 to show the relationship between the depths to the neutral axis, c and c', and the geometry of the strip under the vertical deflection, .

Fig. 76 Mechanism of Restrained Strip

Fig. 77 Portion of Strip Between Yield
Sections A and B of Fig. 76

Because of axial tensile strain,
ϵ, elongation of the middle portion
BC of the strip $= \epsilon L (1 - 2\beta)$

Due to symmetry, the distance by
which the ends of portion BC will
move away from the center of strip $= 0.5 \; \epsilon L (1 - 2\beta)$

Since there is no outward horizontal
displacement at supports, the hori-
zontal distance from each end of
portion BC to the adjacent support $= \beta L - 0.5 \; \epsilon L (1 - 2\beta)$

Owing to axial tensile strain, ϵ,
the lengths of end portion AB and
CD $= (1 + \epsilon) \; \beta L$

From geometry, this distance A'B' $= \left\{ \beta L - 0.5 \; \epsilon L \; (1 - 2\beta) \right\} \sec \theta$

$$= (1 + \epsilon) \; \beta L + (h - c) \tan \theta \; - c' \tan \theta \qquad (30)$$

where $\quad \theta$ = angle that segment AB makes with the horizontal

$\quad c$ = distance of neutral axis from topmost fiber

$\quad c'$ = distance of neutral axis from bottom fiber

Equation 30 can be rearranged as follows:

$$h - c - c' = \frac{2\beta L \; \text{Sin}^2 \; \theta/2 \; - \epsilon\beta \; L \; \text{Cos}\,\theta \; - 0.5(1 - 2\beta)L}{\text{Sin}} \qquad (31)$$

For this equation, since ϵ and θ are small

$$\text{Sin}\,\theta \; = 2 \; \text{Sin} \; \theta/2 = \frac{\delta}{\beta L} \; , \text{ and Cos}\,\theta \; = 1.0$$

$$c + c' = h - \frac{\delta}{2} + \frac{\beta L^2}{2\delta} \qquad (32)$$

Also, for equilibrium, the membrane forces acting on Sections A
and B of segment AB of the strip are equal. Therefore:

$$C'_c + C'_s - T' = C_c + C_s - T \qquad (33)$$

where $\quad C'_c$ = concrete compressive force at Section A

$\quad C'_s$ = steel compressive force at Section A

$\quad T'$ = steel tensile force at Section A

$\quad C_c$ = concrete compressive force at Section B

C_s = steel compressive force at Section B

T = steel tensile force at Section B

Using ACI concrete compressive stress block (Fig. 78) the concrete compressive forces for a strip of unit width can be written as:

$$C_c' = 0.85 \ f_c' \ \beta_1 \ (c' - d_s) \tag{34}$$

$$C_c = 0.85 \ f_c' \ \beta_1 \ (c - d_s) \tag{35}$$

where f_c' = concrete cylinder strength

β_1 = ratio of the depth of equivalent rectangular stress block to the neutral axis depth, as defined by ACI 318-77 (26)

i.e., β_1 = 0.85 for $f_c' \leqslant$ 4 ksi, and

$\qquad$ = 0.85 - 0.05 (f_c' - 4) f_c' > 4 ksi

c = distance of neutral axis from topmost fiber

d_s = depth of spalled concrete

Substituting Eqs. 34 and 35 into Eq. 33 and rearranging gives:

$$c' - c = \frac{T' - T - C_s' + C_s}{0.85 \ f_c' \ \beta_1} \tag{36}$$

By solving Eqs. 32 and 36 simultaneously, the neutral axis depths at the critical sections are given as:

$$c' = \frac{h}{2} - \frac{\delta}{4} + \frac{\beta \epsilon L^2}{4} + \frac{T' - T - C_s' + C_s}{1.7 \ f_c' \ \beta_1} \tag{37}$$

$$c = \frac{h}{2} - \frac{\delta}{4} + \frac{\beta \epsilon L^2}{4} - \frac{T' - T - C_s' + C_s}{1.7 \ f_c' \ \beta_1} \tag{38}$$

Figure 78 shows conditions at a positive moment yield section of unit width. The forces at the section, C_c, C_s and T are statically equivalent to the tensile membrane force n_u, acting at mid-depth, and the resisting moment m_u. Therefore, for a strip of unit width:

$$n_u = T - C_c - C_s = T - C_s - 0.85 f_c' \ \beta_1 \ (c - d_s) \tag{39}$$
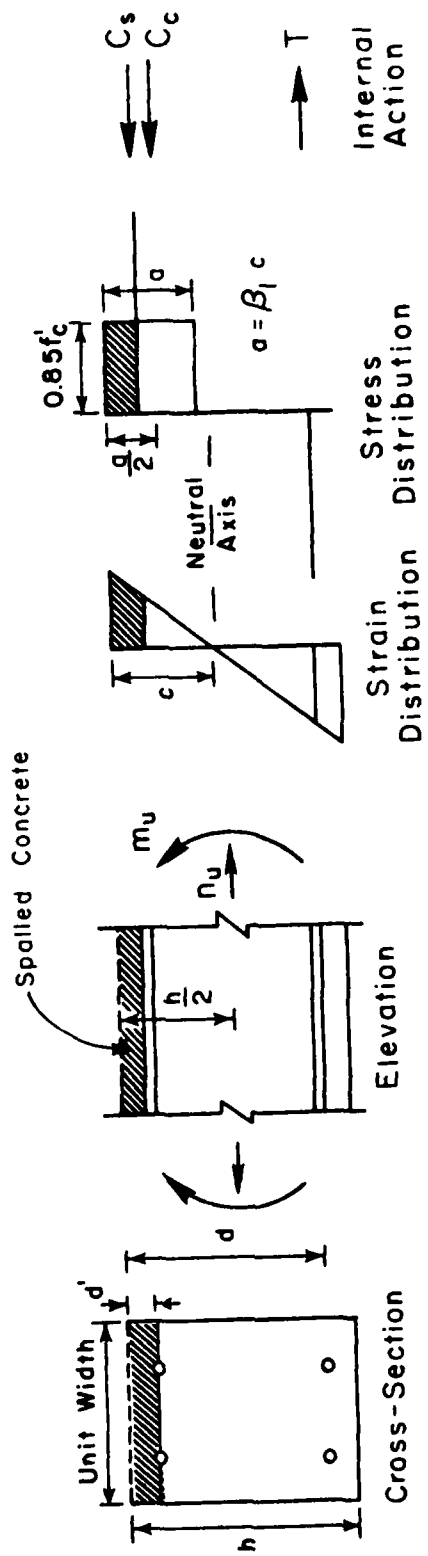
Fig. 78 Conditions at Positive Yield Section

$$m_u = 0.85f'_c \; \beta_1 \left\{ c(0.5h - 0.5\,\beta_1 c) - d_s\,(0.5h - 0.5d_s) \right\}$$

$$+ \; C_s(0.5h - d') + T(d - 0.5h) \tag{40}$$

For a negative moment yield section of unit width, m'_u is given by an equation similar to Eq. 40, and $n'_u = n_u$ for equilibrium.

For each of the segments AB and CD of the strip, the moment sum sum about one end is $m'_u + m_u + n_u\delta$. Shear forces have been neglected since their net contribution to the analysis by virtual work will be zero. On substituting c' and c for Eqs. 36 and 37 into the equation for m'_u, m_u and n_u, it is found that:

$$m_u + m'_u + n_u\delta = 0.425f'_c\;\beta_1 \left\{ c(h - \beta_1 c) - 2d_s(h - d_s) + \right.$$

$$\left. c'(h - \beta_1 c') \right\} + (C_s + C'_s)(0.5h - d') + T + T'(d - 0.5h) +$$

$$\delta \left\{ T - C_s - 0.85f'_c\;\beta_1\,(c - d_s) \right\} \tag{41}$$

The value of unit elongation, ϵ, required in Equation 41 can be determined as follows:

$$\epsilon = \frac{n_u}{hE} \tag{42}$$

where E = effective modulus of elasticity of strip

Substituting values of n_u and c from Equations 38 and 39, ϵ may be written as follows:

$$\epsilon = \frac{T - C_s - 0.85f'_c\;\beta_1\left\{ \dfrac{h}{2} - \dfrac{\delta}{4} - \dfrac{T' - T - C'_s + C_s}{1.7f'_c\;\beta_1} - d_s \right\}}{hE\left\{ 1 + \dfrac{0.2125\;f'_c\;\beta_1\;\beta L^2}{\delta} \right\}} \tag{43}$$

If portion AB or CD of the strip is given a virtual rotation $\Delta\theta$, the virtual work done by the actions at the yield sections of the portion is:

$$(m'_u + m_u + n_u\delta)\,\Delta\theta$$

Work done by the actions at the yield section of the strip portions given by Eq. 44 may be equaled to the work done by the loading on the strip in undergoing the virtual displacement. From this, an equation can be obtained which relates the strip deflection to the load carried.

For illustration, consider a fixed-end reinforced concrete strip of length L, carrying a uniformly distributed load per unit

length, w. In this case, value of β is 0.5. If end of the strip is given a virtual rotation $\Delta\theta$ about the support, the virtual work done by the loading on each end portion is $\frac{wL}{2} \times \frac{L\Delta\theta}{4}$. Hence the virtual work equation may be written as

$$\frac{wL}{2} \times \frac{L\Delta\theta}{4} = (m_u' + m_u + n_u \delta) \, \Delta\theta$$

$$\frac{wL^2}{8} = m_u' + m_u + n_u \, \delta \tag{45}$$

where the right-hand side of Eq. 27 is given by Eq. 41. Thus, the load-deflection relation of the strip may be arranged as follows:

$$w = \frac{3.40}{L^2} f_c' \beta_1 \left\{ c(h - \beta_1 c) - 2d_s(h - \beta_1 d_s) + c'(h - \beta_1 c') \right\}$$

$$+ \frac{8}{L^2} \left\{ (C_s + C_s')(0.5h - d') + (T + T')(d - 0.5h) \right\}$$

$$+ \frac{8\delta}{L^2} \left\{ T - C_s - 0.85 f_c' \beta_1 (c - d_s) \right\} \tag{46}$$

The required values of c', c and ε are given by Eqs. 37, 38 and 43, respectively. The values of forces T, T', C_s, and C_s' are obtained iteratively in order to satisfy compatibility.

It should be noted that the load-deflection relationship thus obtained assumes that critical sections have reached their strength from the onset of deflections. Therefore, the derived load-deflection relationship is not applicable at small deflections when the critical sections are acting elastically or partially plastically.

8.2 A Comparison with Experimental Results

To evaluate the reasonableness of the assumptions used in the approach, a small computer program was developed. A load-deflection relationship was determined for a single-reinforced strip tested by Roberts (53). A comparison of the experimental load-deflection curve with that determined using the plastic hinge method is shown in Figure 79. Due to simplifications introduced in the analytical method calculated deflections at small deflections exhibit a trend that is unrealistic when compared to the experimental results. As mentioned, Eq. 46 applies only when critical sections in the slab have developed their full flexural (plastic) strength. For these reasons, the calculated values at small deflections have not been shown in Fig. 79.
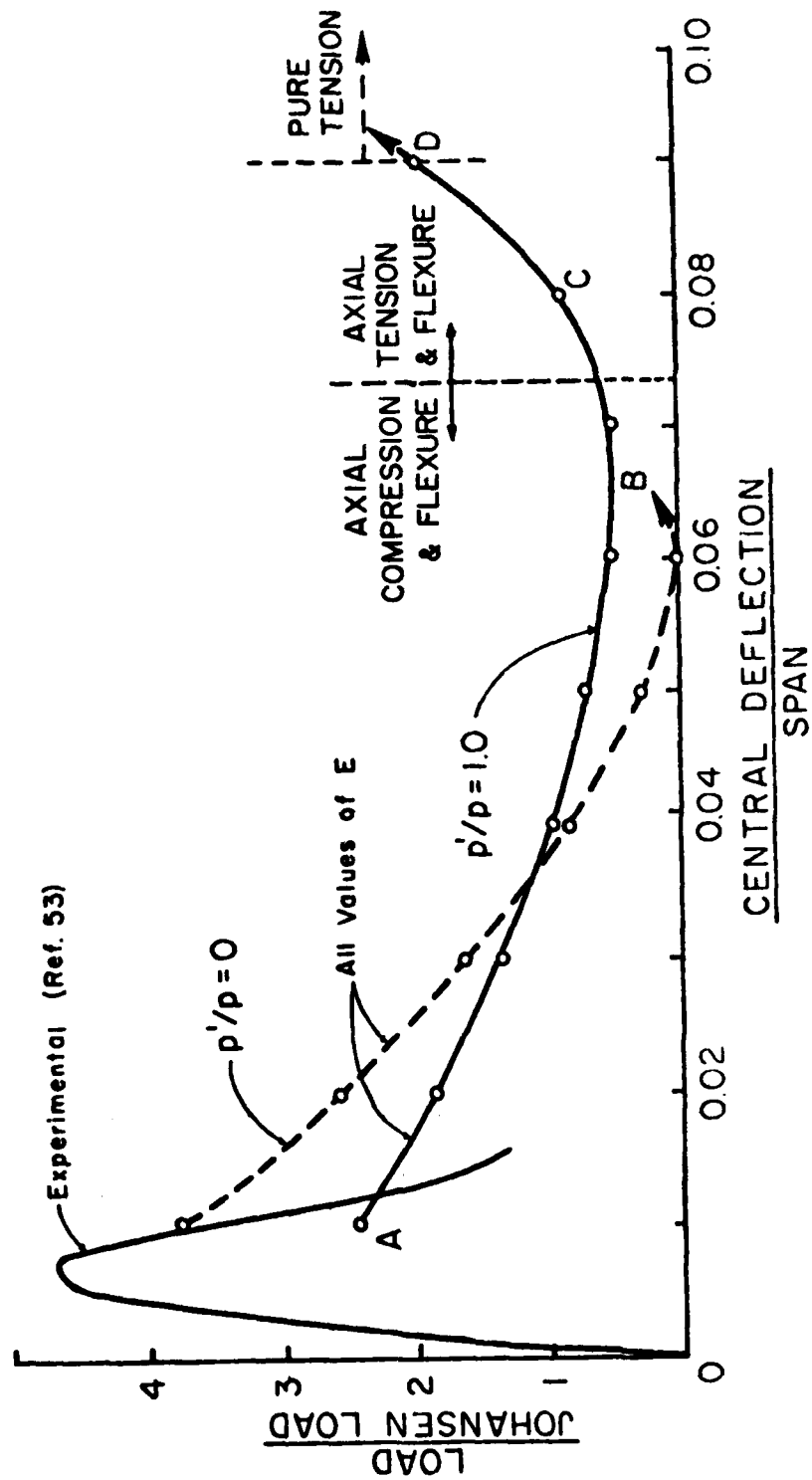
Fig. 79 Analytical and Experimental Load-Deflection Relationships for a
One-Way Slab Strip

Of primary interest is the behavior of the slab at moderately large deflections as predicted by Eq. 46. The analytical curve marked "p'/p = 0" in Fig. 79, shows that the slab capacity drops to zero as both axial thrust and depth to the neutral axis diminish. In the absence of any flexural capacity, the model represents a slab acting as a linkage deforming under pure tension.

As a further application of Eq. 46, another strip was analyzed. The strip was identical to the one analyzed above in all but one aspect. This slab was doubly reinforced, with top and bottom steels having identical areas. As the curve marked "p'/p = 1.0" in Fig. 79 indicates, the load drops from A to B and then rises to D. At level D, the associated depth of the neutral axis is zero. Beyond D, the strip acts as a tensile membrane.

After the moment capacity in the plastic hinges drops to zero, the link model considered in Eq. 46 degenerates into a truss, with its members subjected to tension only. At this stage, a model that assumes the deflected shape of the slab to take the form of a catenary or parabola would be more realistic. However, as will be shown in the next chapter, the use of a parabolic or similar deflected shape to represent the slab in the tensile membrane range yields values of the incipient collapse deflection considerably greater than those observed in experiments. In using such an approach, investigators have found it necessary to apply an empirical constant to the analytical results in order to bring them into agreement with experimental data. Thus, the plastic hinge approach developed here, as reflected in Eq. 46, has limited utility with respect to shedding light on the behavior of a slab in the tensile membrane range, and particularly with reference to the incipient collapse deflection. The approach is more appropriate in the range of behavior when the slab flexural capacity is intact and has not been lost as a result of cracks penetrating the entire slab thickness.

9. DEVELOPMENT OF DESIGN CRITERIA

9.1 Introduction

The primary objective of this investigation is to develop design criteria for conventionally reinforced concrete slabs under static uniform load based on the incipient collapse condition, with emphasis on deflection capacity.

The literature review shows that considerable data exist on the behavior of slabs beyond the Johansen Load. It was noted that the load-deflection relationship of uniformly loaded reinforced concrete slabs is significantly influenced by the restraint conditions along the edges, as shown in Fig. 3.

Available data indicate that most test specimens were not loaded into the tensile membrane regime. Instead, the tests were terminated once the specimen showed a decrease in load-carrying capacity. This would be just after the stage represented by point D in Fig. 3. Tests carried to a deflection level equal to or near that corresponding to incipient collapse are of particular interest in determining deflection capacity of conventionally reinforced concrete slabs.

This chapter summarizes the experimental work on restrained reinforced concrete slabs. It is followed by a comparison of experimental values of incipient collapse deflection with analytical predictions using formula proposed by Park (41), Keenan (42), Black (44), Herzog (45), and Hawkins-Mitchell (47). Finally, the data on experimental incipient collapse deflection capacity is examined to determine the influence of various parameters.

9.2 Restrained Two-Way Slabs

The review of two-way restrained slab test data indicates that both compressive and tensile membrane actions, though occurring at different deflection stages, enhance slab load-carrying capacity. When sufficient lateral restraint exists at boundaries of a slab, slab capacity is increased to several times that predicted by Johansen's yield-line theory, as shown in Table 1. The ratio of slab deflection at the peak load, δ_D, to the slab thickness, h, for a restrained slab does not have a constant value of 0.5 as suggested by Park but varies between 0.11 and 0.97, as summarized in Table 4. Major parameters affecting the ratio δ_D/h are degree of edge restraint, span-depth ratio, and reinforcement ratio.

Near the end of the compressive membrane action range, corresponding to point E in Fig. 3, the large stretch in the central region of the slab surface causes cracks there to penetrate the

entire thickness of the slab. At this stage, load in the central region is carried mainly by the reinforcing bars acting as a tensile membrane.

For a fully restrained slab, as point E in Fig. 3 is approached, the membrane forces change from compression to tension in the central region of the slab. Beyond this stage, the boundary restraints begin to resist inward movement of the slab edges. Initially, the outer regions of the slab will act with the edge restraint as part of the compressive ring supporting the tensile membrane action in the inner region of the slab. With further deflection beyond point E, tensile membrane action gradually spreads throughout the slab. Subsequently, the load carried by the yielding reinforcement increases until the steel starts to fracture at point F. Point F represents the condition of incipient failure for restraint slabs.

Knowledge of the region DE is important since the load will drop suddenly as soon as point D is reached unless the slab is ductile enough to "catch" the load. Thus, tensile membrane action is useful in preventing a catastrophic failure. This assumes that a resistance greater than that corresponding to point D can be developed. Test data show that for heavily reinforced slabs the collapse or ultimate load at point F in Fig. 3 can significantly exceed the peak load at point D. The maximum load associated with tensile membrane action tends to increase with increasing reinforcement ratio, as shown in Figs. 25 and 26.

It is important to note that most restrained slab specimens reviewed in the preceding chapters were not loaded into the tensile membrane range. Instead, the tests were terminated once a slab showed a decrease in load-carrying capacity. This would usually be just after the stage represented by point D in Fig. 3 is reached. Available test data on tensile membrane action indicate that the ultimate deflection before rupture of steel lies between 10 and 15 percent of the slab span (Table 5). The associated maximum edge rotation ranges between 11 and 16 degrees. Herzog (45), and Hawkins and Mitchell (47) pointed out that the breaking strain of steel, in addition to span length, influences ultimate deflection.

The methods used for computing slab behavior in the compressive and tensile membrane action ranges have been examined. No single method of analysis is available for determining the entire load-deflection relationship up to incipient failure. The available methods are semi-empirical in nature and some may have only limited predictive capacity.

9.3 Simply-Supported Two-Way Slabs

For two-way slabs with simply-supported edges, the geometry of deformation permits development of some membrane forces in the slab. This occurs in uniformly loaded two-way slabs at rela-

tively large deflections when the slab regions at the edges tend to move inwards, but are restrained from doing so by the adjacent outer regions. The result is an outer ring of compression resisting tensile membrane forces in the inner region of the slab, as shown in Fig. 50. A representative load-deflection curve for a simply-supported two-way slab is shown as a dashed curve in Fig. 3.

Test results of 65 two-way simply-supported slab specimens show that slab capacity is always greater than that predicted by Johansen's yield-line theory. Measured maximum edge rotations range from 2.2 to 12.4 degrees, as listed in Table 2. A major reason behind such scatter is that not all test specimens were loaded to incipient collapse. Some tests were terminated earlier either due to the loading system being inoperable at large deflections, or disinterest in slab behavior in the region where tensile membrane action predominates.

9.4   Restrained One-Way Slabs

The section on behavior of one-way slab strips presents data and test results on forty-four restrained and simply-supported specimens. These are listed in Table 4. A significant number of tests were carried out using two equal loads at the middle-third points.

Test results on restrained slab strips indicate a maximum edge rotation close to one degree. The reason for this low edge rotation is that the tests were stopped before tensile membrane action developed. Measured maximum edge rotation for simply-supported slab strips ranged from 3.8 to 10.5 degrees. A comparison of test results by Geymayer and McDonald (49) and by Iqbal (54) clearly shows that measured deflection capacity is significantly influenced by the investigator's objective in testing a specimen.

No data is available for one-way strips tested under uniformly distributed load.

9.5   Parameters Affecting Slab Behavior

The major objective in examining the available data has been to get a better understanding of slab behavior near incipient collapse and to identify the most important parameters affecting the deflection capacity at incipient collapse. Park (41), Keenan (42), and Black (44) suggested that the short span of a slab is the only parameter affecting incipient collapse deflection capacity. Herzog (45), and Hawkins and Mitchell (47) hypothesized that, in addition to slab span, the steel breaking strains affect deflection capacity. There has been a tendency to believe that the deflection capacity may be dependent on other slab parameters such as: span-depth ratio, aspect ratio, size of specimen, boundary conditions, etc. An examination of

the correlation between selected parameters and incipient collapse deflection using available experimental data is given below.

As mentioned, most tests were not carried to deflection levels equal to or near the incipient collapse deflection capacity. Thus, in this parametric study, not all test results listed in Tables 1-3 can be employed. Only those carried to the incipient collapse deflection are used.

9.5.1 <u>Short Span of Slab</u>. The effect of short span length on the slab deflection capacity is quite significant, as shown in Fig. 80. The incipient collapse deflection, δ_{ult}, increases almost linearly with an increase in slab's short span. The relationships

$$\delta_{ult} = 0.1 \, L_y, \text{ and}$$

$$\delta_{ult} = 0.15 \, L_y$$

provide almost lower and upper bounds for the experimental data, covering slab spans ranging from 15 inches to 72 inches. The median δ_{ult}-span ratio was 0.13, as shown in Fig. 81.

9.5.2 <u>Lateral Movement of Slab Edges</u>. A comparison between restrained and simply-supported two-way slab test results showed that the deflection capacity-span ratio of simply-supported slabs is slightly greater than that of restrained slabs. The average δ_{ult}-span ratio of simply-supported slabs is 0.18 whereas the δ_{ult}-span of restrained slabs is 0.14. This is indicated in Fig. 81.

9.5.3 <u>Span-Depth Ratio</u>. A plot of incipient collapse deflection, δ_{ult}, and short span-depth of restrained two-way slabs shows a wide scatter (Fig. 82). This implies that short span-depth has no notable affect on δ_{ult}. This observation lends support to the hypothesis that a slab acts essentially as a cable net in the tensile membrane action range.

9.5.4 <u>Combined Short Span-Steel Breaking Strain</u>. Two approaches are available to relate δ_{ult} with a combined effect of short span and breaking strain of the reinforcement. Herzog (45) hypothesized that

$$\delta_{ult} \propto L_y \sqrt{\epsilon_u}$$

Hawkins and Mitchell (47) suggest that

$$\delta_{ult} \propto \frac{L_y \, \epsilon_u}{\sin \sqrt{6 \epsilon_u}}$$

-116-
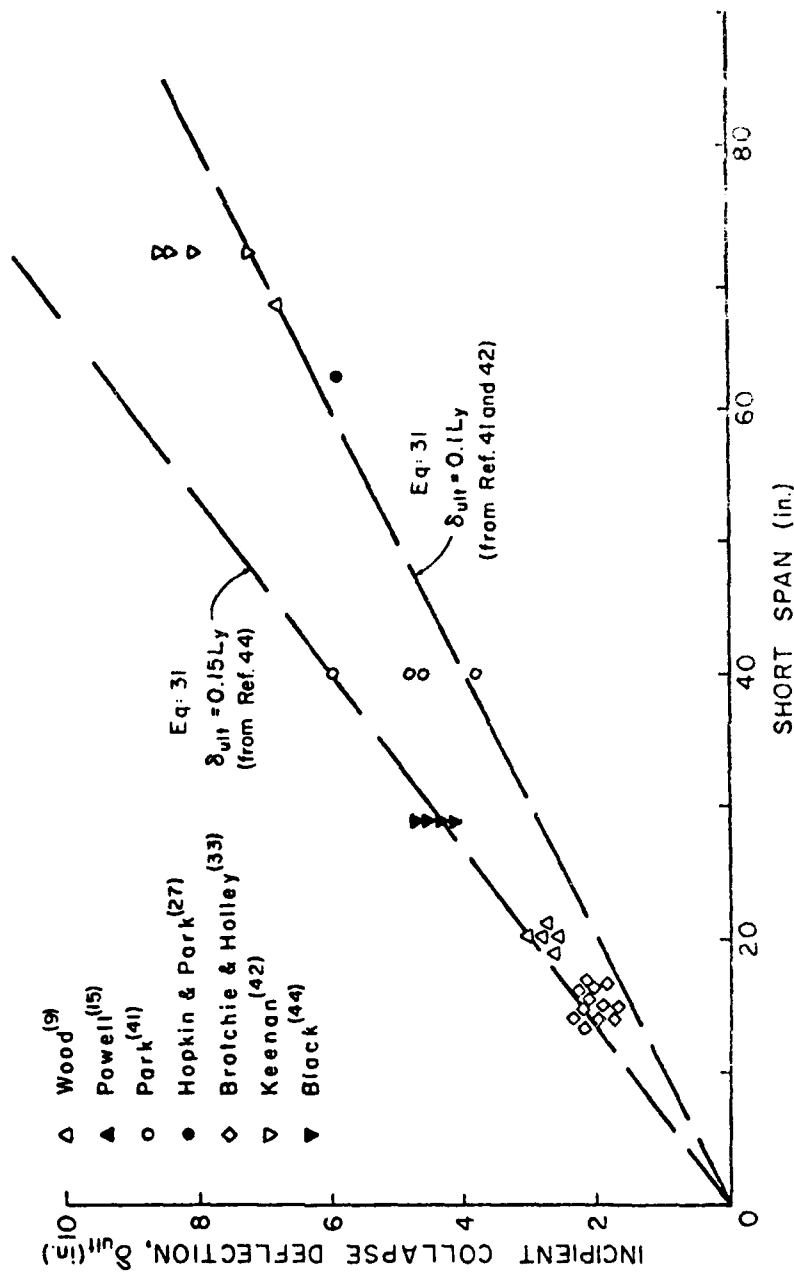
Fig. 80 Effect of Short Span Length on Incipient Collapse Deflection
Capacity of Restrained Two-Way Slabs
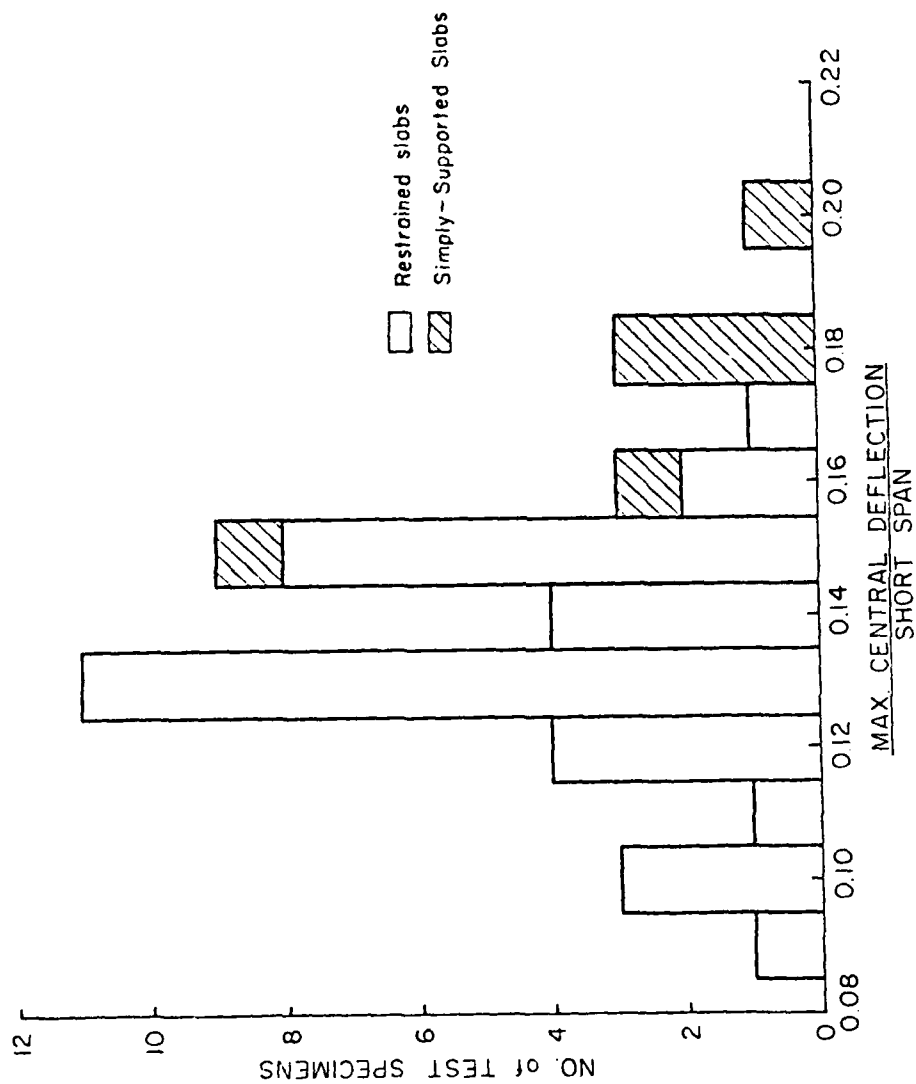
Fig. 81 Effect of Lateral Edge Movement on Incipient Collapse
Deflection Capacity of Two-Way Slabs

Fig. 82   Effect of Span-Depth Ratio on Incipient Collapse
Deflection Capacity of Restrained Two-Way Slabs
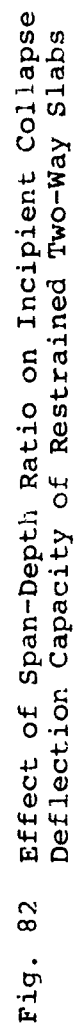
Figures 83 and and 84 show plots of the above relationships. Both show strong positive relationship with δ_{ult}. The scatter seems identical in both cases. The experimental data available for which this combined effect can be considered is quite limited. The reason is that few investigators have reported the breaking strains of reinforcement used in their respective test specimens. However, it should be noted that the data cover a wide range of specimens sizes. The smallest slabs were 29 in. square while the largest was 72 in. square.

9.6 Comparison of Existing Design Methods and Test Data

Park (41) and Keenan (42) determined empirically the safe maximum value for central deflection of restrained slabs, δ_{ult}, in tensile membrane actions to be:

$$\delta_{ult} = 0.1L_y \tag{30}$$

where L_y = short span of slab

Later, Black (44) determined Eq. 30 to be too conservative an estimate of the deflection capacity. Black suggested the deflection capacity, δ_{ult}, to be:

$$\delta_{ult} = 0.15\ L_y \tag{31}$$

A comparison of Eqs. 30 and 31 with available test data indicates that Eq. 30 yields a lower bound whereas Eq. 31 yields an upper bound on the test data.

Herzog (45) determined that the incipient collapse deflection capacity, δ_{ult}, depends on two parameters: short span of slab, and steel elongation at rupture. Assuming the slab to take the shape of a parabolic cable, taking into account the irregular strain distribution in slab reinforcement, Herzog obtained for the midspan deflection after tensile membrane action:

$$\delta_{ult} = L_y\sqrt{\frac{3\varepsilon_u}{32}} = 0.31\ L_y\sqrt{\varepsilon_u} \tag{32}$$

where L_y = short span of slab

              ε_u = steel strain at rupture

A comparison of Eq. 32 with available test data, shown in Fig. 83, indicates that the equation gives a reasonable estimate of the incipient collapse deflection capacity of restrained slabs. For large specimens, Eq. 32 appears to be slightly on the unsafe side.

-120-
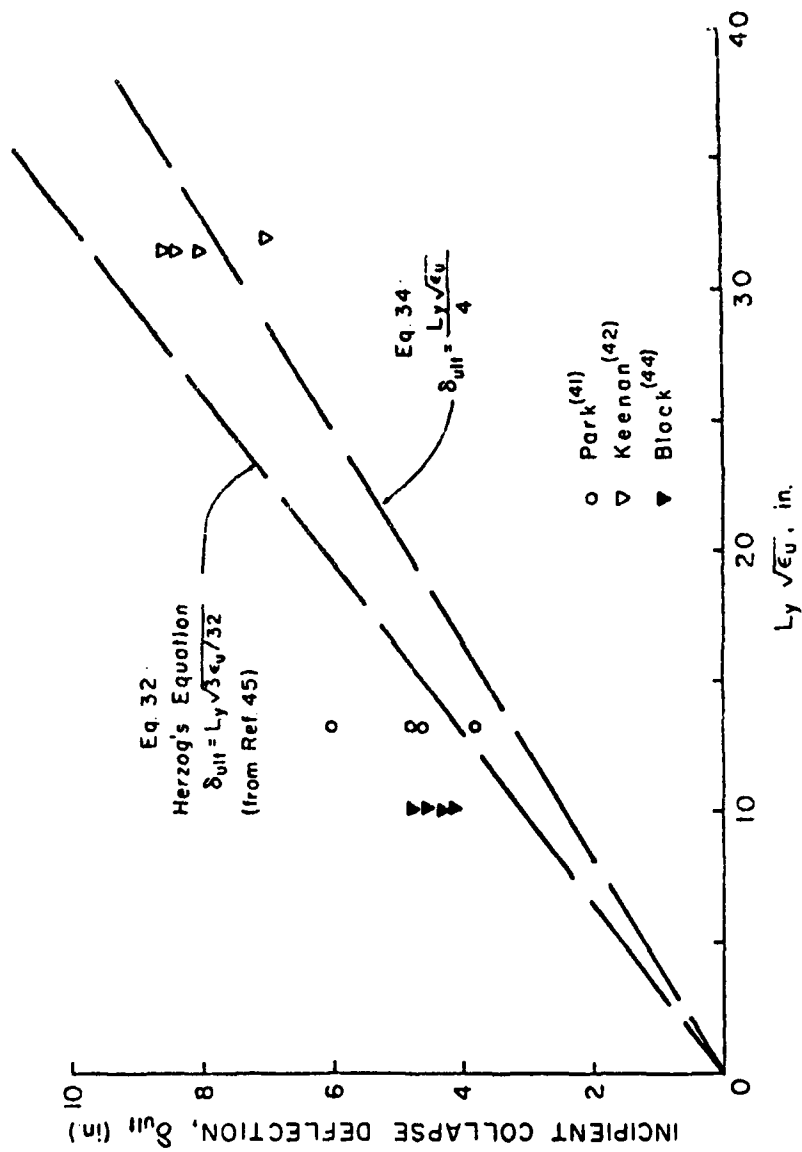
Fig. 83 Combined Short Span-Steel Breaking Strain Effect on
Incipient Collapse Deflection Capacity, as Proposed
by Herzog (from Ref. 45)
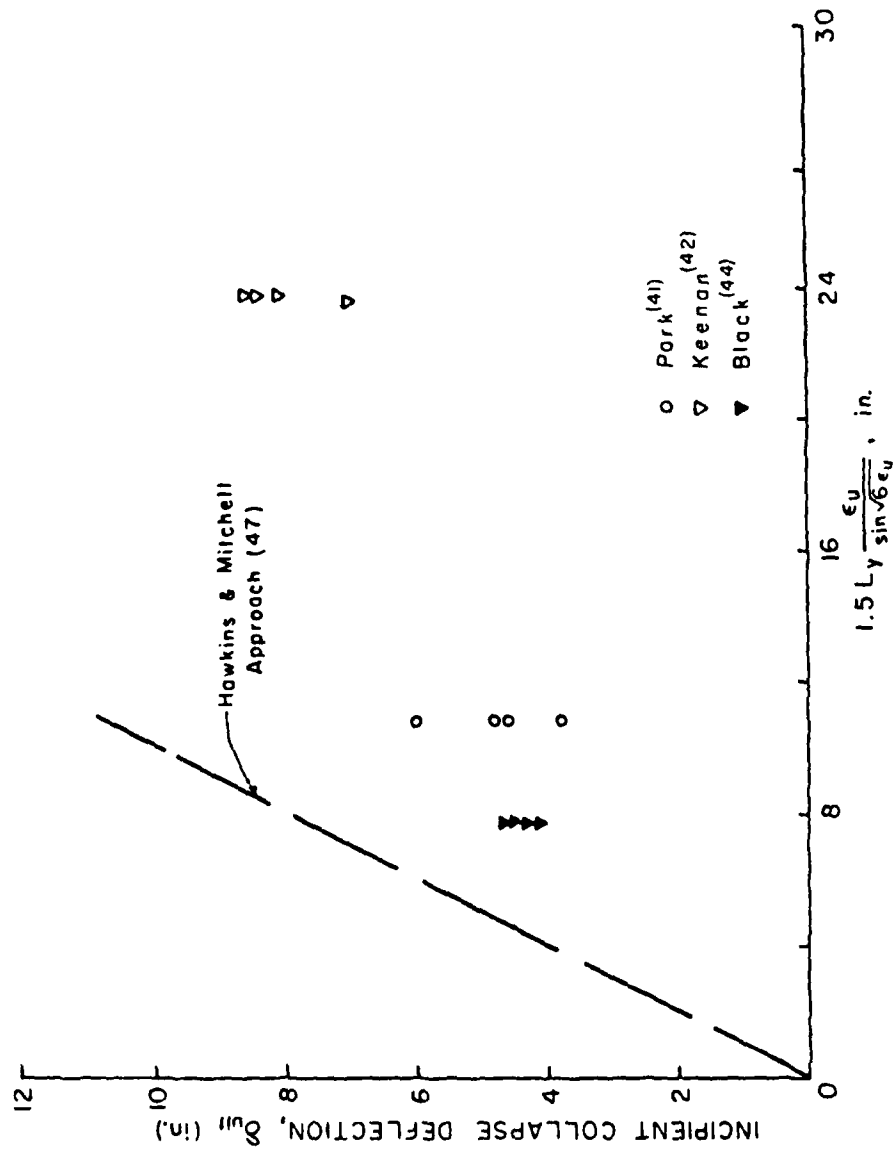
Fig. 84 Combined Short Span-Steel Breaking Strain Effect on
Incipient Collapse Deflection Capacity, as Proposed
by Hawkins and Mitchell (from Ref. 47)

-122-

Hawkins Mitchell (47) assumed that the tensile membrane takes
the shape of a circular arc and developed the following express
for δ_{ult}

$$\delta_{ult} = \frac{1.5\ L_y\ \epsilon_u}{\sin\sqrt{6\epsilon_u}} \qquad (33)$$

Figure 84 shows that Eq. 33 grossly overestimates the incipient
collapse deflection of the test slabs considered. A probable
reason for this discrepancy is the assumption that the slab
behaves merely as a cable net, and that there is no rigidity
provided by concrete enclosed by the steel mesh.

9.7 Selection of Approach to Determine Incipient Collapse Deflection

A comparison of the test data with the existing approaches
indicates that two reasonable approaches exist to determine the
incipient collapse deflection of slabs, δ_{ult}. One approach
assumes that δ_{ult} depends only on short span of the slab.
The second approach stipulates that both short span of slab and
steel strain at breaking point are needed to determine δ_{ult}.

When only the short span of a slab is used to determine δ_{ult},
Eq. 30 provides a conservative estimate. However, it seems
more realistic to include both breaking strain of steel and
short span of slab in predicting δ_{ult}. Both Eqs. 32 and 33
use these two parameters in predicting δ_{ult}, but neither pro-
vides a safe estimate. It is proposed that the following equa-
tion be used to determine the incipient collapse deflection:

$$\delta_{ult} = 0.25\ L_y\sqrt{\epsilon_u} \qquad (34)$$

A comparison of Eq. 34 with the test data is shown in Fig. 83.
It should be noted that the Eq. 34 is slightly more conservative
than Herzog's equation and provides a practical lower bound to
the test data.

There are several points that should be noted in relation to
the proposed Eq. 34. First, the test data on which it is based
include both square and rectangular slabs. The short span of
the slabs range from a low value of 29 in. to a high value of
72 in., more than twice the shortest span. Finally, the test
results are from the work of not just one investigator but of
three different investigators. In spite of the scarcity of
data, the fact that the proposed relationship (i.e., design
criterion) represents a reasonable lower bound on data covering
a wide range of conditions provides some assurance of its
reliability.

As mentioned earlier, the incipient collapse deflection of sim-
ply-supported slabs was, on the average, higher than that of

-123-

restrained slabs. Since no data was available on their steel breaking strain, no separate relationship is proposed. It is believed that Eq. 34 can provide a safe estimate for two-way simply supported slabs. As Eq. 34 was derived using a single cable, its use for one-way slabs seem realistic.

It should be borne in mind that incipient collapse as defined here is assumed to be initiated by rupture of flexural steel. It is further assumed that the slab is designed so that premature failure due to bond or shear does not occur. The design construction requirements to develop tensile membrane behavior so that incipient collapse will occur by tensile rupture of flexural steel will be examined in the report on Phase II of this investigation.

10. SUMMARY AND RECOMMENDATIONS

This report, which covers the work on Phase I of the investigation, presents a review and evaluation of literature on analytical and experimental work on conventionally reinforced concrete slabs. Included are simply-supported as well as restrained one-way and two-way slabs under static loading.

Primary attention in the investigation was focused on the incipient collapse deflection capacity of conventionally reinforced concrete slabs under static loading. For the purpose of this study, incipient collapse is defined as that state of a slab characterized by a drop in the load capacity following mobilization of tensile membrane action. The collapse condition is associated with tensile rupture of the flexural reinforcement. Emphasis was thus placed on the tensile membrane behavior of slabs.

The main objective of work in Phase I has been the evaluation of proposed analytical methods for predicting incipient collapse deflection of slabs. Comparison of analytically predicted deflections with available experimental data was used as the principal basis for determining the reliability of an analytical method.

The literature review showed that although a large number of tests on slabs have been done, very few tests have been carried out to the point of incipient collapse. This reflects the limited interest that slab researchers as a group have had in the behavior of reinforced concrete slabs in the range approaching total collapse.

In terms of analytical prediction, some approaches to determining the load-deflection curve for simply-supported slabs have shown reasonably close agreement with measured curves. However, none of these methods was developed for predicting incipient collapse deflection capacity. Also, no single, rigorous analytical method is available for predicting the entire load-deflection relationship of restrained two-way slabs. Proposed methods for predicting load-deflection curves for restrained two-way slabs have consisted essentially in trying to predict the general trends of separate segments of the overall curve, without clearly defining the endpoints of these segments. Available methods for predicting incipient collapse deflection of two-way slabs are approximate and based on the assumption of pure membrane action, i.e., on the assumption that a typical slab strip behaves as a cable in the tensile membrane range.

The assumption of pure membrane action implies a uniform strain distribution along the length of the slab reinforcement. This results in a predicted collapse deflection

(corresponding to rupture of the reinforcement) considerably greater than that observed in tests. It is obvious that because of cracking, the strain distribution in the flexural reinforcement of an actual slab, even in the tensile membrane range, is non-uniform. The magnitude of the strains at various points along the reinforcement may also be affected by previous flexural response history.

From a correlation of the basic expression for pure membrane action and available experimental data, an expression which provides a reasonable lower bound to the test data is proposed. This expression for the incipient collapse deflection of two-way reinforced concrete slabs under static uniform load is given by

$$\delta_{ult} = 0.25 \, L_y \, \sqrt{\epsilon_u} \, ,$$

where

$$L_y = \text{short span of slab}$$

$$\epsilon_u = \text{breaking strain of flexural steel.}$$

The above expression indicates that the incipient collapse deflection is primarily a function of two parameters, namely, the short span of the slab and the rupture strain of the reinforcement. As indicated in Fig. 83, the above equation provides a reasonably safe estimate of the incipient collapse deflection capacity of two-way restrained slabs. The equation is slightly more conservative when applied to simply-supported slabs. It is therefore recommended that the same expression be used for both restrained and simply supported slabs.

The proposed expression for δ_{ult} implies an angle of rotation at the support (in the direction of the short span) of about 10 degrees for an $\epsilon_u = 0.11$ or about 13 degrees for $\epsilon_u = 0.20$.

In recommending the above expression for estimating the incipient collapse deflection of conventionally reinforced concrete slabs subjected to static uniform loads, it is implicitly assumed that the slab will be properly designed to preclude premature failure due to shear or bond.

- - - - - - - - - -

ACKNOWLEDGMENT

REFERENCES

1. Anonymous, "Structures to Resist the Effects of Accidental Explosions," Department of Navy Publication, NAVFAC P-397, June 1969.

2. Johansen, K.W., Brudlinieteorier, Copenhagen, 1943; English Edition, "Yield-Line Theory," Cement and Concrete Association, London, 1962.

3. Timoshenko, S.P. and Krieger, W., "Theory of Plates and Shells," 2nd Edition, McGraw-Hill, 1959.

4. Wood, R.H., "Plastic and Elastic Design of Slabs and Plates," Thames and Hudson, 1961.

5. Kemp, K.O., "A Lower Bound Solution to the Collapse of an Orthogonally Reinforced Slab on Simple Supports," Magazine of Concrete Reserch, Vol. 14, No. 41, July 1962, pp. 79-84.

6. Vijayarangan, B., "Lower Bound Solutions for Continuous Orthotropic Slabs," Journal of Structural Division, ASCE, Vol. 99, No. ST3, March 1973, pp. 443-452.

7. Hillerborg, A., "A Plastic Theory for the Design of Reinforced Concrete Slabs," Prel. Publication, 6th Congress of the International Association of Bridge and Structural Engineering, Stockholm, 1960.

8. Crawford, R.E., "Limit Design of Reinforced Concrete Slabs," Journal of the Engineering Mechanics Division, ASCE, Vol. 90, No. EM5, October 1964, pp. 321-342.

9. Wood, R.H. and Armer, G.S.T., "Theory of the Strip Method for the Design of Slabs," Proc. of the Institution of Civil Engineers (London), Vol. 41, October 1968, pp. 285-311.

10. Swedish State Concrete Committee, "Massive Concrete Slabs, Specifications for Design Methods, Etc.," Stockholm, 1958.

11. Armer, G.S.T., "Ultimate Load Tests of Slabs Designed by the Strip Method," Proc. of the Institution of Civil Engineers (London), Vol. 41, October 1968, pp. 313-331.

12. Ockleston, A.J., "Load Tests on a Three Storey Reinforced Concrete Building in Johannesberg," Structural Engineer, Vol. 33, No. 10, October 1955, pp. 304-322.

13. Ockleston, A.J., "Arching Action in Reinforced Concrete Slabs," Structural Engineer, Vol. 36, No. 6, June 1958, pp. 197-201.

REFERENCES
(Cont'd)

14. Kemp, K.O., "Yield of a Square Reinforced Concrete Slab on Simple Supports Allowing for Membrane Action," Structural Engineer, Vol. 45, No. 7, July 1967, pp. 235-240.

15. Powell, D.S., "The Ultimate Strength of Concrete Panels Subjected to Uniformly Distributed Loads," Cambridge University Thesis, 1956.

16. Wood, R.H., "Discussion on the Paper: Ultimate Strength of Rectangular Concrete Slabs under Short Term Uniform Loading with Edges Restrained Against Lateral Movement," Proc. Institution of Civil Engineers (London), Vol. 32, September 1965, pp. 97-102.

17. Sawczuk, A., "Membrane Action in Flexure of Rectangular Plates with Restrained Edges," Flexural Mechanics of Reinforced Concrete, ACI/ASCE, SP-12, Detroit, 1965, pp. 347-358

18. Sawczuk, A. and Winnicki, L., "Plastic Behavior of Simply Supported Plates at Moderately Large Deflections," International Journal of Solids and Structures, Vol. 1, No. 1, February 1965, pp. 97-111.

19. Hung, T.Y. and Nawy, E.G., "Limit Strength and Serviceability Factors in Uniformly Loaded Isotropically Reinforced Two-Way Slabs," Cracking, Deflection and Ultimate Load of Concrete Slab Systems, ACI, SP-30, Detroit 1971, pp. 301-311.

20. Park, R., "Ultimate Strength of Rectangular Concrete Slabs Under Short Term Uniform Loading with Edges Restrained Against Lateral Movement," Proc. Institution of Civil Engineers (London), Vol. 28, June 1964, pp. 125-150.

21. Park, R., "The Ultimate Strength and Long-Term Behaviour of Uniformly Loaded Two-Way Concrete Slabs with Partial Lateral Restraint at All Edges," Magazine of Concrete Research, Vol. 16, No. 48, September 1964, pp. 139-152.

22. Park, R., "The Lateral Stiffness and Strength Required to Ensure Membrane Action at the Ultimate Load of a Reinforced Concrete Slab and Beam Floor," Magazine of Concrete Research, Vol. 17, No. 50, March 1965, pp. 29-38.

23. Park, R., "Further Test on a Reinforced Concrete Floor Designed by Limit Procedures," Cracking, Deflection and Ultimate Load of Concrete Slab Systems, ACI SP-30, 1971, pp. 251-270.

REFERENCES
(Cont'd)

24. Park, R. and Gamble, W., "Reinforced Concrete Slabs," John Wiley, New York, to be published.

25. Iwankiw, N.R. and Longinow, A., "Structural Response of Floor Assemblies to Fire," preprint ASCE Annual Convention, October 1978, Chicago, Illinois.

26. ACI Standard, "Building Code Requirements for Reinforced Concrete," ACI 318, 1977.

27. Hopkins, D.C. and Park, R., "Test on a Reinforced Concrete Slab and Beam Floor Designed with Allowance for Membrane Action," Cracking, Deflection and Ultimate Load of Concrete Slab Systems, ACI, SP-30, Detroit, 1971, pp. 251-269.

28. Morley, C.T., "Yield Line Theory for Reinforced Concrete Slabs at Moderately Large Deflections," Magazine of Concrete Reserch, Vol. 19, No. 61, December 1967, pp. 211-221.

29. Nawy, E.G. and Blair K., "Further Studies on Flexural Crack-Control in Structural Slab Systems," Cracking, Deflection and Ultimate Load of Concrete Slab Systems, ACI SP-30, 1971, pp. 1-41.

30. Nawy, E.G., et al, "Crack Control, Serviceability and Limit Design of Two-Way Action Slabs and Plates," Rutgers University, Engineering Research Bulletin 53, 1972.

31. Nawy, E.G., "Crack Control Through Reinforcement Distribution in Two-Way Acting Slabs and Plates," Journal of ACI, Vol. 69, No. 4, April 1972, pp. 217-219.

32. Jacobson, A., "Membrane Flexural Modes of Restrained Slabs," Journal of Structural Division, ASCE, Vol. 93, No. ST5, October 1967, pp. 85-112.

33. Brotchie, J.F. and Holley, M.J., "Membrane Action in Slabs," Cracking, Deflection and Ultimate Load of Concrete Slabs Systems, ACI, SP-30, Detroit, 1971, pp. 345-377.

34. Moy, S.S.J. and Mayfield B., "Load Deflection Characteristics of Reinforced Concrete Slabs," Magazine of Concrete Research, Vol. 24, No. 81, December 1972, pp. 209-218.

35. Massonet, C., "General Theory of Elastic-Plastic Membrane Plates," Paper presented at Conference on Engineering Plasticity, Cambridge University, March 1968.

36. Ramesh, C.K. and Datta, T.K., "Ultimate Strength of Reinforced Concrete Slab-Beam Systems," The Indian Concrete Journal, Vol. 47, No. 8, August 1973, pp. 301-308.

37. Datta, T.K. and Ramesh, C.K., "Some Experimental Studies on a Reinforced Concrete Slab-Beam System," Magazine of Concrete Research, Vol. 27, No. 91, June 1975, pp. 111-120.

38. Hognestad, E., Hanson, N.W. and McHenry, ... Concrete Stress Distribution in Ultimate Strength Design," Proceedings ACI, Vol. 52, 1955-1956, pp. 455-479.

39. Girolami, M.A., Sozen, M.A. and Gamble, W.L., "Flexural Strength of Reinforced Concrete Slabs with Externally Applied In-Place Forces," and Gamble, W.L., Flung, E. and Sozen, M.A., "Strength of Slab subjected to Multiaxial Bending and Compression," Civil Engineering Studies, Structural Research Series No. 369, University of Illinois, Urbana, 1970.

40. Desayi, P. and Kulkarni, A.B., "Load-Deflection of Restrained R/C Slabs," Journal of Structural Division, ASCE, Vol. 103, No. ST2, February 1977, pp. 405-419.

41. Park, R., "Tensile Membrane Behavior of Uniformly Loaded Rectangular Reinforced Concrete Slabs with Fully Restrained Edges," Magazine of Concrete Research, Vol. 16, No. 46, March 1964, pp. 39-44.

42. Keenan, W.A., "Strength and Behavior of Restrained Reinforced Concrete Slabs Under Static and Dynamic Load," Technical Report R621, U.S. Naval Civil Engineering Laboratory, Port Hueneme, California, April 1969.

43. Denton, D.R., "A Dynamic Ultimate Strength Study of Simply Support Two-Way Reinforced Concrete Slabs," U.S. Army Engineer Waterways Experiment Station, Vicksburg, Mississippi, Technical Report 1-789, July 1967.

44. Black, M.S., "Ultimated Strength Study of Two-Way Concrete Slabs," ASCE Proc., Journal of Structural Division, Vol. 101, No. ST1, January 1975, pp. 311-324.

45. Herzog, M., "The Membrane Effect in Reinforced Concrete Slabs According to Tests," Beton and Stahlbetonbau, Vol. (71), 1976, pp. 270-275 (in german).

46. Gilbert, R.I. and Warner, R.F., "Tension Stiffening in Reinforced Concrete Slabs," Journal of Structural Division, ASCE, Vol. 104, No. ST12, December 1978.

47. Hawkins, N.M. and Mitchell, D., "Progressive Collapse of Flat Plate Structures," ACI Journal, Vol. 76, No. 7, July 1979, pp. 775-808.

48. Taylor R., "A Note on a Possible Basis for a New Method of Ultimate Load Design of Reinforced Concrete Slabs," Magazine of Concrete Research, Vol. 17, No. 53, December 1965, pp. 183-186.

49. Taylor R., Maher, D.R.H. and Hayes B., "Effect of the Arrangement of Reinforcement on the Behavior of Concrete Slabs," Magazine of Concrete Research, Vol. 18, No. 55, June 1966, pp. 85-94.

50. Hayes, B., "Allowing for Membrane Action in the Plastic Analysis of Rectangular Reinforced Concrete Slabs," Magazine of Concrete Research, Vol. 20, No. 65, December 1968, pp. 205-211.

51. Geymayer, H.G. and McDonald, J.E., "Influence of Reinforcing Details on Yield-Line Pattern and Ultimate Load-Carrying Capacity of Reinforced Concrete Slabs," Miscellaneous Paper No. 6-911, U.S. Army Engineer Waterways Experimental Station, Vicksburg, Mississippi, August 1967.

52. Desayi, P. and Kulkarni, A.B., "Load-Deflection Behavior of Simply-Supported Rectangular Reinforced Concrete Slabs," International Association for Bridge and Structural Engineering, Proceedings P-11/78, February 1978.

53. Comite Europeen du Beton, "Recommendations for an International Code of Practice for Reinforced Concrete," Comite Europeen du Beton, Paris, 1964.

54. Christiansen, K.P., "The Effect of Membrane Stresses on the Ultimate Strength of the Interior Panel in a Reinforced Concrete Slab," Structural Engineer, Vol. 41, No. 8, August 1963, pp. 261-265.

55. Roberts, E.H., "Load Carrying Capacity of Slab Strips Restrained Against Longitudinal Expansion," Concrete, Vol. 3, No. 9, September 1969, pp. 369-378.

56. Iqbal, M., "Behavior and Strength of R. C. Plates Reinforced with Hot and Cold-Rolled High Strength Steels," M.S. Thesis, Middle East Technical University, Ankara, Turkey, August 1969.

57. Birke, H., "Arch Action in Concrete Slabs," Meddelande NR 108, Institutionen for Byggnadsstatik, KTH, Stockholm, Sweden, 1975. (In Swedish with English Abstract.)

REFERENCES
(Cont'd)

58. Komori, K., "Studies on Strength and Deflection of Reinforced Concrete One-Way Slabs (Part 1)," Transactions of the Architectural Institute of Japan, Vol. 269, July 1978, pp. 61-72. (In Japanese with English Abstract.)

59. Bazant, Z.P., Schnobrich, W.C. and Scordelis, A.C., "Finite Element Analysis of Reinforced Concrete Structures," Fratelli Presenti Specialty Course on Reinforced Concrete Construction, Milan Polytechnic, Milan, Italy, June 1978.

60. Ngo, D. and Scordelis, A.C., "Finite Analysis of Reinforced Concrete Beams," Journal of the American Concrete Institute, Vol. 64, No. 3, March 1967, pp. 152-160.

61. Nilson, A. H., "Nonlinear Analysis of Reinforced Concrete by the Finite Element Method," Journal of the American Concrete Institute, Vol. 65, No. 9, September 1968.

62. Mufti, A.A., Mirza, M.S., Cutcheon, J.O. and Houde, J., "A Study of the Nonlinear Behavior of Structural Concrete Elements," Proceedings of the Specialty Conference of Finite Element Method in Civil Engineering, Montreal, Quebec, Canada, June 1972.

63. Rashid, Y.R., "Ultimate Strength Analysis of Prestressed Concrete Pressure Vessels," Nuclear Engineering Design, Vol. 7, p. 334, 1968.

64. Isenberg, J. and Adham, S., "Analysis of Orthotropic Reinforced Concrete Structure," Journal of the Structural Division, ASCE, Vol. 96, No. ST12, December 1970, pp. 2607-2624.

65. Valliappan, S. and Doolan, T.F., "Nonlinear Stress Analysis of Reinforced Concrete," Journal of the Structural Division, ASCE, Vol. 98, No. ST4, April 1972, pp. 885-898.

66. Nam, C.H. and Salmon, C.G., "Finite Element Analysis of Concrete Beams," Journal of the Structural Division, ASCE, Vol. 100, No. ST12, December 1974, pp. 2419-2432.

67. Bell, J.C. and Elms, D.G., "Nonlinear Analysis of Reinforced Concrete Slabs," Magazine of Concrete Research, Vol. 24, No. 79, June 1972, pp. 63-70.

68. Jofriet, J.C., "Flexural Cracking of Concrete Flat Plates," Journal of ACI, Vol. 70, No. 12, December 1973, pp. 805-809.

REFERENCES
(Cont'd)

69. Jofriet, J.C., "Short Term Deflection of Concrete Flat
    Plates," Journal of Structural Division, ASCE, Vol. 99,
    No. ST1, January 1973, pp. 163-182.

70. Scanlon, A. and Murray, D.W., "An Analysis to Determine
    the Effects of Cracking in Reinforced Concrete Slabs,"
    Proceeding Conference on Finite Element Methods in Civil
    Engineering, McGill University, 1972, p. 841.

71. Lin, C.S., Scordelis, A.C., "Nonlinear Analysis of RC
    Shells of General Form," Journal of Structural Division,
    ASCE, Vol. 101, No. ST3, March 1975, pp. 523-538.

72. Hand, F.A., Pecknold, D.A. and Schnobrich, W.C., "Layered
    Finite Element Procedure for Inelastic Analysis of Rein-
    forced Concrete Slabs," Civil Engineering Studies, Struc-
    tural Research Series No. 389, University of Illinois,
    Urbana, Illinois, August 1972.

73. Kupfer, H.B., Hilsdorf, H.K. and Rusch, H., "Behavior of
    Concrete Under Biaxial Stresses," Journal of the American
    Concrete Institute, Vol. 66, No. 8, August 1969, pp.
    656-668.

74. Wanchoo, M.K. and May, G.W., "Cracking Analysis of Rein-
    forced Concrete Plates," Journal of Structural Division,
    ASCE, Vol 101, No. ST1, January 1975, pp. 201-215.

75. Backlund, J., "Finite Element Analysis of Nonlinear
    Structures," Chalmers Tekniska Hogskola, Gotenberg,
    Sweden, 1973.

76. Berg, S., "Nonlinear Finite Element Analysis of Reinforced
    Concrete Plates," Norwegian Institute of Technology,
    University of Trondheim, Norway, 1973.

77. Knopfel, H., "Calculation of Rigid Plastic Slabs by Finite
    Element Method," Institut for Baustatik, ETH, Switzerland,
    Bericht No. 47, August 1973.

78. Bashur, F.K. and Darwin, D., "Nonlinear Model for Rein-
    forced Concrete Slabs," Journal of Structural Division,
    ASCE, Vol. 104, No. ST1, January 1978, pp. 157-170.

79. Kabir, A.F., "Nonlinear Analysis of Reinforced Concrete
    Panels, Slabs, and Shells for Time Dependent Effects,"
    University of California, Report SESM 76-6, December 1976.

80. Kabir, A.F., "Analysis of RC Shells for Time Dependent
    Effects," preprints, ASCE Annual Convention held in
    Boston, April 1979.

REFERENCES
(Cont'd)

81. Bathe, K.J. and Ramaswamy, S., "On Three-Dimensional Nonlinear Analysis of Concrete Structures," Massachusetts Institute of Technology, Cambridge, Massachusetts, 1978.

82. Bathe, K.J., "ADINA-A Finite Element Program for Automatic Dynamic Incremental Nonlinear Analysis," MIT Reports 82448-1 and 82448-2, 1976.

83. Jain S. and Kennedy, J., "Yield Criterion for Reinforced Concrete Slabs," Journal of Structural Division, ASCE, Vol. 100, March 1974, pp. 631-644.

84. Suidan, M. and Schnobrich, W.C., "Finite Element Analysis of Reinforced Concrete," Journal of Structural Division, ASCE, Vol. 99, No. ST10, October 1973, pp. 2109-2122.

85. Murray, D.W. and Wilson, E.L., "Finite-Element Large Deflection Analysis of Plates," Journal of Engineering Mechanics Division, ASCE, Vol. 95, No. EM1, February 1969, pp. 143-166.

86. Personal Communication with the Naval Civil Engineering Laboratory Staff, Port Hueneme, California, June 1979.

Table 1 Properties and Test Results of Two-Way Restrained Slabs

Investigators	Configuration and Boundary Conditions	Mark	Cylinder Comp. Strength f'c (psi)	Clear Slab Dimension Lx×Ly h	d (in.)	Lx/Ly	Ly/h	Reinforcement Size	Dia. (in.)	Spac. (in.)	Short Span Top	Short Span Bottom	Long Span Top	Long Span Bottom	Steel Yield Strength fy (ksi)	Load wD (psi)	Deflection δD (in.)	Support Rotation θD (degrees)	Johansen Load wj (psi)	Enhancement Ratio wD/wj	δD/L
Ockleston[12]	Rectangular, Orthotropic	B1		190×160×t4		1.20	36.0				0.37	0.24	0.21	0.15		5.23	2.5	1.8	2.05	2.55	0.36
		B2		190×160×t4		1.20	36.0				0.37	0.24	0.21	0.15		5.85	2.5	1.8	2.14	2.74	0.36
Powell[11]	Rectangular, Isotropic	B46	5,810	36×20.6×1.29		1.25	16.0				0.35	0.35	0.35	0.35		45.0			5.5	8.2	
		B47	6,500	36×20.6×1.29		1.25	16.0				0.25	0.25	0.25	0.25		38.0			5.5	7.0	
		B50	5,600	36×20.6×1.29		1.25	16.0				0.45	0.45	0.45	0.45		48.6			9.8	4.9	
		B54	5,940	36×20.6×1.29		1.75	16.0				0.71	0.71	0.71	0.71		52.9			15.4	3.4	
		B55	5,340	36×20.6×1.29		1.75	16.0				0.71	0.71	0.71	0.71		53.0			15.4	3.6	
		B58	5,800	36×20.6×1.29		1.75	16.0				0.97	0.97	0.97	0.97		49.6			25.0	2.0	
		B59	5,700	36×20.6×1.29		1.75	16.0				0.97	0.97	0.97	0.97		50.8			24.9	2.0	
		B62	5,950	36×20.6×1.29		1.75	16.0				1.53	1.53	1.53	1.53		61.0			38.6	1.6	
		B63	5,270	36×20.6×1.29		1.75	16.0				1.53	1.53	1.53	1.53		67.3			38.1	1.8	
Mayol[14]	Square, Isotropic	P812	4,720	58×58×2.7	1.81	1.0	30.0		0.180	3.75	0	0.23	0	0.23	33.8	16.9	1.50	2.7	1.5	10.8	0.70
		P813	3,840	58×58×2.7	1.81	1.0	30.0		0.180	3.75	0.23	0.23	0.23	0.23	33.8	12.3	1.13	1.9	3.0	4.10	0.50
Park[20]	Rectangular, Orthotropic	A1	5,250	40×60×2	1.63	1.5	20.0	D4.6	0.242	8×8	0.38	0.19	0.41	0.20	45.50	30.8	1.10	3.2	8.5	3.67	0.55
		A2	4,710	40×60×2	1.58	1.5	20.0	D2.9	0.191	4×4	0.04	0.42	0.43	0.21	45.50	31.3	1.0	2.9	11.5	2.72	0.50
		A3	5,500	40×60×2	1.53	1.5	20.0	D2.9		4×4	1.44	0.72	0.45	0.22	45.50	37.0	0.90	2.6	20.1	1.84	0.43
		A4	4,620	40×60×2	1.48	1.5	20.0	D4.6	0.242	6×6	2.42	1.21	0.47	0.23	45.50	37.3	0.75	2.2	25.7	1.45	0.38
Hung and Nasy[19]	Square, Isotropic	C1-1	5,590	60×60×2½	2.0	1.0	24.0	D4.6	0.242		0.38	0.38	0.38	0.38	64.3	22.7	2.22	4.2	16.8	1.35	0.89
		C1-2	5,590	60×60×2½	2.0	1.0	24.0	D2.9	0.191		0.36	0.36	0.36	0.36	60.9	18.9	2.07	3.9	10.7	1.35	0.81
		C1-3	4,800	60×60×2½	2.0	1.0	24.0	D4.6	0.242		0.20	0.20	0.20	0.23	64.3	17.6	2.20	4.2	8.3	2.04	0.88
		C1-4	5,590	60×60×2½	2.0	1.0	24.0	D2.9	0.159		0.23	0.23	0.23	0.23	64.8	17.6	2.05	3.9	7.4	2.38	0.82
		C1-5	4,990	60×60×2½	2.0	1.0	24.0	D2.9	0.191		0.36	0.36	0.36	0.36	60.9	29.3	2.04	3.9	1542	1.79	0.82
		C1-6	4,990	60×60×2½	2.0	1.0	24.0	D4.6	0.242		0.38	0.38	0.38	0.38	64.3	20.2	2.16	4.1	10.7	1.79	0.66
		C1-7	5,640	60×60×2½	2.0	1.0	24.0	F3	0.375	9½×9½	0.38	0.38	0.38	0.38	41.6	21.4	2.04	3.9	14.0	1.67	0.82

a Corresponding to point D in Fig. 3.

Continued on next page....

-136-

Table 1 Properties and Test Results of Two-Way Restrained Slabs (Continued)

Investigator	Configuration and Boundary Conditions	Mark	Cylinder Comp. Strength f'c (psi)	Clear Slab Dimension Lx×Ly×h	d (in.)	Lx/Ly	Ly/h	Reinforcement			Steel Percentage				Steel Yield Strength fy (ksi)	Experimental Results at D			Johansen Load wj (psi)	Enhancement Ratio wb/wj	δb/Lb
								Size	Dia. (in.)	Spac. (in.)	Short Span Top / Bottom		Long Span Top / Bottom			Load wb (psi)	Deflection δb (in.)	Support Rotation θb (degrees)			
Hung and Blair (29)	Rectangular, Isotropic	CA-1	6,780	42×60×2½	2.0	1.0	16.0	#3	0.375	9½×9½	0.39 / 0.39	0.39 / 0.39			41.6	30.7	1.86	1.9	13.3	2.0	0.74
		CA-2	5,770	42×60×2½	2.0	1.43	16.0		0.262	8×8	0.28 / 0.28	0.28 / 0.28			64.1	29.0	1.61	3.1	13.7	2.04	0.65
		CA-3	3,770	42×60×2½	2.0	1.43	16.0		0.262	4×4	0.58 / 0.58	0.58 / 0.58			66.1	32.1	1.39	2.0	25.0	1.25	0.52
		CA-4	5,020	42×60×2½	2.0	1.43	16.0		0.191	4×4	0.36 / 0.36	0.36 / 0.36			60.7	29.1	1.79	3.2	17.3	1.67	0.60
		CA-5	5,070	42×60×2½	2.0	1.43	16.0		0.262	6×6	0.39 / 0.38	0.38 / 0.38			64.1	19.1	1.79	2.1	2520	1.67	0.63
	Square, Isotropic	WS1	3,300	60×60×3	2.65	1.0	20.0	24.6	0.262	6×6	0.47 / 0.47	0.47 / 0.47			83.5	33.7	1.69	1.7			0.47
		WS2	3,300	60×60×3	2.65	1.0	20.0	24.6	0.262	8×8	0.47 / 0.47	0.47 / 0.47			83.5	29.92	1.48	2.0			0.63
		WS3	4,070	60×60×3	2.56	1.0	20.0	22.0	0.159	4×4	0.17 / 0.17	0.19 / 0.19			86.3	27.4	1.18	2.3			0.33
		WS4	4,070	60×60×3	2.66	1.0	20.0	22.0	0.159	4×4	0.18 / 0.18	0.18 / 0.18			86.3	22.1	1.52	2.9			0.31
		WS5	5,800	60×60×3	2.65	1.0	20.0	22.0	0.159	6×6	0.24 / 0.24	0.24 / 0.24			86.3	23.1	1.94	3.7			0.63
		WS6	5,800	60×60×3	1.90	1.0	20.0	22.0	0.159	4×4	0.26 / 0.26	0.26 / 0.26			86.3	19.2	1.50	2.9			0.30
		WS7	2,830	60×60×3	2.56	1.0	20.0	22.9	0.191	6×6	0.28 / 0.28	0.28 / 0.28			93.0	22.8	1.66	2.8			0.45
		WS8	2,830	60×60×3	2.56	1.0	20.0	22.9	0.191	6×6	0.28 / 0.28	0.28 / 0.28			93.0	23.3	2.38	2.6			0.46
		WS9	6,170	60×60×3	2.25	1.0	20.0	22.3	0.191	4×4	0.32 / 0.32	0.32 / 0.32			93.0	20.5	1.63	3.1			0.34
		WS10	6,170	60×60×3	2.25	1.0	20.0	22.9	0.191	4×4	0.32 / 0.32	0.32 / 0.32			93.0	22.8	1.44	3.2			0.36
		WS11	4,400	60×60×3	2.62	1.0	20.0	24.6	0.262	8×8	0.22 / 0.22	0.22 / 0.22			87.5	21.1	1.36	2.6			0.63
		WS12	4,400	60×60×3	2.62	1.0	20.0	24.6	0.262	8×8	0.27 / 0.27	0.27 / 0.27			61.5	23.3	1.62	2.7			0.67
		WS13	4,070	60×60×3	1.75	1.0	20.0	48.6	0.331	8×8	0.62 / 0.62	0.62 / 0.62			83.5	25.4	1.92	4.0			0.84
		WS14	4,070	60×60×7	7.00	1.0	20.0	48.6	0.331	8×8	0.34 / 0.34	0.34 / 0.34			83.5	32.4	2.60	5.5			0.30
		WS15	3,870	60×60×3	1.64	1.0	20.0	42.1	0.167	4×4	0.27 / 0.27	0.27 / 0.27			72.0	29.0	2.44	4.0			0.31
		WS16	6,330	60×60×3	2.32	1.0	20.0	47.1	0.167	4×4	0.22 / 0.22	0.22 / 0.22			72.6	17.5	1.72	3.1			0.33
		WS17	4,330	60×60×3	2.72	1.0	20.0	47.1	0.167	4×4	0.27 / 0.27	0.27 / 0.27			72.0	26.5	1.66	3.1			0.36
		WS18	3,930	60×60×3	1.67	1.0	20.0	47.1	0.162	6×6	0.28 / 0.28	0.28 / 0.28			72.0	26.5	.96	3.7			0.63
		WS19	4,850	60×60×3	1.81	1.0	20.0	42.6	0.159	3×3	0.37 / 0.37	0.37 / 0.37			81.7	19.0	1.34	2.9			0.65
		WS20	4,620	60×60×3	2.25	1.0	20.0	42.6	0.159	3×3	0.30 / 0.30	0.30 / 0.30			81.7	28.3	1.98	3.0			0.31

* corresponding to point D in Fig. 3.

Continued on next page.

-137-

Table 1 Properties and Test Results of Two-Way Restrained Slabs
(Continued)

Investigators	Configuration and Boundary Conditions	Mark	Cylinder Comp. Strength f'c (psi)	Clear Slab Dimension Lx×Ly×h	d (in.)	Lx/Ly	Ly/h	Reinforcement Size	Dia. (in.)	Spac. (in.)	Steel Percentage Short Span Top	Short Span Bottom	Long Span Top	Long Span Bottom	Steel Yield Strength fy (ksi)	Load wD (psi)	Deflection δD (in.)	Support Rotation θD (degrees)	Enhance Load wj (psi)	Enhance anit Ratio wD/wj	δD/h
		WS21	4,470	60×60×3	2.25	1.0	20.0	D2.0	0.159	3x3	0.090	0.090	0.30	0.30	81.9	20.3	1.37	2.6			0.46
		WS22	4,850	60×60×3	1.94	1.0	20.0	D2.0	0.159	3x3	0.34	0.34	0.34	0.34	81.9	20.0	1.42	2.7			0.47
		WS23	4,190	60×60×3	2.25	1.0	20.0	D2.0	0.159	4x4	0.22	0.22	0.22	0.22	81.9	19.0	1.55	3.0			0.52
		WS24	4,190	60×60×3	1.75	1.0	20.0	D2.0	0.159	4x4	0.29	0.29	0.29	0.29	81.9	17.4	1.92	3.7			0.64
		WS29	3,800	60×60×3	1.25	1.0	20.0	D4.6	0.242	6x6	0.44	0.44	0.46	0.44	67.5	20.3	2.24	4.3			0.75
		WS30	3,800	60×60×3	1.62	1.0	20.0	D4.6	0.242	6x6	0.47	0.47	0.47	0.47	67.5	19.7	1.76	3.4			0.59
		WS31	3,780	60×60×3	1.25	1.0	20.0	D4.6	0.242	6x6	0.61	0.61	0.61	0.61	67.5	19.0	1.84	3.3			0.61
		WS32	3,780	60×60×3	1.25	1.0	20.0	D4.6	0.242	6x6	0.61	0.61	0.61	0.61	67.5	14.4	1.76	3.4			0.59
		WY1	5,590	60×60×2½	2.0	1.0	24.0	D4.6	0.242	4x4	0.58	0.58	0.58	0.58	68.3	22.7	2.22	4.2			0.89
		WY2	5,590	60×60×2½	2.0	1.0	24.0	D2.9	0.191	4x4	0.36	0.36	0.36	0.36	68.9	18.0	2.03	3.9			0.81
		WY3	4,810	60×60×2½	2.0	1.0	24.0	D4.6	0.242	8x8	0.28	0.28	0.28	0.28	68.3	17.6	2.20	4.2			0.88
		WY4	5,590	60×60×2½	2.0	1.0	24.0	D2.0	0.159	4x4	0.13	0.13	0.15	0.23	68.7	17.6	2.03	3.9			0.82
		WY5	4,990	60×60×2½	2.0	1.0	24.0	D2.9	0.191	4x4	0.36	0.36	0.36	0.36	68.9	19.3	2.04	3.9			0.82
		WY6	4,990	60×60×2½	2.0	1.0	24.0	D4.6	0.242	6x6	0.38	0.38	0.38	0.38	68.3	20.3	2.14	4.1			0.86
		WY7	5,660	60×60×2½	2.0	1.0	24.0	(3)	0.375	9½x9½	0.58	0.58	0.58	0.58	41.6	23.3	2.04	3.9			0.82
	Square, Orthotropic	WS25	3,800	60×60×3	1.87	1.0	20.0	D4.6	0.242	4x8	0.62	0.62	0.31	0.31	67.5	23.3	2.46	4.7			0.82
		WS26	2,400	60×60×3	1.87	1.0	20.0	D4.6	0.242	4x8	0.62	0.62	0.31	0.31	67.5	23.9	1.94	3.7			0.65
		WS27	3,550	60×60×3	1.87	1.0	20.0	D4.6	0.242	4x8	0.62	0.62	0.31	0.31	67.5	22.0	1.92	3.7			0.64
		WS28	3,550	60×60×3	1.87	1.0	20.0	D4.6	0.242	4x8	0.62	0.62	0.31	0.31	67.5	20.3	1.80	3.6			0.60
	Rectangular, Isotropic	WY18	3,370	42×60×2½	1.83	1.43	16.8	D9.2	0.342	8x8	0.63	0.63	0.63	0.63	62.0	23.9	2.10				0.84
		WY19	4,200	42×60×2½	1.92	1.43	16.8	D2.9	0.171	4x4	0.36	0.36	0.36	0.36	68.0	26.2	1.77				0.71
		WY20	3,750	42×60×2½	1.91	1.43	16.8	D2.3	0.177	3x3	0.43	0.43	0.43	0.43	91.0	33.1	1.41				0.56
		WY21	4,280	42×60×2½	1.66	1.43	16.8	D2.5	0.177	3x3	0.49	0.49	0.49	0.49	91.0	35.1	1.64				0.66
		WY22	5,700	42×60×2½	1.88	1.43	16.8	D4.6	0.242	6x6	0.41	0.41	0.41	0.41	91.0	35.1	1.70				0.68
		WY23	5,700	42×60×2½	1.83	1.43	16.8	D9.2	0.342	12x12	0.62	0.62	0.42	0.42	76.0	29.3	2.28				0.91
		WY24	5,690	42×60×2½	1.71	1.43	16.8	D9.2	0.342	8x8	0.95	0.95	0.95	0.95	62.0	23.9	1.90				0.76

a Corresponding to point B in Fig. 3.

Table 1 Properties and Test Results of Two-Way Restrained Slabs
(Continued)

Investigators	Configuration and Boundary Conditions	Mark	Cylinder Comp. Strength f'c (psi)	Clear Slab Dimension Lx Ly h	d (in.)	Lx/Ly	Ly/h	Reinforcement Size	Dia. (in.)	Spac. (in.)	Steel Percentage Short Span Top	Short Span Bottom	Long Span Top	Long Span Bottom	Steel Yield Strength fy (ksi)	Load w (psi)	Deflection δ_D (in.)	Support Rotation θ_D (degrees)	Johansen Load w_j (psi)	Enhancement Ratio w/w_j	δ_D/h
		WV25	4,780	42x60x2½	2.0	1.43	16.0	D3	0.375	9¾x9¾	0.58	0.58	0.58	0.58	41.4	16.1	1.04				0.74
		WV26	5,270	42x60x2½	2.0	1.43	16.0	D4.6	0.242	8x8	0.28	0.28	0.28	0.28	60.3	26.4	1.62				0.65
		WV27	5,770	42x60x2½	2.0	1.43	16.0	D4.6	0.242	4x4	0.58	0.58	0.58	0.58	60.3	25.4	1.54				0.62
		WV28	5,020	42x60x2½	2.0	1.43	16.0	D2.9	0.191	4x4	0.36	0.36	0.36	0.36	60.9	26.6	1.70				0.68
		WV29	5,020	42x60x2½	2.0	1.43	16.0	D4.6	0.242	6x6	0.41	0.41	0.41	0.41	60.3	25.4	1.70				0.68
Brotchie and Holley (33)	Square; Isotropic; Restrained against lateral elongation only	27	4,205	15x15x1.5	1.5	1.0	10.0	0	0		0	0	0	0	—	154.8	0.156	1.5			0.13
		28	4,774	15x15x1.5	1.22	1.0	10.0	wire No. 10	0.135		0.5	0.5	0	0.5	55	190.0	0.262	1.9			0.16
		29	4,487	15x15x1.5	1.22	1.0	10.0		0.135		1.0	1.0	0	1.0	55	276.0	0.271	2.1			0.18
		30	6,518	15x15x1.5	1.22	1.0	10.0		0.135		2.0	2.0	0	2.0	55	259.0	0.334	2.4			0.27
		31	3,620	15x15x1.5	1.22	1.0	10.0		0.135		3.0	3.0	0	3.0	55	276.0	0.327	2.5			0.22
		32	4,721	15x15x0.75	0.75	1.0	20.0	0	0		0.5	0.5	0	0.5	—	35.8	0.279	2.1			0.36
		33	4,721	15x15x0.75	0.56	1.0	20.0	wire No. 13	.0915		0.5	0.5	0	0.5	55	40.1	0.292	2.7			0.39
		34	5,041	15x15x0.75	0.56	1.0	20.0		.0915		1.0	1.0	0	1.0	55	41.4	0.311	2.4			0.47
		35	5,041	15x15x0.75	0.56	1.0	20.0		.0915		2.0	2.0	0	2.0	55	43.9	0.393	2.7			0.46
		36	5,540	15x15x0.75	0.56	1.0	20.0		.0915		3.0	3.0	0	3.0	55	42.1	0.371	2.8			0.55
Square; Isotropic; Clamped		42	5,057	15x15x0.75	0.75	1.0	20.0	—			0	0	—	0	—	35.6	0.366	2.0	0		0.48
		44	4,321	15x15x0.75	0.75	1.0	20.0	—			0	0	—	0	—	25.0	0.272	2.1	0		0.36
		45	4,373	15x15x1.5	1.5	1.0	10.0	—			1.0	1.0	—	1.0	—	16.4	0.167	1.3	0		0.11
		46	5,991	15x15x0.75	0.56	1.0	20.0	wire No. 13	.0915		1.0	1.0	—	1.0	60	39.5	0.325	2.5	18.8	3.17	0.44
		47	4,565	15x15x1.5	1.22	1.0	10.0		0.135		1.0	1.0	—	1.0	55	200	0.160	1.2	81.1	2.50	0.21
		48	6,090	15x15x0.75	0.56	1.0	20.0		.0915		2.0	2.0	—	2.0	60	55	0.425	3.1	34.3	1.60	0.57
		49	4,610	15x15x1.5	1.22	1.0	10.0		0.135		2.0	2.0	—	2.0	55	220	0.155	1.3	150.1	1.47	0.10

a Corresponding to point D in Fig. 3.

Continued on next page

-139-

Table 1 Properties and Test Results of Two-Way Restrained Slabs
(Continued)

Investi- gators	Configuration and Boundary Conditions	Geometrical and Material properties of Slab Specimens						Reinforcement			Steel Percentage				Steel Yield Strength f_y (ksi)	Experimental Results at D*			Johansen Load w_J (psi)	Enhance- ment Ratio w_D/w_J	δ_D/h
		Mark	Cylinder Comp. Strength f'_c (psi)	Clear Slab Dimension l_x, l_y, h	d (in.)	l_x/l_y	l_x/h	Size	Dia. (in.)	Spac. (in.)	Short Span		Long Span			Load w_D (psi)	Deflection δ_D (in.)	Support Rotation θ_D (degrees)			
											Top	Bottom	Top	Bottom							
Hopmans [12]		3S1	3,550	72x72x3	2.25	1.0	24.0	#3	0.375	6x6	0.82	0.82	0.82	0.82	49.6	37.2	1.53	2.4	17.7	1.07	0.51
		3S2	4,140	72x72x3	2.25	1.0	24.0	#3	—	—	0	0	0	0	—	23.6	0.99	1.6	0	—	0.33
		3S3	4,120	72x72x3	2.25	1.0	24.0	#3	0.375	6x6	0.82	0.82	0.82	0.82	49.6	39.6	1.35	2.2	17.9	1.94	0.45
		3S4	1,300	72x72x3	2.25	1.0	24.0	#3	0.375	6x6	0.82	0.82	0.81	0.81	49.6	37.1	1.35	2.1	13.6	1.83	0.45
		4,3S1	3,120	72x72x6.75	3.75	1.0	15.2	#4	0.5	6x6	0.89	0.89	0.89	0.89	47.4	85.0	0.93	1.5	50.6	1.68	0.18
		6S1	3,620	72x72x6	5.0	1.0	12.0	#4	0.5	3x3	1.33	1.33	1.33	1.33	47.4	102.0	1.00	1.7	138.1	1.35	0.18
Rl-w-k [6]		S1	3,750	29x29x0.89	0.8	1.0	33.0	wire #14	0.080	0.95x 0.55	0	0.87	0	0.87	43.6	17.1	0.63	2.3			0.71
		S2	3,680	29x29x0.89	0.8	1.0	33.0		0.080	—	—	0.87	—	0.87	43.6	15.5	0.45	1.8			0.51
		S3	3,620	29x29x0.89	0.8	1.0	33.0		0.080	—	—	0.87	—	0.87	43.6	13.8	0.60	2.4			0.61
		S1-S1	3,790	29x29x0.89	0.8	1.0	33.0		0.080	0.82x 0.52	1.17	1.17	—	—	43.6	18.2	0.30	1.2			0.34

* Corresponding to point D in Fig. 3.

-140-

Table 2 Properties and Test Results of Two-Way Simply Supported Slabs

Investigators	Configuration and Boundary Conditions	Mark	Cylinder Strength f'_c (psi)	Clear Slab Dimension $L_x L_y h$	d_x (in.)	L_x/L_y	L_x/L_y	Size	Dia. (in.)	Spac. (in.)	Steel Percentage Short Span Top	Bottom	Long Span Top	Bottom	Steel Yield Strength f_y (ksi)	Maximum Load w_{mx} (psi)	Maximum Deflection δ_{mx} (in.)	Support Rotation θ_{mx} (degree)	Enhanced Load w_j (psi)	Enhancement Ratio $\frac{w_{mx}}{w_j}$	$\frac{\delta_{mx}}{a}$
Wood[4]	Supported on four encased steel beams	65		72x72x4	1.81	1.0	32.0		0.25	3.0	0	0.00	0.00	0	0.00		7.04	2.48	3.9	4.65	1.57	1.10
		66		72x72x4	1.81	1.0	32.0		0.25	3.0	0	0.00	0.00	0	0.00		6.70	0.95	4.5	4.00	1.64	0.65
	Simply supported on all edges	L7		24x24x1		1.0	24.0	1/8" dia. bar			0	0.00	0.00	0	0.00		8.10	3.2	3.1	5.01	1.61	1.62
Capnyer and McDonald[45]	Reinforcement detail was the variable	1-2	2,650	60x60x1	0.75	1.0	60.0		0.12	2.0	0	0.0	0.0	0	0.8	70.4	390	4.17	7.0	328	1.0	4.17
		3-7	2,850	60x60x1	0.75	1.0	60.0		0.12	2.0	0	0.0	0.0	0	0.8	79.0	315	3.29	7.1	278	0.88	3.29
		4	2,860	60x60x1	0.75	1.0	60.0		0.12	2.0	0	0.0	0.0	0	0.8	79.0	374	3.00	7.2	400	1.09	3.00
		5	2,860	60x60x1	0.75	1.0	60.0		0.12	2.0	0	0.0	0.0	0	0.8	79.0	374	3.40	6.8	424	1.13	7.40
		6	2,860	60x60x1	0.75	1.0	60.0		0.12	2.0	0	0.0	0.0	0	0.8	79.0	374			445	1.19	
		7	3,140	60x60x1	0.75	1.0	60.0		0.12	2.0	0	0.0	0.0	0	0.8	79.0	374			361	0.98	
Sozen and Wimich[18]		11	2,690	43x63x1.18	1.02	1.45	37.0		0.12	1.18	0	0.01	0.01	0	0.01	38.3	6.3	4.75	12.6	3.09	1.48	4.05
		12	2,490	39x79x1.18	1.02	2.0	33.0		0.12	1.18	0	0.01	0.01	0	0.01	38.3	7.0	5.01	6.6	3.09	2.3	3.0
		111	2,490	43x63x1.18	1.02	1.45	37.0		0.12	2.36	0	0.45	0.45	0	0.45	38.3	3.1	3.34	9.4	1.61	2.09	3.0
Taylor, Maher and Hayes[46]	Square; four reinforcement configurations. See Fig. 52	81	4,040	72x72x2		1.0	36.0	3/16 in. dia. bars	0.19	See Fig. 54	0	0.46	0.46	0	0.46	54.5	6.27	3.2	5.1	3.44	1.8	1.5
		82	4,320	72x72x2		1.0	36.0		0.19		0	0.46	0.46	0	0.46	54.5	3.75	3.0	4.0	3.44	1.07	1.5
		83	4,480	72x72x2		1.0	—		0.19		0	0.46	0.46	0	0.46	54.5	4.36	1.8	2.9	3.44	1.26	0.7
		84	3,920	72x72x2		1.0	36.0		0.19		0	0.46	0.46	0	0.46	54.5	6.09	3.2	3.1	3.33	1.6	1.5
		85	3,912	72x72x2		1.0	36.0		0.19		0	0.46	0.46	0	0.46	54.5	5.17	2.2	3.2	3.33	1.3	1.5
		86	3,984	72x72x2		1.0	36.0		0.19		0	0.46	0.46	0	0.46	54.5	5.35	3.1	5.1	3.33	1.6	1.5
		87	4,320	72x72x1.75		1.0	41.0		0.19		0	0.52	0.52	0	0.52	54.5	5.66	3.8	6.1	3.44	1.6	2.10
		88	4,480	72x72x1.75		1.0	41.0		0.19		0	0.51	0.52	0	0.51	54.5	5.66	3.31	5.5	3.44	1.6	1.7
		89	3,472	72x72x3		1.0	24.0		0.19		0	0.31	0.31	0	0.31	54.5	5.53	3.31	9.3	3.44	1.6	1.10
		810	3,768	72x72x3		1.0	24.0		0.19		0	0.31	0.31	0	0.31	54.5	5.53	3.31	9.3	3.43	1.5	1.10

* Maximum recorded by investigator. The values may or may not correspond to the incipient collapse deflection capacity at point C.

-141-

Table 2 Properties and Test Results of Two-Way Simply Supported Slabs
(Continued)

Investigators	Configuration and Boundary Conditions	Mark	Cylinder Strength f'c (psi)	Clear Slab Dimension Lx × Ly h	d (in.)	Lx/Ly	Ly/h	Reinforcement			Steel Percentage				Steel Yield Strength fy (ksi)	Experimental Results			Johansen Load wj (psi)	Enhance. Ratio
								Size	Dia (in.)	Spac (in.)	Short Span Top	Short Span Bottom	Long Span Top	Long Span Bottom		Maximum Load wmax (psi)	Maximum Deflection δmax (in.)	Support Rotation θmax (degrees)		
Brotchie and Holley (35)	Square, Isotropic	8	4,413	15x15x0.75	0.56	1.0	20.0	wire #11	.0915		0	1.0	0	1.0	40.0	17.2	0.23	3.6		0.?
		9	4,063	15x15x0.75	0.56	1.0	20.0	wire #11	.0915		0	1.0	0	1.0	40.0	42.0	0.46	3.5		0.?
		12	4,223	15x15x1.5	1.22	1.0	10.0	wire #10	.1350		0	1.0	0	1.0	40.0	73.3	0.33	4.0		0.?
		13	3,473	15x15x1.5	1.22	1.0	10.0	q dia	.1350		0	3.0	0	3.0	40.0	156.0	0.29	2.3		0.?
Desayi and Kulkarni (50)		S1	2,607	40x60x2		1.5	20.0		0.16			0.25		0.25	80.3				4.61	
		T1	2,494	40x60x1.5		1.5	26.7		0.16			0.33		0.33	80.3				4.45	
		S2	2,607	40x60x2		1.5	20.0		0.16			0.33		0.28	80.3				7.45	
		T2	2,494	40x60x1.5		1.5	26.7		0.16			0.44		0.27	80.3				4.49	
		S3	2,688	40x60x2		1.5	20.0		0.16			0.50		0.28	80.3				9.94	
		T3	2,688	40x60x1.5		1.5	26.7		0.16			0.67		0.37	80.3				6.30	
		S4	2,784	40x30x2		1.5	20.0		0.16			0.25		0.25	80.3	11.76	1.6		2.55	1.56
		T4	2,506	40x50x1.5		1.5	26.7		0.16			0.33		0.33	80.3	6.16	1.7		3.06	1.27
		S5	2,784	40x30x2		1.5	20.0		0.16			0.44		0.20	80.3				8.11	
		T5	2,506	40x50x1.5		1.5	26.7		0.16			0.50		0.27	80.3				3.57	
		S6	3,090	40x30x2		1.5	20.0		0.16			0.50		0.20	80.3				10.70	
		T6	3,090	40x50x1.5		1.5	26.7		0.16			0.67		0.37	80.3				8.81	

Table 3 Properties and Test Results for One Way Slabs

Investigator(s)	Slab				Reinforcement			Cylinder Strength f'c (psi)	Measured Maximum		Edge Reaction at max. Load δmax (degrees)	Ultimate Load W (lbs.)	Wexp/W	δmax/h	Remarks
	Mark	Dimension Lx × Ly × h (in.)	d (in.)	L/h	Type	p %	fy (ksi)		Load Wmax (lbs.)	Deflection δmax (in.)					
Christiansen [52]	1	60×b×3	2.62	20	2 - #2	0.62		3990	2530			1715	1.46		Restrained; See ref. 53 for reinforcement arrangement
	2	60×b×3	2.62	20	2 - #2	0.62		3750	3180	0.65	1.24	2240	1.42	0.2	
	3	60×b×3	2.62	20	2 - #2	0.62		3270	3970			2700	1.67		
	4	60×b×3	2.62	20	2 - #2	0.62		6330	4400			1150	3.83		
Roberts [53]	RB10	54×9×2		28	3/16" Diam. Bars	0.56	35.0	5840		0.58	1.17		6.14	0.29	Restrained in a surround with stiffness equal to 61% that of an infinitely rigid surround.
	RB11	54×9×2		28		0.56	35.0	2870		0.51	1.03		3.95	0.25	
	RB11	54×9×2		28		0.56	35.0	2870		0.52	1.05		3.92	0.26	
	RB11	54×9×2		28		0.56	35.0	2870		0.49	1.00		4.05	0.25	
	RB12	54×9×2		28	Diam. Bars	0.74	35.0	3830		0.54	1.10		4.05	0.27	
	RB12	54×9×2		28		0.74	35.0	3830		0.54	1.14		4.10	0.28	
	RB13	54×9×2		28		0.74	35.0	3500		0.56	1.14		3.51	0.28	
	RB13	54×9×2		28		0.74	35.0	3500		0.48	0.97		3.10	0.26	
	RB13	54×9×2		28		0.74	35.0	3500		0.48	0.92		3.33	0.24	
	RB14	54×9×2		28		0.74	35.0	5760		0.62	1.26		4.31	0.31	
	RB14	54×9×2		28				5760		0.58	1.18		4.59	0.29	
	RB14	54×9×2		28				5760		0.62	1.26		4.85	0.31	
	RB15	54×9×2		28		0.93		2800		0.54	1.10		2.91	0.27	
	RB15	54×9×2		28		0.93		2800		0.48	0.97		2.87	0.24	
	RB17	54×9×2		28		0.93		6180		0.52	1.05		3.45	0.26	
	RB17	54×9×2		28		0.93		6180		0.60	1.22		3.27	0.30	
	RB18	54×9×3		19		0.58		3130		0.43	0.87		4.72	0.14	
	RB18	54×9×3		19		0.58		3130		0.50	1.01		4.46	0.17	
	RB19	54×9×3		19		0.58		3690		0.57	1.16		5.54	0.19	
	RB19	54×9×3		19		0.58		3690		0.54	1.10		5.63	0.18	
	RB20	54×9×3		19		0.58		5550		0.50	1.01		7.43	0.17	
	RB20	54×9×3		19		0.58		5550		0.45	0.91		6.78	0.15	
	RB21	54×9×3		19		0.92		2110		0.42	0.85		3.19	0.14	
	RB21	54×9×3		19		0.92		2110		0.47	0.95		3.01	0.16	
	RB22	54×9×3		19		0.92		3500		0.46	0.93		3.33	0.15	
	RB22	54×9×3		19		0.92		3500		0.46	0.93		3.63	0.15	
	RB23	54×9×3		19		0.92		6530		0.51	1.03		5.06	0.17	
	RB23	54×9×3		19		0.92		6530		0.52	1.05		4.79	0.17	
	RB24	54×9×3		28		0.37		6010		0.54	1.10		9.60	0.27	
	RB24	54×9×3		28		0.37		6010		0.56	1.14		8.50	0.28	
	RB25	54×9×3		28		0.37		3850		0.48	0.97		6.80	0.24	
	RB25	54×9×3		28		0.37		3850		0.52	1.05		7.21	0.26	
	RB26	54×9×3		19		0.23		6040		0.48	0.97		16.30	0.16	
	RB26	54×9×3		19		0.23		6040		0.42	0.85		17.24	0.14	
	RB27	54×9×3		19		0.23		2900		0.39	0.79		10.91	0.13	
	RB27	54×9×3		19		0.23		2900		0.32	0.65		1.72	0.16	
Grewencver and McDonald [49]	a	60×12×1	0.75	60	1/8 in. diam.	0.8	79.0	3150	435	2.0	3.8	381	1.14	2.0	Simply supported; loaded at middle-third points.
	b	60×12×1	0.75	60	1/8 in. diam.	0.8	79.0	3150	421	2.5	4.8	381	1.10	2.5	
Iqbal [54]	1	43×15-3/4 ×1-3/4	1.62	24	8 mm diam.	0.56	71.1	3770	1874	3.94	10.3	1830	1.02	2.22	Steel with definite yield point
	2		1.62	24		0.56	61.2	3770	1995	4.02	10.5	1720	1.16	2.27	Steel with no definite yield point

Table 4 Measured Central Deflection/Slab Thickness at
Ultimate Load of Uniformly Loaded Laterally
Restrained Slabs

Investigator(s)	Number of Slabs	L_x/L_y	L_y/h	Range of δ_D/h
Wood [4]	2	1.0	30	0.50 − 0.70
Ockleston [12]	2	1.20	36	0.56
Powell [15]	15	1.75	16	0.33 − 0.44
Hung and Nawy [19]	7	1.0	24	0.81 − 0.89
"	5	1.43	17	0.62 − 0.74
Park [20-23]	5	1.5	20	0.39 − 0.50
"	1	1.5	27	0.48
"	3	1.5	40	0.37 − 0.50
Nawy and Blair [29]	28	1.0	20	0.39 − 0.89
"	12	1.4	17	0.56 − 0.91
Brotchie and Holley [33]	9	1.0	20	0.36 − 0.57
"	8	1.0	10	0.10 − 0.22
Keenan [42]	4	1.0	24	0.33 − 0.51
"	1	1.0	15	0.20
"	1	1.0	12	0.18
Black [44]	4	1.0	33	0.34 − 0.71

Total No. of Slabs: 107

Table 5 Measured Maximum Deflection/Span Ratio for
Two-Way Slabs Acting as Tensile Membrane

Investigator(s)	Boundary Conditions of Slabs	Number of Slabs	$\frac{L_x}{L_y}$	$\frac{L_y}{h}$	Maximum Deflection Short Span
Wood[4]	Restrained, Single Panel	1	1.0	20.0	0.1
Park[22]	Restrained, Single Panel	4	1.5	20.0	0.10-0.12
Hopkins and Park[27]	Interior Panel in 9-Panel Slab-Beam Floor System	1	1.0	36.0	0.09
Brotchie and Holley[35]	Restrained,	3	1.0	20.0	0.14-0.17
	Simply-Supported	4	1.0	20.0	0.14-0.17
	Restrained,	3	1.0	10.0	0.13-0.14
	Simply-Supported	3	1.0	10.0	0.14-0.17
Keenan[42]	Restrained	4	1.0	24.0	0.11
		1	1.0	15.2	0.09
		1	1.0	12.0	0.06
Black[44]	Restrained	4	1.0	33.0	0.14-0.16
Geymayer and McDonald[49]	Simply-Supported	5	1.0	60.0	0.06-0.07
Sawczuk and Winnicki[18]	Simply-Supported	2	1.45	37.0	0.08-0.11
		1	2.0	33.0	0.15
Taylor, Maher and Hayes[46]	Simply-Supported	1-6	1.0	36.0	0.03-0.04
		7-8	1.0	41.0	0.05
		9-10	1.0	24.0	0.05
Desayi and Kulkarni[50]	Simply-Supported	1	1.2	20.0	0.08
		1	1.2	26.7	0.06